PROCEEDINGS OF
THE GHRSST XIX SCIENCE TEAM MEETING

Darmstadt, Germany
4th – 8th June 2018

ISSN 2049–2529
Issue 2

Edited by the GHRSST Project Office

Meeting hosted by:

EUMETSAT

GHRSST International Project Office

Gary Corlett, Project Director
gpc@ghrsst.org

Silvia Bragaglia-Pike, Project Administrator
gpa@ghrsst.org

www.ghrsst.org

The GHRSST Project Office is funded by the European Union

Table of Contents

SECTION 1: AGENDA

Agenda with links to individual presentations available on the GHRSST website under 'Resources' of the G-XIX meeting page (https://www.ghrsst.org/meetings/19th-international-ghrsst-science-team-meeting-ghrsst-xix/)

MONDAY, 4TH JUNE 2018		
Plenary Session I: Introduction ***Chair:*** *Anne O'Carroll* ***Rapporteur:*** *Gary Corlett*		
09:00-09:10	Welcome to G-XIX from EUMETSAT	Cristian Bank
09:10-09:30	Overview of EUMETSAT	Dieter Klaes
09:30-09:50	EUMETSAT SST Activities	Anne O'Carroll
09:50-10:10	EUMETSAT OSI-SAF	Stéphane Saux Picart
10:10-10:30	CMEMS	Rosalia Santoleri
10:30-11:00	**Tea/Coffee Break**	
Plenary Session II (part 1): Review of activities since G-XVIII ***Chair:*** *Eileen Maturi* ***Rapporteur:*** *Tim Nightingale*		
11:00-11:10	G-XIX: Logistics	Gary Corlett
11:10-11:20	Update on GHRSST	Gary Corlett
11:20-11:30	GHRSST Connection with CEOS: SST-VC	Anne O'Carroll
11:30-11:40	GHRSST system Components: GDAC	Ed Armstrong
11:40-11:50	GHRSST system Components: EU GDAC	Jean-François Piollé
11:50-12:00	GHRSST system Components: LTSRF	Xuepeng Zhao
12:00-12:10	GHRSST system Components: SQUAM and iQUAM	Alexander Ignatov
12:10-12:20	RDAC Update: ABoM	Helen Beggs
12:20-12:30	RDAC Update: CMC	Dorina Surcel Colan
12:30-12:40	RDAC Update: JAXA	Nodoka Ono
12:40-12:50	RDAC Update: JMA	Toshiyuki Sakurai
12:50-13:00	RDAC Update: Met Office	Simon Good
13:00-14:00	**Lunch**	

MONDAY, 4TH JUNE 2018		
Plenary Session II (part 2): Review of activities since G-XVIII ***Chair:*** *Prasanjit Dash* ***Rapporteur:*** *Charlie Barron*		
14:00-14:10	RDAC Update: NASA	Ed Armstrong
14:10-14:20	RDAC Update: NAVO	Bruce McKenzie
14:20-14:30	RDAC Update: NOAA/NESDIS/STAR 1	Alexander Ignatov
14:30-14:40	RDAC Update: NOAA/NESDIS/STAR 2	Eileen Maturi
14:40-14:50	RDAC Update: NOAA/NCEI	Xuepeng Zhao
14:50-15:00	RDAC Update: RSS	Chelle Gentemann
15:00-15:10	Report from CMA	Sujuan Wang
15:10-15:20	Report from ESA	Craig Donlon
15:20-15:30	Report from MISST	Chelle Gentemann
15:30-16:00	**Tea/Coffee Break (Atrium)**	
16:00-16:20	Report from ECMWF	Hao Zuo
16:20-16:30	Discussion	
16:30-18:30	**Poster Session I**	
See Section 3 for Posters List		
18:30-20:00	**Icebreaker**	

TUESDAY 5TH JUNE 2018		
Plenary Session III: Analysis of SST ***Chairs:*** *Dorina Surcel Colon* ***Rapporteur:*** *Simon Good*		
09:00-09:20	Sea Surface Temperature Analysis within the NCEP GFS	Xu Li
09:20-09:40	A new ensemble optimal interpolation SST analysis system at the Bureau of Meteorology	Helen Beggs
09:40-10:00	Variational bias correction of Satellite Sea Surface Temperature observations	James While
10:00-10:30	Open discussion led by session chair	
10:30-11:00	**Tea/Coffee Break**	
Plenary Session IV: Applications of SST ***Chair:*** *Craig Donlon* ***Rapporteur:*** *Ioanna Karagli*		
11:00-11:20	Skin-subskin SST differences using a collocated nine-year Aqua MODIS/AMSR-E record in support of wave breaking studies	Haifeng Zhang
11:20-11:40	A new synergetic approach for the determination of the sea-surface currents in the Mediterranean Sea	Daniele Ciani
11:40-12:00	Exploring Internal Wave signature on remote sensing infrared SST observations.	Cristina González-Haro
12:00-12:30	Open discussion led by session chair	
12:40-14:00	**Lunch**	

TUESDAY 5TH JUNE 2018		
Plenary Session V: Air-Sea Interaction ***Chair:*** *Rosalia Santoleri* ***Rapporteur:*** *Peter Minnett*		
14:00-14:20	Improved diurnal variability forecast of ocean surface temperature through community model development	Ioanna Karagali
14:20-14:40	The Lampedusa Cal/Val site: assessing heat fluxes and high frequency SST estimates in the Mediterranean Sea	Salvatore Marullo
14:40-15:00	Ensemble SST and air-sea heat flux estimate	Hiroyuki Tomita
15:00-15:30	Open discussion led by session chair	

15:30-16:00	**Tea/Coffee Break**

16:00-18:00	**Poster Session II**
See Section 3 for Posters List.	

WEDNESDAY 6TH JUNE 2018		
Plenary Session VI: Calibration/Validation ***Chair:*** *Werenfrid Wimmer* ***Rapporteur:*** *Lei Guan*		
09:00-09:20	Inter-calibration of HY-1B/COCTS Thermal Infrared Channels with MetOp-A/IASI	Mingkun Liu
09:20-09:40	Using Saildrone autonomous in situ data for satellite validation and research into upper ocean physics	Chelle Gentemann
09:40-10:00	Inference from distributions of difference in sea surface temperature validation data	Christopher Merchant
10:00-10:30	Open discussion led by session chair	
10:30-11:00	**Tea/Coffee Break**	
Plenary Session VII: SLSTR ***Chairs:*** *Anne O'Carroll* ***Rapporteur:*** *Igor Tomazic*		
11:00-11:15	The Sentinel-3 Tandem Mission	Craig Donlon
11:15-11:30	Monitoring and evaluation of SST products in the EUMETSAT METIS framework: a year of S3A SLSTR data and preparation for S3B	Prasanjit Dash
11:30-11:45	An open-source cal/val environment and its application to Sentinel-3A SLSTR	Jean-François Piollé
11:45-12:00	Independent validation of Sentinel 3A SLSTR sea surface temperature products	Gary Corlett
12:00-12:15	Sentinel-3 SLSTR SST Validation using a Fiducial Reference Measurements (FRM) Service	Werenfrid Wimmer
12:15-12:30	Assessment of SLSTR L2P SST data as input to the CMEMS MED L3S/L4 multi-sensor operational system	Rosalia Santoleri
12:30-13:00	Open discussion led by session chair	
13:00-14:00	**Lunch**	
15:00-17:00	**GHRSST Team Building**	
18:30-22:00	**GHRSST Dinner**	

THURSDAY 7TH JUNE 2018		
Plenary Session VIII: SST Products ***Chair:*** *Helen Beggs* ***Rapporteur:*** *Jacob Hoeyer*		
09:00-09:20	OSI SAF Sea Surface Temperature reprocessing of MSG/SEVIRI archive	Stéphane Saux Picart
09:20-09:40	ACSPO hourly SST Products from GOES-R/ABI & Himawari-8/AHI	Irina Gladkova
09:40-10:00	Consistent Line of ACSPO L3U SST Products	Matthew Pennybacker
10:00-10:30	Open discussion led by session chair	
10:30-11:00	**Tea/Coffee Break (Atrium)**	
Plenary Session IX: Tools and Services ***Chair:*** *Jean-François Piollé* ***Rapporteur:*** *Stéphane Saux Picart*		
11:00-11:20	Progress with the NOAA ACSPO Regional Monitor for SST (ARMS) System	Alexander Ignatov
11:20-11:40	Ocean Science Data Analytics using Apache Science Data Analytics Platform	Thomas Huang
11:40-12:00	Improving search relevancy for oceanographic data discovery	Ed Armstrong
12:00-12:30	Open discussion led by session chair	
12:30-13:00	Discussion on GHRSST Training & Planning for G-XX	
13:00-14:00	**Lunch**	

THURSDAY 7TH JUNE 2018

14:00-15:30	Task Teams Session I: 14:00 to 15:00: Evolution of R/GTS (led by Jean-François Piollé) 15:00 to 15:30: GHRSST Product Levels (led by Jean-François Piollé)
15:30-16:00	**Tea/Coffee Break**
16:00-18:00	Task Teams Session II: 16:00 to 16:25: Cloud masking (led by Gary Corlett) 16:25 to 16:50: Spatial resolution (led by Peter Cornillon) 16:50 to 17:15: High latitude SSTs (led by Chelle Gentemann) 17:15 to 17:40: SSES and L4 (led by Andy Harris) 17:40 to 18:00: New topics Climatologies (led by Helen Beggs) Ocean Obs '19 (led by Anne O'Carroll)
18:00-21:00	**Advisory Council**

FRIDAY 8TH JUNE 2018		
Plenary Session X: Retrieval of SST ***Chair:*** *Andy Harris* ***Rapporteur:*** *Sandra Castro*		
09:00-09:20	Improving Satellite Retrieved Infrared Sea Surface Temperatures in Aerosol Contaminated Regions	Bingkun Luo
09:20-09:40	Use of 3.9 µm channel for daytime sea surface temperature retrieval	Prabhat Koner
09:40-10:00	Optimal Estimation of Sea Surface Temperature from AMSR-E	Pia Nielsen-Englyst
10:00-10:30	Open discussion led by session chair	
10:30-11:00	**Tea/Coffee Break**	
Closing Session ***Chair:*** *Anne O'Carroll* ***Rapporteur:*** *Gary Corlett*		
11:00-11:15	Report from AC Meeting	Jacob Hoeyer
11:15-12:00	Task Team planning for next year	
12:15-12:45	Review of action items/AOB	
12:45-13:00	Wrap-up/closing remarks	
Close of GHRSST XIX		
13:00-14:00	**Lunch**	
14:00-18:00	**CEOS SST-VC**	

SECTION 2: PLENARY SESSIONS SUMMARY REPORTS

PLENARY SESSION I: INTRODUCTION

THE SATELLITE APPLICATION FACILITY ON OCEAN AND SEA ICE (OSI SAF).

S. Saux Picart[(1)] & OSI SAF team

(1) Météo-France, Lannion, France, Email: stephane.sauxpicart@meteo.fr

1. Introduction

The EUMETSAT Satellite Application Facilities (SAFs) are dedicated centres of excellence for processing satellite data. They form an integral part of the distributed EUMETSAT Application Ground Segment. The Ocean and Sea Ice SAF has the responsibility of developing, validating and distributing near real time products of Sea Surface Temperature (SST), radiative fluxes, wind and Sea Ice for a variety of platforms/sensors.

The OSI SAF consortium includes Meteo-France, as leading institute, and the following co-operating institutes : MET Norway (Norway), DMI (Denmark), Ifremer (France), KNMI (Netherlands).

The OSI SAF production is based on three subsystems:

- Low and Mid latitude (LML) Centre, under Météo-France responsibility, processes and distributes the SST and Radiative Fluxes products covering LML, North Atlantic Regional (NAR) and Global areas. Ifremer contributes to the products distribution and archiving,
- High Latitude (HL) Centre, under MET Norway responsibility with the co-operation of DMI, processes and distributes the Global Sea Ice products, the High Latitude SST and the High Latitude Radiative Fluxes,
- Wind (WIND) Centre, under KNMI responsibility, processes and distributes the Wind products.

2. OSI SAF products

The OSI SAF develops, processes and distributes, in near real-time, products related to key parameters of the ocean-atmosphere interface: sea-ice concentration, edge, type, emissivity, drift, surface temperature, radiative fluxes, wind speed and direction, and sea surface temperature.

2.1. Operational SST products

OSI SAF operational SST production is based on satellites from the EUMETSAT polar orbiting program Meteorological Operational (Metop) and geostationary program Meteosat Second Generation (MSG), and on satellite from the American NOAA polar orbiting program and geostationary program.

2.1.1. Low Earth orbiting satellites production

Currently OSI SAF is processing data from the Advanced Very High Resolution Radiometer (AVHRR), the Infrared Atmospheric Sounding Interferometer (*IASI*) on-board Metop-B and from the Visible Infrared Imaging Radiometer Suite (VIIRS) on-board Suomi-NPP.

Two global SST products are elaborated:

- Global SST from Metop/AVHRR: Level 2 (granules in satellite projection at full resolution) and Level-3 (12 hourly composite on a regular 0.05° lat/lon grid). An illustration is presented on Figure.
- Global SST from Metop/IASI: Level 2 (swath with a sampling of 12 to 40 km). This product is actually developed by EUMETSAT and formated/distributed by OSI SAF.

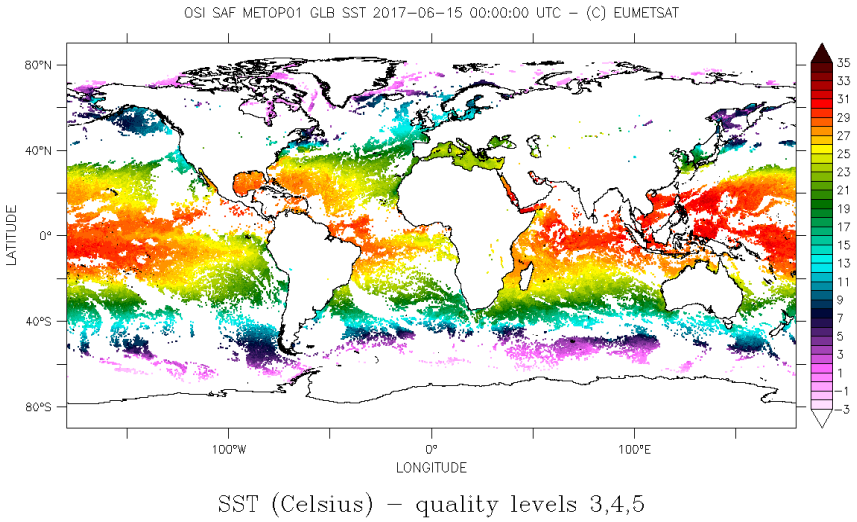

Figure 1: Metop-B/AVHRR global SST 12 hourly composite

Two regional SST products are elaborated:

- North Atlantic Regional SST from Metop/AVHRR and NPP/VIIRS: Level 3 (6 hourly composite mapped onto a 2km stereo-polar grid).
- High latitude Ice and Sea Surface Temperature (IST, SST) and Marginal Ice Zone Temperature (MIZT) from Metop/AVHRR: Level 2 (swath at full spatial resolution). Figureillustrate this product.

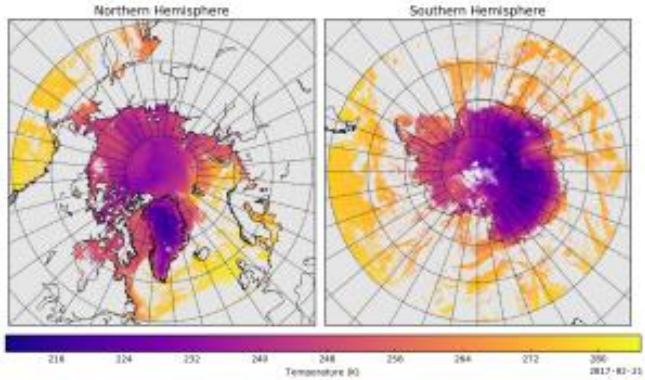

Figure 2: Metop-B/AVHRR high latitude IST, SST and MIZT

2.1.2. From geostationary satellites

OSI SAF is currently processing data from three geostationary satellites: GOES-16 which is in East position (75W), Meteosat-11 (MSG4) in 0E position and Meteosat-8 (MSG1) over Indian Ocean in 41.5E.

Products are Level-3 one hourly composites mapped onto regular lat/lon 0.05° grids.

An illustration is shown on Figure.

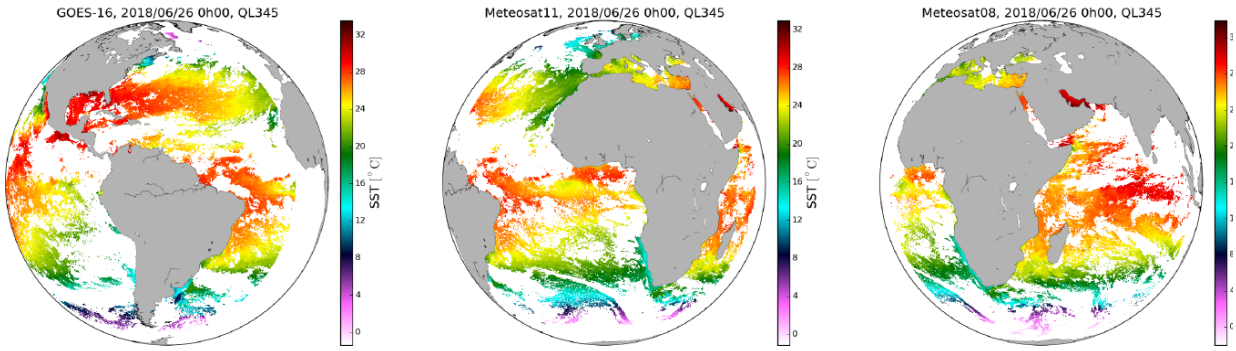

Figure 3: SST from GOES-16, Meteosat-11 and Meteosat-8 at 0h00 on 2018/6/26

2.1.3. Quality assessment

SST products are quality assessed using in situ data, mostly coming from drifting buoys measurements and collected through the Global Telecommunication System (GTS). For each sensor a Match up Data Set (MDS) is assembled. It contains satellite and in situ observation collocated in time and space as well as some intermediate variables of the processing and brightness temperature simulations.

Validation is routinely performed using MDS with a five days delay with respect to near real time data production to ensure most in situ data are captured. Monthly operational validation results are accessible throught the OSI SAF website (http://osi-saf.eumetsat.int) as well as validation reports which are updated

every time a major change occurs in the precessing (new sensor, change in the retrieval methodologies or input data).

2.2. SST reprocessing activities

OSI SAF has achieved a consistent reprocessing of SST from the MSG/SEVIRI archive from 2004 to 2012. For more information see Saux Picart et al (2018) in these proceedings.

3. Sentinel 3/SLSTR cal/val activity

OSI SAF is involved in the calibration/validation activities for the Soil and Land Surface Temperature Radiometer (SLSTR) on-board Copernicus satellite Sentinel 3. A EUMETSAT federated activity has been set up between OSI SAF and EUMETSAT Central Application Facility to collect in situ data build up a MDS and compare SLSTR SST with a variety of in situ sources including measurement from the Infrared Sea Surface Temperature Autonomous Radiometer (ISAR) in high latitude. A validation report has been issued: Dybkjaer et al. (2018).

4. Data access

OSI SAF data are freely accessible to anyone via several means (ftp, EUMETCast, thread server,…). Data are also available through the Physical Oceanography Distributed Active Archive Center (PODAAC) at http://podaac.jpl.nasa.gov, and the data discovery tool exists: Naiad (http://naiad.ifremer.fr).

More information on data access can be found on the OSI SAF website: http://osi-saf.eumetsat.int

5. Conclusion

OSI SAF production is in constant evolution due to the changing satellite capabilities, in particular new satellite missions. The major changes in the coming decade are related to the launch of EUMETSAT new generation sensors such as MetImage on-board Metop-Second Generation platforms, and the Flexible Combined Imager (FCI) on the third generation of geostationary satellites of the program Meteosat Third Generation (MTG). These new generation sensors will be launch by 2022 and it is expected that they will allow for better SST products with for instance higher spatial resolution.

6. References

G. Dybkjaer, A. Marsouin, S. Eastwood, J.-F. Piolle, J. Høyer, H. Roquet, S. Saux Picart, A. O'Carroll, I. Tomazic (2018) Sentinel 3 SLSTR SST Validation Report, A Match-up Data Base for S3A/SLSTR SST products validation. EUMETSAT SAF/OSI/CDOP3/DMI/SCI/RP/307.

S. Saux Picart, A. Marsouin, G. Legendre, S. Péré, H. Roquet (2018), OSI SAF Sea Surface Temperature reprocessing of MSG/SEVIRI archive. These proceedings.

PLENARY SESSION II: REVIEW OF ACTIVITIES SINCE G-XVIII

GLOBAL DATA ASSEMBLY CENTER (GDAC) REPORT TO THE GHRSST SCIENCE TEAM

Edward Armstrong[(1)], Jorge Vazquez[(1)], Wen-Hao Li[(2)], Chris Finch[(1)]

(1) Jet Propulsion Laboratory, California Institute of Technology, Pasadena, CA, 91109 USA
(2) Raytheon Corp., Pasadena, CA 91101
Email: edward.m.armstrong@jpl.nasa.gov

ABSTRACT

In 2017-2018 the Global Data Assembly Center (GDAC) at NASA's Physical Oceanography Distributed Active Archive Center (PO.DAAC) provided ingest, archive, distribution and user services for GHRSST operational data streams with improved and evolved tools, services, and tutorials and interfaced with the user community to address technical inquiries. The GDAC provided access to new GHRSST datasets as well retired a significant number of deprecated GHRSST datasets from its discovery services. The following sections summarize and document the specific achievements of the GDAC to the GHRSST community.

Introduction

The primary contributions to GHRSST for this period are in three categories: Data Management and User Services, Tools and Services, and R/G TS evolution. For data management, the GDAC ingested 12 new GHRSST datasets from multiple data providers (RDACs) and retired 42 obsoleted/superseded datasets, including 26 Level-2, 2 Level-3 and 14 Level-4 datasets (see Appendix I and II). The GDAC continued to support operational data streams for L2P/L3/L4 data from 15 unique RDACs and maintain linkages to the NASA Common Metadata Repository (CMR; https://search.earthdata.nasa.gov/search) and LTSRF archive. For user community engagement the PO.DAAC responded to GHRSST user queries through its help desk and user forum, improved data recipes with data and tutorials (also promulgated on the PO.DAAC user forum) and provided expertise and education in the use and implementation of PO.DAAC Drive, the emerging FTP replacement service. The tools and services set to serve the GHRSST user community needs for data access, subsetting and visualization continues to improve and evolve, and is substantial (see Sections 3 and 4). Members of the PO.DAAC also collaborated on the recommendation to re-architect the Regional Global Task Sharing (R/G TS) framework to decentralize the GHRSST data ingest and distribution nodes that culminated in a formal proposal to the GHRSST Science Team.

Distribution metrics

The following figures show distribution metrics and relative popularity of GHRSST datasets. On a monthly or annual basis GHRSST datasets are consistently among the most popular products in the entire PO.DAAC catalog. Users, data volumes and number of files are all steady or have slightly increased. Users are continuing to leverage services such as OPeNDAP, THREDDS and LAS more so than in the past.

Top 10 Datasets for FTP by users during 2018

Rank	Name	Tool	Files	Volume (GB)	Users
1	PODAAC-GMSLM-TJ142 Global Mean Sea Level Trend from Integrated Multi-Mission Ocean Altimeters TOPEX/Poseidon Jason-1 and OSTM/Jason-2 Version 4.2	FTP	7260	0.76	4183
2	PODAAC-GHMDT-2PJ02 GHRSST Level 2P Global Skin Sea Surface Temperature from the Moderate Resolution Imaging Spectroradiometer (MODIS) on the NASA Terra satellite	FTP	440305	8562.10	3205
3	PODAAC-GMSLM-TJ124 Global Mean Sea Level Trend from Integrated Multi-Mission Ocean Altimeters TOPEX/Poseidon Jason-1 and OSTM/Jason-2 Version 4	FTP	1943	0.21	1134
4	PODAAC-TEMSC-ANTS1 Antarctica Mass Variability Time Series Version 1 from JPL GRACE Mascon CRI Filtered	FTP	5119	0.03	842
5	PODAAC-OSCAR-03D01 OSCAR third degree resolution ocean surface currents	FTP	38410	1109.95	652
6	PODAAC-GHGMR-4FJ04 GHRSST Level 4 MUR Global Foundation Sea Surface Temperature Analysis (v4.1)	FTP	178045	41930.37	573
7	PODAAC-GHGMR-4FJ01 GHRSST Level 4 MUR Global Foundation Sea Surface Temperature Analysis	FTP	181228	29.24	525
8	PODAAC-TEMSC-GRTS1 Greenland Mass Variability Time Series Version 1 from JPL GRACE Mascon CRI Filtered	FTP	4582	0.03	523
9	PODAAC-TEMSC-SFC01 MASCON CLMR4 Scale Factor with CRI Filter	FTP	2905	2.96	451
10	PODAAC-TEMSC-LMC01 MASCON Land Mask used with CRI filter	FTP	2334	2.36	420

Figure 1. Top 10 Datasets for FTP by users during 2018 showing the relative popularity (by Users) of the GHRSST MODIS L2P and MUR L4 datasets.

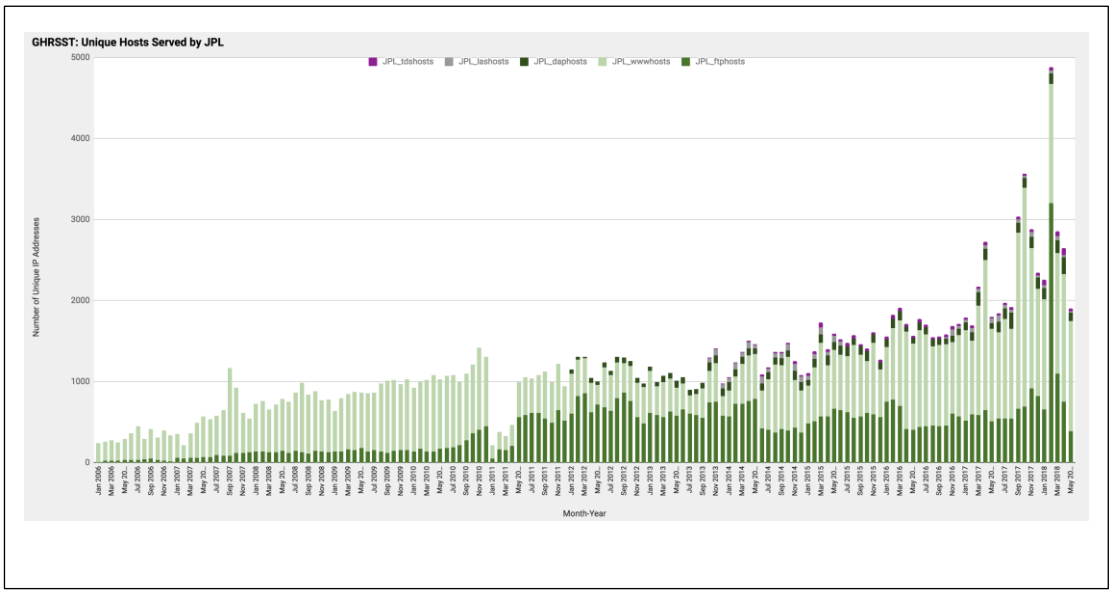

Figure 2. Monthly unique users by FTP, OPeNDAP, THREDDS, LAS or WWW since 2006. Results up to mid-May 2018.

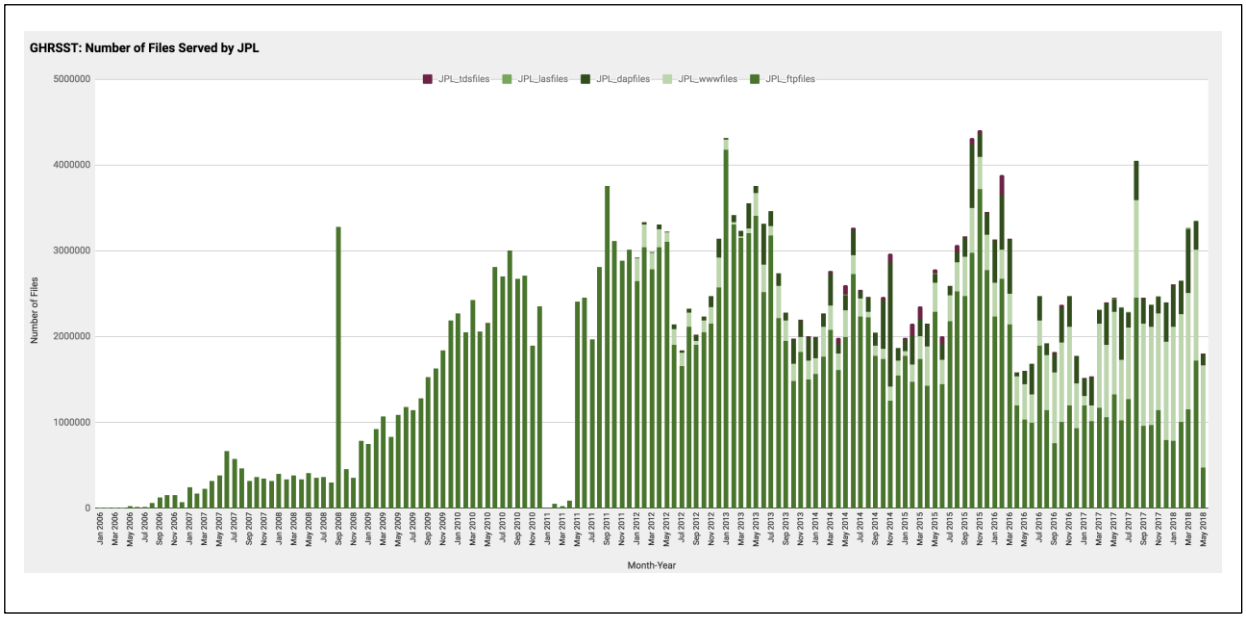

Figure 3. Number of monthly files distributed.

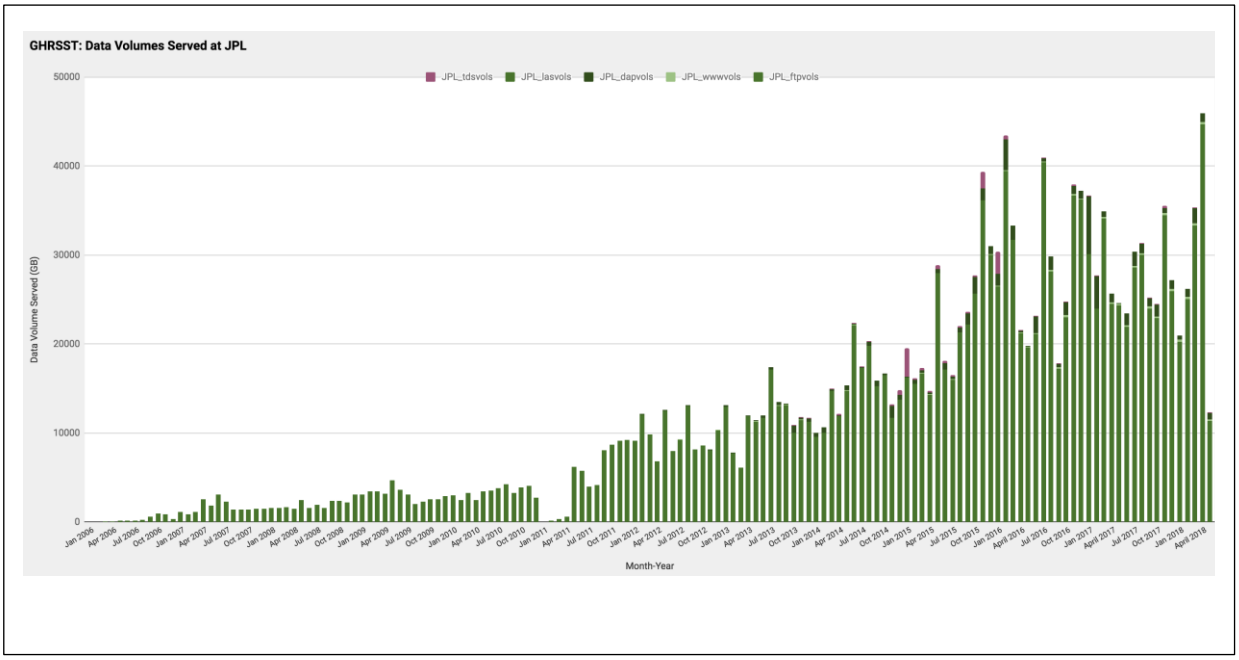

Figure 4. Volume of monthly files (GBs) distributed. Recent record month of 45 TBs distributed (March 2018).

Current Tool Summary

The following list summarizes the list of available tools and services and their locations for GHRSST data.

- SOTO (State of the Ocean version 4.2): visualization including GHRSST MODIS L2P, MUR L4, SMAP SSS.
    - https://podaac-tools.jpl.nasa.gov/soto
- HiTIDE: GUI based L2 subsetting tool, New version to be released in 2018.
    - https://podaac-tools.jpl.nasa.gov/hitide/
- PO.DAAC Web Services: search, discovery, metadata, extract as “chained” services.
    - https://podaac.jpl.nasa.gov/ws
- OPeNDAP: Subsetting for L2/L3/L4
    - https://opendap.jpl.nasa.gov/opendap/OceanTemperature/ghrsst/data/GDS2/contents.html
- THREDDS: Dataset aggregation and subsetting for gridded datasets
    - https://thredds.jpl.nasa.gov/thredds/catalog_ghrsst_gds2.html
- Live Access Server (LAS) for L3/L4 subsetting and visualization
    - https://podaac-tools.jpl.nasa.gov/las/UI.vm
- Webification (w10n-sci): Arbitrary data store exposed as URLs. Subsetting by value.
    - https://podaac-w10n.jpl.nasa.gov/allData/ghrsst/data/GDS2/
- Metadata Compliance Checker: Granule level CF and ACDD metadata reports.
    - https://podaac-uat.jpl.nasa.gov/mcc/

New and Emerging Technologies

The GDAC presentation at the GHRSST-19th Meeting also focused on new emerging tools and services, including the PO.DAAC Drive service which will replace FTP in the very near future. “Drive” can be accessed with this link: https://podaac-uat.jpl.nasa.gov/drive after establishing NASA login credentials here: https://urs.earthdata.nasa.gov/users/new . Tutorials on how to setup PO.DAAC Drive are also found on the PO.DAAC forum. One advantage of Drive is that it allows users to virtually mount the entire PO.DAAC data store as if it were a local directory on their computer. Other emerging technologies include a NASA AIST funded activity called OceanWorks (https://oceanworks.jpl.nasa.gov/) that provides a new paradigm for data storage and fast access to perform dataset discovery, in situ to satellite matchup capability, satellite data analytics including climatologies, visualization and data extraction. Two talks at the GHRSST-19th Meeting focused on this technology and its applications.

Acknowledgements

This work was carried out at the NASA Jet Propulsion Laboratory, California Institute of Technology. Government sponsorship acknowledged. Copyright 2018 California Institute of Technology. Government sponsorship acknowledged.

Appendix I, New and updated GHRSST datasets ingested in the last 12 months

Process Level	Sensors	RDAC	Resolution	Short Name	Persistent ID
Level2	VIIRS	JPL	0.75 km	VIIRS_NPP-JPL-L2P-v2016.0	PODAAC-GHVRS-2PN16
Level2	VIIRS	OSPO	0.75 km	VIIRS_NPP-OSPO-L2P-v2.41	PODAAC-GHVRS-2PO41
Level2	VIIRS	NAVO	0.75 km	VIIRS_NPP-NAVO-L2P-v3.0	PODAAC-GHVRS-2PN30
Level2	AMSR2	RSS	25 km	AMSR2-REMSS-L2P-v8a	PODAAC-GHAM2-2PR8A
Level3	SEVERI	OSI SAF	5 km	SEVIRI_IO_SST-OSISAF-L3C-v1.0	PODAAC-GHSIO-3CO01
Level3	AMSR2	RSS	25 km	AMSR2-REMSS-L3U-v8a	PODAAC-GHAM2-3UR8A
Level3	WindSat	RSS	25 km	WindSat-REMSS-L3U-v7.0.1a	PODAAC-GHWSA-3UR7A
Level3	GMI	RSS	25 km	GMI-REMSS-L3U-v8.2a	PODAAC-GHGMI-3UR8A
Level3	TMI	RSS	25 km	TMI-REMSS-L3U-v7.1a	PODAAC-GHTMI-3UR71
Level3	VIIRS	OSPO	2 km	VIIRS_NPP-OSPO-L3U-v2.41	PODAAC-GHVRS-3UO41
Level4	mw_ir_OI	REMSS	8 km	MW_IR_OI-REMSS-L4-GLOB-v5.0	PODAAC-GHMWI-4FR05
Level4	mw_ir_rt_OI	REMSS	25 km	MW_OI-REMSS-L4-GLOB-v5.0	PODAAC-GHMWO-4FR05

Appendix II, Retired GHRSST dataset table

Process Level	Sensors	RDAC	Resolution	Short Name	Persistent ID
Level2	AVHRR	NAVO	8.8 km	EUR-L2P-AVHRR16_G	PODAAC-GH16G-2PE01
Level2	AVHRR	NAVO	2.2 km	EUR-L2P-AVHRR16_L	PODAAC-GH16L-2PE01
Level2	AVHRR	NAVO	8.8 km	EUR-L2P-AVHRR17_G	PODAAC-GH17G-2PE01
Level2	AVHRR	NAVO	2.2 km	EUR-L2P-AVHRR17_L	PODAAC-GH17L-2PE01
Level2	AVHRR	NERC	1.1 km	NEODAAS-L2P-AVHRR17_L	PODAAC-GH17L-2PS01
Level2	AVHRR	NERC	1.1 km	NEODAAS-L2P-AVHRR18_L	PODAAC-GH18L-2PS01
Level2	AVHRR	OSI-SAF	2 km	EUR-L2P-NAR16_SST	PODAAC-GHN16-2PE01
Level2	AVHRR	OSI-SAF	3 km	EUR-L2P-NAR17_SST	PODAAC-GHN17-2PE01
Level2	AVHRR	OSI-SAF	4 km	EUR-L2P-NAR18_SST	PODAAC-GHN18-2PE01
Level2	AMSRE	REMSS	25 km	REMSS-L2P_GRIDDED_25-AMSRE	PODAAC-GHAMS-2GR01
Level2	AMSRE	REMSS	25 km	REMSS-L2P-AMSRE	PODAAC-GHAMS-2PR01
Level2	AMSRE	OSI SAF	25 km	EUR-L2P-AMSRE	PODAAC-GHAMS-2PE01
Level2	AATSR	EUM	0 km	EUR-L2P-ATS_NR_2P	PODAAC-GHATS-2PE01
Level2	GOES	OSDPD	4 km	OSDPD-L2P-GOES11	PODAAC-GHG11-2PO01
Level2	GOES	OSDPD	4 km	OSDPD-L2P-GOES12	PODAAC-GHG12-2PO01

Process Level	Sensors	RDAC	Resolution	Short Name	Persistent ID
Level2	GOES	OSDPD	4 km	OSDPD-L2P-GOES13	PODAAC-GHG13-2PO01
Level2	GOES	OSDPD	4 km	OSDPD-L2P-GOES15	PODAAC-GHG15-2PO01
Level2	MODIS	JPL	1 km	JPL-L2P-MODIS_A	PODAAC-GHMDA-2PJ01
Level2	MODIS	JPL	1 km	JPL-L2P-MODIS_T	PODAAC-GHMDT-2PJ01
Level2	SEVIRI	CMS	11.6	EUR-L2P-SEVIRI_SST	PODAAC-GHSEV-2PE01
Level2	SEVIRI	OSDPD	4.5	OSDPD-L2P-MSG02	PODAAC-GHMG2-2PO01
Level2	MTSAT	OSDPD	4 km	OSDPD-L2P-MTSAT1R	PODAAC-GHMT1-2PO01
Level2	MTSAT	OSDPD	4 km	OSDPD-L2P-MTSAT2	PODAAC-GHMT2-2PO01
Level2	TMI	REMSS	25 km	REMSS-L2P_GRIDDED_25-TMI	PODAAC-GHTMI-2GR01
Level2	TMI	REMSS	25 km	EUR-L2P-TMI	PODAAC-GHTMI-2PE01
Level2	TMI	REMSS	25 km	REMSS-L2P-TMI	PODAAC-GHTMI-2PR01
Level3	AVHRR	OSI SAF	5 km	EUR-L3P-GLOB_AVHRR_METOP_A	PODAAC-GHGMT-3PE01
Level3	AVHRR	OSI SAF	2 km	EUR-L3P-NAR_AVHRR_METOP_A	PODAAC-GHNMT-3PE01
Level4	AVHRR_OI	NCDC	25 km	NCDC-L4LRblend-GLOB-AVHRR_OI	PODAAC-GHAAO-4BC01
Level4	MUR	JPL	1 km	JPL-L4UHfnd-GLOB-MUR	PODAAC-GHGMR-4FJ01

Process Level	Sensors	RDAC	Resolution	Short Name	Persistent ID
Level4	ODYSSEA	ODYSSEA	10 km	EUR-L4HRfnd-GLOB-ODYSSEA	PODAAC-GHGOY-4FE01
Level4	ODYSSEA	ODYSSEA	2 km	EUR-L4UHRfnd-GAL-ODYSSEA	PODAAC-GHLOY-4FE01
Level4	EUR	ODYSSEA	2 km	EUR-L4UHFnd-MED-v01	PODAAC-GHMED-4FE01
Level4	ODYSSEA	ODYSSEA	2 km	EUR-L4UHRfnd-MED-ODYSSEA	PODAAC-GHMOY-4FE01
Level4	mw_ir_OI	REMSS	8 km	REMSS-L4HRfnd-GLOB-mw_ir_OI	PODAAC-GHMWI-4FR01
Level4	mw_ir_rt_OI	REMSS	8 km	REMSS-L4HRfnd-GLOB-mw_ir_rt_OI	PODAAC-GHMWR-4FR01
Level4	MUR	JPL	1 km	JPL-L4UHfnd-NCAMERICA-MUR	PODAAC-GHNMR-4FJ01
Level4	ODYSSEA	ODYSSEA	2 km	EUR-L4UHRfnd-NWE-ODYSSEA	PODAAC-GHNOY-4FE01
Level4	MODIS-AMSRE	JPL	1 km	JPL-L4UHblend-NCAMERICA-RTO_SST_Ad	PODAAC-GHRAD-4FJ01
Level4	MODIS-AMSRE	JPL	1 km	JPL-L4UHblend-NCAMERICA-RTO_SST_An	PODAAC-GHRAN-4FJ01
Level4	MODIS-AMSRE	JPL	1 km	JPL-L4UHblend-NCAMERICA-RTO_SST_Td	PODAAC-GHRTD-4FJ01
Level4	MODIS-AMSRE	JPL	1 km	JPL-L4UHblend-NCAMERICA-RTO_SST_Tn	PODAAC-GHRTN-4FJ01

THE EU GDAC AND IFREMER RELATED ACTIVITIES

Jean-François Piollé[(1)], Emmanuelle Autret[(1)], Cédric Prevost[(1)]

(1) Institut Français de Recherche pour l'Exploitation de la Mer (Ifremer), Brest, France, Email: jfpiolle@ifremer.fr

Introduction

Ifremer's Satellite Data Center (CERSAT) operates as a GHRSST producer and Global Data Assembly Center (G-DAC) for Europe since Medspiration (2005). It delivers a wide range of L2P, L3 and L4 products together with different access services. It also maintains the felyx system for match-up production, in particular in the context of Sentinel-3 cal/val.

Products

Distributed products

As a DAC, Ifremer distributes the L2P and L3 products from OSI SAF, pushed to US-GDAC, and also mirror several products from US-GDAC for European users. All these data are used as input to multi-sensor products or match-up databases processed at Ifremer.

Since 2018, Ifremer is also the main DAC for all in situ radiometer data from the shipborne radioemeter network (http://www.shipborne-radiometer.org/).

The distribution statistics of these products show a steady number of users and distributed volume over the last few years. The equally steady number of newly registered users compared to the two previous numbers also seem to demonstrate that most usages are still occasional rather than continuous operational applications.

Generated products

- Ifremer processes and deliver several global and regional multi-sensor products, including: the continuation of Medspiration project time series for regional L4 products over Mediterranean Sea, South Africa, and Brazil/Tropical Atlantic
- an operational global multi-sensor L3S and a L4 over Europe North Western Shelves (now extended to Iberian sea and canary islands) in the context of Copernicus Marine Service (CMEMS). These products are exclusively distributed at CMEMS (http://marine.copernicus.eu/).

In the last year, we have focused on two main activities:

- the reprocessing of a long time series (1982-2017) of the multi-sensor L4 over Europe North Wester Shelves (NWS) for Copernicus Marine Environment Monitoring Service (CMEMS), using the AVHRR Pathfinder v5.3 (PFv53) archive extended over 2017 with AVHRR GAC data (figure 1). A new analysis methodology was used for this product based on a Kalman smoother (Tandéo et al., 2011). This product is available on CMEMS portal and used to derive the annual CMEMS State of the Ocean report.

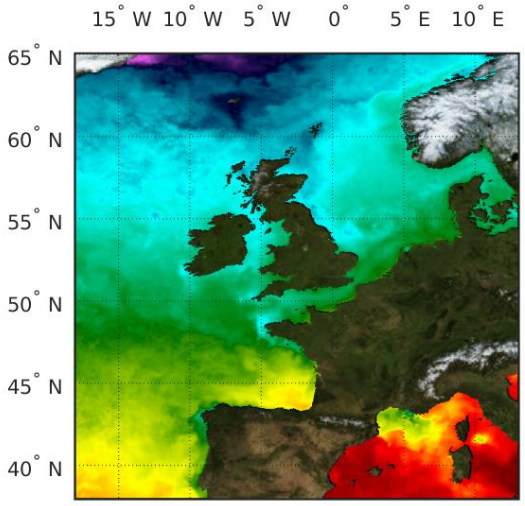

Figure 1: new reprocessed time series over Europe North Western Shelves

- A new product extending the NWS area down to the Morocco upwelling and including Iberian, Biscay and Irish seas (IBI), as a request by CMEMS (figure 2). Available daily at 2km resolution, this product will eventually supersede the smaller NWS product and a full reprocessing from 1982-2017 covering the complete area will be available by October 2018

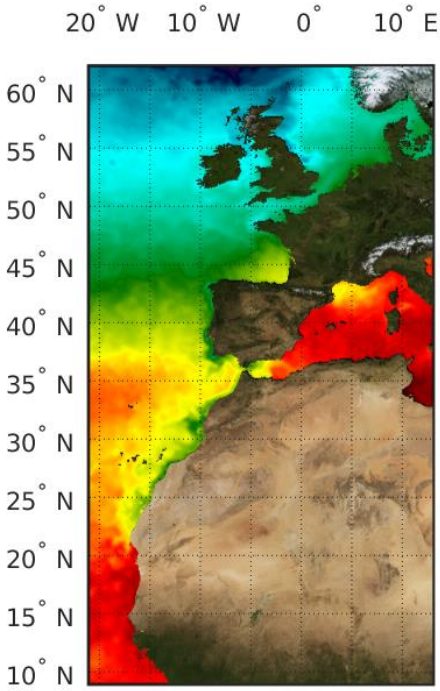

Figure 6: new regional L4 product over IBI area

1 felyx

felyx is an open-source system developed and maintained by Ifremer (http://hrdds.ifremer.fr) to extract data subsets and build multi-sensor match-up databases.

Usage

Felyx is used to produce daily match-ups from Sentinel-3A (and soon Sentinel-3B) SLSTR with in situ measurements from CMEMS In Situ TAC, in the context of OSI SAF project (http://www.ifremer.fr/cerweb/sentinel-3/mdb-slstr/). It is also operated similarly at Eumetsat to generate match-ups from Sentinel, Metop AVHRR and IASI SST products. It was a great asset in the context of Sentinel-3 SLSTR cal/val including for more specific usages for lake SST validation.

It is also demonstrated as a possible support to implement the GHRSST Climate Data Record Assessment Framework (CDAF), as show in the poster session (“A tool for the quantitative assessment of long time series of satellite SST “, JF Piolle et al.).

Soon it will be also used in the context of the In Situ Radiometer Network (ISFRN) to produce match-ups from in situ radiometers with Sentinel-3 and Metop.

Further developments

Further developments are ongoing to improve the performances and usability of felyx, including:

- integration with production system such as Apache Airflow for complex processing chains monitoring and scheduling
- integration with existing big data analytics (for dashboard reporting, analysis,…) such as Grafana or Kibana (available in Elasticsearch ecosystem) : this makes more and more easy the monitoring of match-up production (status, extent, data density,...) and eventually sensor performances(alerts, trends, etc…).
- management of in situ data directly into elastic search instead of external sqlite files, which allow to take also advantages of above analytics tools
- better error management in the system

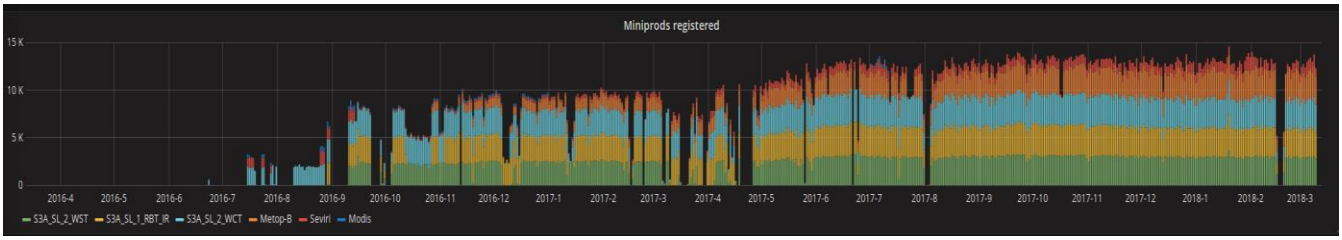

Figure 7: Investigation of match-up distributions with on-the-shelf analytics tools such as kibana or grafana

RDAC UPDATE: JMA

REPORT TO GHRSST XIX FROM JMA

Toshiyuki SAKURAI [(1)], Hiromu KOBAYASHI[(1)], Mika KIMURA[(1)], Yukio KURIHARA[(1*)], Akiko SHOJI[(1*)], Toshiyuki KITAJIMA[(2)] and Kouki MOURI[(3)]

(1) Global Environment and Marine Department, Japan Meteorological Agency, Tokyo (Japan),
(2) Observation Department, Japan Meteorological Agency, Tokyo (Japan),
(3) Meteorological Satellite Center, Japan Meteorological Agency, Tokyo (Japan)
** affiliation is valid until March 2018*
Email: tsakurai@met.kishou.go.jp

ABSTRACT

The Japan Meteorological Agency (JMA) produces and maintains two SST analysis products: (1) a daily global SST analysis with 0.25° grid resolution (MGDSST) and (2) a daily SST analysis with 0.1° grid resolution for the western North Pacific (HIMSST). JMA has operated a series of geostationary meteorological satellites (Himawari-8 and -9), and produces hourly HIMAWARI L3 SST with 0.02° grid resolution. This report describes an overview of these SST products and recent activities related to them.

1 Introduction

JMA has operated an SST analysis system to generate global daily SST data (Merged satellite and in-situ data Global Daily Sea Surface Temperature: MGDSST) on a routine basis since 2005. The system adopts an optimal interpolation (OI) method which considers not only spatial correlation but also temporal correlation. It produces 0.25° resolution, daily global SST analysis, using both satellite and in-situ SST observation. The satellite data currently ingested to MGDSST are: AVHRR SST (NOAA-18, NOAA-19 and MetOp-A), WindSat SST and AMSR2 SST. Prompt analysis of MGDSST is running within JMA'S NWP System in operational basis, and delayed analysis is conducted five-months later in principle. Since long term, consistent time series of the SST analysis is needed for climate research, JMA also conducted the reanalysis of MGDSST for the 1982 – 2006 period using AVHRR Pathfinder Version 5.0/5.1 SST and AMSR-E SST. MGDSST analysis contributes to the GHRSST Multi-Product Ensemble (GMPE) system (Martin et al, 2012) as one of input data.

JMA has developed a regional daily high resolution (0.1°) SST analysis for the western North Pacific region. This regional product was named HIMSST (HIgh resolution Merged satellite and in-situ data Sea Surface Temperature) and has been in operation since November 2016. Analysis framework is based on that of MGDSST. In addition to the satellite data used in MGDSST, the components of smaller spatial-temporal scale derived from Himawari-8 L3 SST are ingested to HIMSST.

JMA has operated a series of geostationary meteorological satellites (Himawari-8 and -9) that observe the East Asia and Western Pacific Region, contributing to the space-based global observation system.

JMA's Meteorological Satellite Center (MSC) has routinely produced Himawari-8 L3 SST since October 2015. The L3 SST is produced hourly with 0.02° horizontal grid resolution and the coverage of 60°S – 60°N, 80°E – 160°W. JMA adopts the same SST retrieval algorithm as used by

JAXA based on a quasi-physical algorithm (Kurihara et al. 2016). One of the main differences between JMA's and JAXA's product is the method of cloud masking. For cloud screening on Himawari-8 L3 SST, JMA uses the Fundamental Cloud Product for Himawari-8 (Imai and Yoshida, 2016) and JAXA adopts the Bayesian inference method (Kurihara et al. 2016).

2 Main activities since GHRSST XVIII

Himawari-9 SST

Himawari-9 was launched on 2 Nov. 2016 and was put into in-orbit standby as backup for Himawari-8 on 10 Mar. 2017. Several non-operational observations (e.g. health check) have been conducted. The comparison against buoy SSTs shows that Himwari-9 SSTs have a larger negative bias compared to Himawari-8 SSTs (Fig. 1).

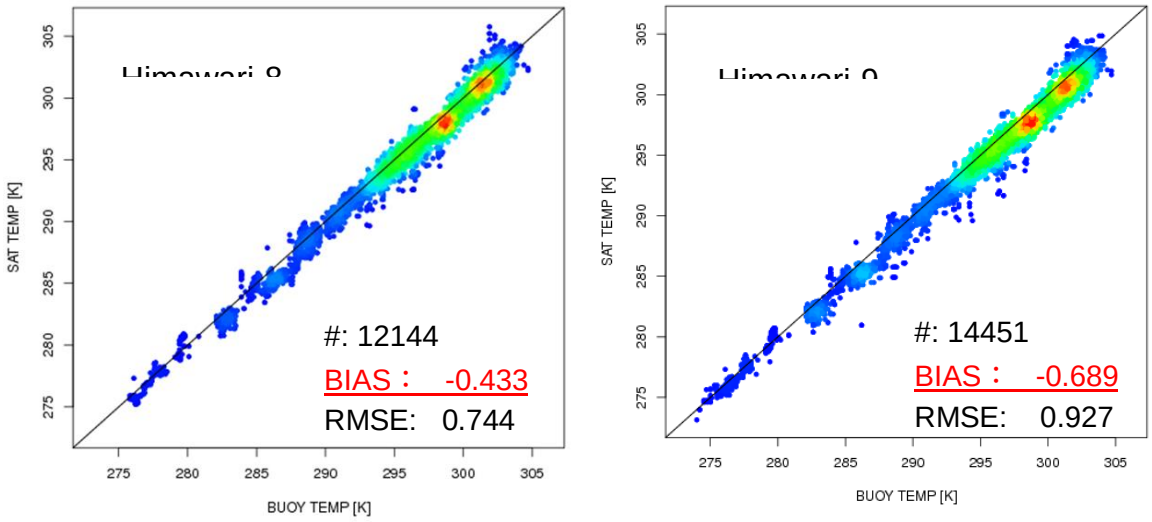

Figure 1: Comparison of Himawari-8 SSTs (left) and Himawari-9 SSTs (right) against buoy SSTs for the period from 2 to 16 Feb. 2018.

Some points to be improved in HIMSST and HIMAWARI-8 SST

Unnatural warm SSTs from Himawari-8 were sometimes seen in the Sea of Okhotsk and east of the Kuril Islands in summer night-time (Fig. 2). These are considered to be caused by relatively lower SST accuracy due to large satellite zenith angle in this area and cloud classification difficulties: (1) Temperatures at the top of lower clouds over this area are sometimes warmer than SSTs in summer. (2) Visible bands are not able to be used in the night-time.

In the HIMSST analysis, the abnormal Himawari-8 SST are removed by Quality Control (QC) using AMSR-2 SST for the area north of 42°N and east of 143°E. Along the boundary of the area where QC applied, an artificial SST front is occasionally found. We are exploring other QC methods which can be applied for the whole region.

In Himawari-8 SST, false clouds were often detected over inner bay area, such as the Seto Inland Sea in winter. In the top temperature tests of the cloud mask algorithm, estimated SST is

compared with MGDSST, which has a large positive bias over the Seto Inland Sea in winter. Not using MGDSST for cloud screening reduced false clouds detections over the Seto Inland Sea.

Although low SSTs in winter were ingested into HIMSST analysis, the positive bias of HIMSST over the Seto Inland Sea was not remarkably reduced. We considered that excluding the long-term and large scale (LL scale) component of Himawari-8 SST caused the positive bias. We have a plan to extend the area where MGDSSTs are not used in the cloud mask, and to introduce Himawari-8 SST for LL scale analysis.

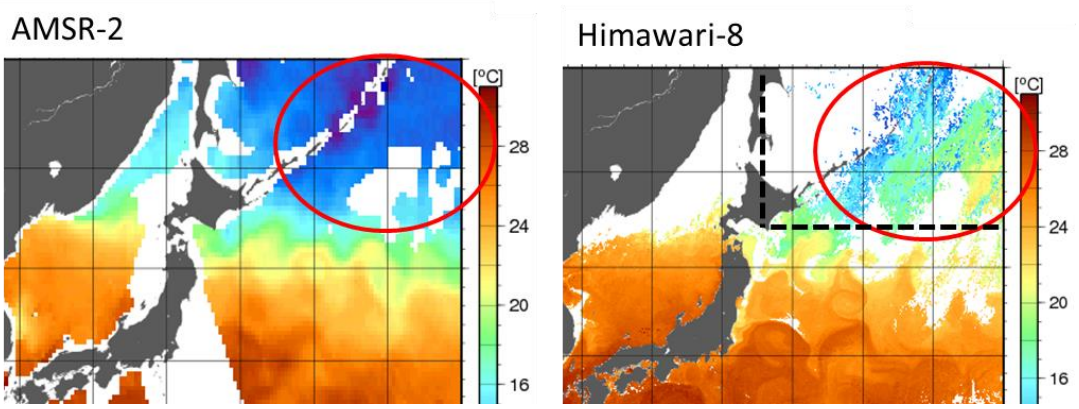

Figure 2: Daily-mean AMSR2 SST (left) and night-time composite of Himawari-8 SST (right) for 20 July 2017. Unnatural warm SSTs from Himawari-8 are seen in the red circle of the right figure. The black dotted line shows the border of the area north of 42°N and east of 143°E, where Quality Control by using AMSR2 SST are applied.

Impact test of VIIRS data for delayed MGDSST analysis

We investigated the impact of assimilating NOAA ACSPO VIIRS L3U SST (ver.2.40) for the delayed MGDSST analysis. The configuration of test run was the same as the control run (i.e. routine analysis), except that VIIRS SSTs are used in place of NOAA18/AVHRR data. The SSES bias was removed from the VIIRS L3U SSTs. Comparison against In-situ observation shows that RMSE for test run was reduced by 0.016 K in global area. The improvement was relatively large in the southern mid- and high- latitude. We will make an impact test for prompt analysis of MGDSST and HIMSST.

Future plan of a global 0.1 degree analysis

JMA has a plan to develop a 0.1° daily global SST analysis as a natural extension of HIMSST (regional high resolution SST analysis for the western North Pacific). Analysis method will be almost the same as HIMSST, however, SST data of additional geostationary satellites, such as GOES-16, GOES-17 and Meteosat are essential for the new analysis. Firstly, GOES-16/ABI SST data (NOAA/ACSPO v2.50) have been downloaded since Jan. 2018 from NOAA CoastWatch/OceanWatch Ftp site.

3 Data availability

MGDSST are available from January 1982 via NEAR-GOOS Regional Real Time Database (RRTDB) as text format. HIMSST data were opened in the NEAR-GOOS RRTDB on March 2017, and are available from February 2017 as text format. We are preparing the GDS 2.0 implementation of MGDSST to facilitate the use of JMA's SST products in GHRSST activities.

4 References

Imai T and Yoshida R., Algorithm theoretical basis for Himawari-8 Cloud Mask Product, Meteorological Satellite Center Technical Note, 61,1-7, 2016.

Kurihara Y, Murakami H and Kachi M., Sea surface temperature from the new Japanese geostationary meteorological Himawari-8 satellite, Geophysical Research Letters, 43(3), 1234-40, 2016.

Martin, M., P. Dash, A. Ignatov, V. Banzon, H. Beggs, B. Brasnett, JF Cayula, J. Cummings, C. Donlon, C. Gentemann, R. Grumbine, S. Ishizaki, E. Maturi, R. Reynolds and J. Roberts-Jones, Group for High Resolution Sea Surface temperature (GHRSST) analysis fields inter-comparisons. Part 1: A GHRSST multi-product ensemble (GMPE), Deep Sea Research Part II: Topical Studies in Oceanography, 77–80, 21–30, doi:10.1016/j.dsr2.2012.04.013. 2012.

SESSION II REPORT (PART 2)

Chair: Prasanjit Dash[(1)] – Rapporteur: Charlie Barron[(2)]

(1) NOAA NESDIS STAR, USA, Email: prasanjit.dash@noaa.gov
(2) U.S. Naval Research Laboratory, USA Email: charlie.barron@nrlssc.navy.mil

ABSTRACT

The session featured ten presentations by nine speakers offering a review of activities since GHRSST XVIII from nine organizations and one US national project.

Summary of Speakers and Organizations

1. RDAC update from NASA (10min) – Ed Armstrong
2. RDAC update from NAVOCEANO (10min) – Bruce McKenzie
3. RDAC update from NOAA/NESDIS/STAR 1 (10min) – Sasha Ignatov
4. RDAC update from NOAA/NESDIS/STAR 2 (10min) – Eileen Maturi
5. RDAC update from NOAA/NCEI (10min) – Xuepeng Zhao
6. RDAC update from RSS (10min) – Chelle Gentemann
7. Report from CMA (10min) – Sujuan Wang
8. Report from ESA (10min) – Craig Donlon
9. Report from MISST (10min) – Chelle Gentemann
10. Report from ECMWF (20min) – Hao Zuo

Summary of presentations

The highlights for each talk and floor discussion are given below.

1 RDAC update from NASA – *Ed Armstrong*

Components of the NASA RDAC include the JPL RDAC (L2P Aqua/Terra and L2P VIIRS; G1SST blended global L4 SST; L4 MUR) and JPL_OUROCEAN (L4 COVERAGE product). Following an overview of the L2 Aqua/Terra and VIIRS data streams, Ed noted that the G1SST might be the only data still provided to GHRSST in the GDS1 format. Bruce McKenzie later commented that he believes the NAVO K10 product is provided only in the GDS1 format as well.

Since a non-trivial effort is required to appropriately map the present output and processing update the format, would members of the GHRSST community interested in this product prefer that it be upgraded to the latest GDS format? The NASA RDAC has also been upgrading the MUR L4 product and is working on upgrades to ECCO-2 2km global L4 SST. Is there interest from the GHRSST community in simulated L2 SST samples from the ECCO-2 product? The NASA RDAC has also been contributing to a “COVERAGE” effort that utilizes data from all four of the virtual constellation components to make a L4 product mapping these 4 fields onto a common ~25km (1/4°) globally gridded product. What is the interest in this product? An overview of recent NASA physical oceanography initiatives reveals proposals to special topics including MISST-high latitude SST.

Discussion:

Andy Harris and Chris Merchant report that there would be interest in simulated high-resolution SST sampled from ECCO-2 (simulating observing system output). Some discussion on whether/how these would be used.

Helen Beggs: Do the composite fields in the COVERAGE product have companion gridded metadata indicating the source of the data as a function of grid cell and are these more properly presented as an L3 product?

Chelle Gentemann (following on the question from Helen): Said that this gridded metadata indicating sensor source would be useful for assessing the credibility of the COVERAGE fields. Chelle would expect the COVERAGE product to be popular with many downstream users of the remote sensing data who want a low resolution indication of basic ocean properties. Such users also gravitated toward coarse SST products from RSS because they were not interested in considering the impact of the finer-scale SST variations and they found the small file sizes convenient.

Action items/questions to GHRSST:

a. Upgrade of G1SST to latest GDS format. Send positive response to Ed Armstrong: Would members of the GHRSST community interested in G1SST prefer that it be upgraded to the latest GDS format?
b. Simulated L2 samples from L4 ECCO-2 SST. Is there interest from the GHRSST community in simulated L2 SST samples from the ECCO-2 product?
c. 25km COVERAGE product. What is the community interest in a global product providing data from each of the fields provided by the virtual constellation? Discuss with Jorge Vazquez at his poster.

2 RDAC update from NAVOCEANO – *Bruce McKenzie*

Bruce notes that he is at the moment replacing Keith Willis as the Navy representative to the GHRSST science team, as Keith has moved on to a new position at NAVOCEANO with different responsibilities. The products shown in the NAVOCEANO presentation are developed and tested by the U.S. Naval Research Laboratory (Charlie Barron/Jean Francois Cayula) before transition to operations at NAVOCEANO. NAVOCEANO provides several L2 and L4 products to GHRSST including one in GDS1 format, the K10 composite SST. Should the K10 SST be upgraded to latest GDS format or should it be superseded by other composite or gridded L4 products?

NAVO has updated processing for L2P NPP VIIRS SST and has discontinued NOAA-18 processing (~24 May). NAVO daily provides its L2 and L4 data to JPL for distribution, and it acquires GHRSST data from the PODAAC and L2P SLSTR SST from NOAA STAR. AMSR2 data is presently downloaded 2x per day with 12-34 hour latency, and NAVO is evaluating a path for future work acquiring/producing AMSR-2 fields or products.

Discussion:

Helen Beggs: The Australian Bureau of Meteorology had been using the NOAA-18 feed and was surprised when the NOAA-18 feed stopped. Bruce said that NAVO did send notices but perhaps the distribution of notice was insufficient. NOAA-18 has degraded to a level that it will no longer be processed by NAVO to make SST retrievals. Gary Corlett said that in the future such notices could be sent to the GHRSST program office for redistribution.

Helen Beggs: Is NAVO intending to make GAC versions of its L2 products? Bruce: no.

Gary Corlett and Chelle Gentemann: Questions on how NAVO plans to move forward with AMSR2 now and in the future. Bruce: NAVO/NRL are evaluating options, and some of the discussions can continue after the session.

Action items/questions to GHRSST:

a. Send GHRSST program office future notification of changes to products to facilitate wider redistribution of notification.
b. Future plans for developing/maintaining software to derive SST from AMSR2

3 RDAC update from NOAA/NESDIS/STAR 1 – *Sasha Ignatov*

An update on the ACSPO system included pointers to associated oral or poster presentations later in the week. NOAA has two new constellations of sensors, one polar and one geostationary. The design characteristics of sensors in these new constellations are superior to the prior versions they have replaced. A second VIIRS was launched in Nov. 2017 under the auspices of JPSS; it has been redesignated as NOAA-20. In its initial stages after launch, NOAA-20 VIIRS had some biases relative to SNPP VIIRS, but by March 2018 these have been resolved and the two VIIRS instruments are showing similar performance. NOAA-20 SST will be released in the near future.

GOES-R ABI and Himawari-8/9 AHI have superior SST sensors relative to prior generation sensor versions on geostationary platforms. GOES-16 has moved into the role as the operational GOES-EAST platform. GOES-17 remains in an initial intermediate placement and will move to GOES-WEST if its cooling problems are resolved and sensor noise is reduced to acceptable levels. GOES-16 is working well, as expected with the latest solution algorithm. Plans are in development to reprocess the full ABI record with consistent software. Lists of ACSPO products and users are accompanied by a discussion on future plans for N20 VIIRS, G17 ABI, and reanalyses.

Discussion:

No time for further questions/discussion

Action items/questions to GHRSST:

None

4 RDAC update from NOAA/NESDIS/STAR 2 – *Eileen Maturi*

Reports on reprocessing work on data from earlier versions SST sensors from 1995-2002, with plans to make geo-polar blended SST analyses in various versions such as day, night, and diurnally-corrected day/night. These reanalyses would include data from Meteosat 8, Meteosat 11, and GOES-15. Prabhat has developed physical retrieval methodology and updated software for cloud masks and diurnal models. Low biases are expected from the physical retrievals. The impact of new retrieval methods is evident in MSG 8 coverage. Future work is planned on blended SSTs and physical SST retrievals.

Discussion:

Peter Cornillion: What is the space/time resolution of the L3 global SST.

Andy Harris: 1 day composite coverage sampling super-obbed to a 5-km gridded composite.

Peter Cornillion: I would like hourly high-resolution L4 composite SST.

Action items/questions to GHRSST:

None

5 RDAC update from NOAA/NCEI – *Xuepeng Zhao*

In this presentation, the NOAA NCEI SST portfolio is presented. ICOADS is the most extensive marine and meteorological data set and provides stewardship of climate-quality data. Its GHRSST products are authoritative reconstructed monthly SST products. Efforts are underway to include uncertainty fields. The 1/4° daily optimal interpolation SST adds improvements to the Arctic and focuses on climate scales. There are specifics on updates to the Pathfinder SST climate data record based on the AVHRR time series. Future plans include producing V6 SST anomaly products based on PFv5.3, to be extended to cover 1981-present and to included SSES-Bias and SSES-STDDEV variables.

Discussion:

Helen Beggs: Is glad that the error characteristics are being included with the reanalyses and would like to know how to get the product.

Xuepeng Zhao: Products are currently available from NCEI.

Chris Merchant: As the plan in the past has been to include only AVHRR, what are plans to extend pathfinder into the post-AVHRR era?

Xuepeng Zhao: We are evaluating options for the post-AVHRR error but at present no decisions.

Action items/questions to GHRSST:

a. Plans to extend into the post-AVHRR era.

6 RDAC update from RSS – *Chelle Gentemann*

The primary RSS contributions to GHRSST are the L2P and L3U microwave SST products. When RSS updates processing of microwave retrievals for a particular product, the entire time series of that product is reprocessed to enable delivery of a consistent reanalysis over the lifetime of the data set. The most recent update to L3U has been delivered to the PODAAC. However, the L2P product has been undergoing validation of almost a year. The evaluation should be complete in the next couple of months. The main RSS activities since GHRSST XVIII center on upgrades to the RSS V8 calibration standards. The absolute radiation calibration is based on OMI; further details of this calibration are not available at this time. RSS has also delivered a new microwave AO + I. In prior versions of the L2 product, not all fields were L2p compliant.

Discussion:

Question on versioning: There is little documentation of differences between different versions.

Chelle Gentemann: I agree. This should be resolved.

Sasha Ignatov: Since the data are quite small at 25 km grid spacing, data sizes are small, less than 100 GB for the whole data set. So why was work on L3U prioritized over L2P?

Chelle Gentemann: Right now RSS is missing personnel with technical capability and expertise to run L3P. RSS made an internal decision that users would likely care more about L3u. Chelle thinks that historically, users are likely to care more about L2p.

Action items/questions to GHRSST:

a. Complete version L2P validation
b. Better documentation on characteristics of different versions.

7 Report from CMA – *Sujuan Wang*

CMA provided an overview of the status of their constellation. The geostationary satellite SST FY3D was launched 11 Dec 2016 and is in the post-launch test phase. The retrieval algorithms and quality control have been updated with validation relative to OSTIA and OISST products. Example products and matchups are shown for day and nighttime products. Bias has high correlation with the block body temperature. Other FY3C work has focused on reprocessing based on new monthly coefficients. Comparisons to OISST and IQUAM shows standard deviation of

about 0.6° K. CMA is working to convert output to GHRSST formats. Future work will focus on data quality and move to comply with GHRSST formats.

Discussion:

none

Action items/questions to GHRSST:

none

8 Report from ESA – *Craig Donlon*

Discussion of ESA developments begins with the Sentinel-3B launch. The launch put S3B in a tandem flight on the same ground track with S3A and separated by 30 seconds in equatorial crossing time. Current testing of instruments indicates that SLSTR aboard S3B is working as expected.

Sentinel 3C, 3D are in production with only a few small changes from the baseline version. Follow-on contracts cover calibration and launch are being put in place, with launch date to be determined based the expected operational lifetime of S3A, S3B. Planning on next-generation spacecraft is beginning. At this time there is a movement (not endorsed by Craig) to put the SSH and optical packages on separate, individual satellite platforms. Sun-synchronous orbit must be guaranteed in the topographic (altimeter) component. With combined or divided missions must be adjusted to determine how to best meet requirements. Matchup land, ice, and sea surface temperature data are being reserved for confirmation matchups with reports in preparation, There is also more SLSTR validation with shipboard radiometers (Fred Wimmer presentation Wednesday). The ESA S3-View service is being prototyped including the ESA ocean virtual laboratory. Preparations are also underway for GHRSST XX and a future 30-50m resolution land temperature mission.

Discussion:

none

Action items/questions to GHRSST:

a. Preparation for GHRSST XX

9 Report from MISST – *Chelle Gentemann*

The MISST project for Arctic SST is a $5M NOPP project extending over 2018-2023 to do new science in the Arctic. Working with a new data model, MISST-related products will comply with updates to GHRSST formats. SST algorithm development will acknowledge the challenges posed by very sparse in situ matchup data availability north of 60°N. SST retrieval algorithms are not validated in increasingly ice free areas of the Arctic. MISST for the Arctic will gather Arctic data from various sources and incorporate these sets into the ICOADS data set available for the

community to use in development of retrieval algorithms. This will be supplemented by 5 Arctic cruises of a Saildrone with temperature observations distributed across the air-sea interface via sensors distributed from the drone sail to the drone keel. SST algorithms will be reformatted for IR and passive MW. Evidence was shown to reveal that dynamic variability of Arctic SST follows patterns and ranges similar to variability in lower latitudes. Other Arctic challenges include the representativeness of a foundation SST given extreme seasonal variations in solar insolation.

MISST will have an open data policy and encourage development of open source retrieval and other software. For example, this would include open source software converter for in situ data to ICOADS format.

Discussion:

Irina Gladkova: Regarding Ice extent and Ice mask, how will this effort deal with sea surface retrievals across the transition from ocean to ice?

Chelle Gentemann: The state of the art ice mask is patchy. Some users will likely combine indicators of ice from analyzing the retrievals with ice mask. These need to be considered for QC of Arctic data.

Action items/questions to GHRSST:

a. Open source software for passive microwave SST
b. Incorporating ice indicators and ice mask in SST retrieval processing and QC.

10 Report from ECMWF – *Hao Zuo*

This presentation covered the increasing role of SST observations in assimilative forecasts at ECMWF. The ensemble prediction system (EPS) uses a coupled model with a partial coupling scheme that has unsatisfactory performance in its traditional use with a rather coarse SST background; its performance is improved when provided with the level 4 OSTIA SST that more accurately represents structures of the temperature field. SST is incorporated in this approach via full gridded L4 fields rather than direct assimilation of the irregularly distributed L1 or L2 products. Global mean SST bias shows large differences when the EPS is run with and without nudging to the SST analysis. Similarly, the AMOC transport varies when incorporating different SST fields. The calibration and skill assessments use forecasts initialized from SST reanalyses. The impact of in situ SST observations in forecasts was revealed in a case when they captured cooling under the clouds of Hurricane Irma, enabling a more accurate representation of the air-sea conditions that in the case using a background SST limited to using IR satellite observations that were unable to view the cooling temperatures through the clouds.

Advancements in development of a weakly coupled atmosphere-ocean data assimilation will provide boundary conditions for the HRES atmospheric forecasts, with HRES in turn providing boundary conditions for the ocean. The impact of SST in coupled forecasts shows an impact of the ocean-atmosphere feedback on ocean temperature and salinity, More timely SST under tropical cyclones should have significant positive impact in reducing the present delay in ocean cooling under TC conditions. ECMWF is working toward assimilation of L2 SST. A January SST/ice

workshop developed a vision for more effective use of SST in the future, recommending movement toward coupled data assimilation with assimilation of radiances running with fully coupled systems. Considerations were offered on making better use of L4 products with recommendations for transition to L3 or L2.

Discussion:

Charlie Barron: The presentation showed results coupling a relatively fine scale atmosphere with a coarser, 25 km ocean; coupling results were favorable in the low latitudes and mixed or unfavorable outside the tropics. What would happen if the ocean model were run at resolutions better able to represent the western boundary currents and eddies important at higher latitudes?

Hao Zuo: Higher resolution in coupling will solve part of the problem, but there are also systematic errors that will not be resolved by increased resolution alone

Andy Harris: On slide 15, the field labeled AVHRR looks to have a narrow swath that is more similar to SLSTR. Perhaps these are mislabeled.

Hao Zuo: I received this slide from a colleague and at the moment I am unable to affirm the data source for that particular plot.

Peter Cornillion: What are the space time scales of the model components and what would happen if you were assimilating L2 or L3 data rather than the L4 fields?

Hao Zuo: We used a 9 km atmosphere and 25 km ocean, so assimilating SST at about a quarter-degree. If we used L2 or L3 SST data, we would have been forced to super-ob the data.

Chris Merchant: What is the source of differences on slide 6? There seems to be a gap in performance that decreases after 2002.

Hao Zuo: This may be due to operational changes in the source data or other aspects of the system.

Peter Cornillion: For a L4 SST provided to your system, what impact would a 0.75°C bias over a 150 km x 150 km area have?

Hao Zuo: I would speculate that if such a bias were persistent it would have a significant impact on a seasonal forecast. If it were a transient bias, I would speculate that it would have a larger impact if it were in frontal or western boundary current regions and perhaps a smaller impact if in other, less dynamic regions.

James While: In our operational system at the Met Office, such a bias would be unlikely to actually get through to influence the forecast because it would be detected and corrected by an online bias correction. This bias correction to the input data would prevent the scenario Peter was suggesting.

Xu Li: Regarding some of the issues you raised regarding the timeliness of L4 data, I would suggest that assimilating the L1 data directly as radiances would enable the observations to be introduced to the forecasts in a much more timely manner.

Hao Zuo: At the present time, we are not able to assimilate L data.

Chris Merchant: If you were to attempt to assimilate L1 data directly, it would be a lot of work to derive the appropriate treatment of the data to enable appropriate representation of the SST. In effect, the system directly assimilating the SST system would have to attempt to capture the collective expertise represented in this room to derive an appropriate representation of the SST.

Hao Zuo: We seek collaborations to leverage or build on capabilities previously developed. We do not intend to attempt reinventing such capabilities from scratch.

Chris Merchant: What do you need now?

Hao Zuo: SST with higher time/space resolution and characterization of errors.

Action items/questions to GHRSST:

a. More timely SST observations in the assimilation system reduce forecast errors.
b. Uncertainty information associated with the L4 or L2/L3 data would be useful for data assimilation and quality control.
c. SST with higher time/space resolution.

RDAC UPDATE: NASA

Edward Armstrong[(1)], Jorge Vazquez[(1)], Wen-Hao Li[(2)], Toshio Chin[(1)], Zhijin Li[(1)]

Jet Propulsion Laboratory, California Institute of Technology, Pasadena, CA, USA
Raytheon, 300 N Lake Ave, Pasadena, CA 91101
Email: edward.m.armstrong@jpl.nasa.gov

ABSTRACT

The NASA JPL and JPL_OUROCEAN RDACs continued their scientific contributions to GHRSST community for providing valuable GHRSST Level-2 and Level-4 products, of which the MUR and Terra MODIS L2P have been listed at the top 10 most active GHRSST data in 2018 (See GDAC Report in these proceedings). The JPL RDAC has continually produced the MODIS Aqua/Terra L2P, VIIRS L2P and MUR L4 datasets, while JPL_OUROCEAN RDAC has produced and supported the G1SST L4 dataset. The report will also discuss NASA contributions to the COVERAGE project and the US GHRSST community in general.

1 Introduction

The summary accomplishments and milestones performed by the two RDACs are noted below:

- GHRSST datasets provided by JPL RDAC
    1. MODIS Aqua and Terra L2P, version 2014.0.
        - Data landing page: https://podaac.jpl.nasa.gov/dataset/MODIS_T-JPL-L2P-v2014.0
        - The data have been used as input layer in State of The Ocean (SOTO) visualization tool.
    2. VIIRS L2P, version 2016.
        - Data landing page: https://podaac.jpl.nasa.gov/dataset/VIIRS_NPP-JPL-L2P-v2016.0
        - Fully completed the 2012-2018 time series by March 2018.
    3. MUR L4 version 4.1.
        - Data landing page: https://podaac.jpl.nasa.gov/dataset/MUR-JPL-L4-GLOB-v4.1.
        - The data have been used as input layer in State of The Ocean (SOTO) visualization tool.
        - Experimental field "dt_1km_data" was introduced in mid-2016 to indicate temporal proximity to MODIS L2P samples at each grid. Enables MUR L4 to be use as a L3C
        - Smoothness optimization (given the L2P sampling patterns and timing) using simulated SST dynamics (from 2km global ECCO2 runs)
        - 25-km grid MUR product create as a by-product of the full MUR production line for COVERAGE project

- GHRSST datasets provided by JPL_OUROCEAN RDAC
    1. G1SST Level 4.
        * The G1SST 2DVAR blending algorithm has been revised for blending L2 VIIRS SSTs, with emphasis on keeping small-scale features resolved by VIIRS.

2 COVERAGE (CEOS Ocean Variables Enabling Research and Applications for GEO)

COVERAGE is a collaborative effort within CEOS and 3-year NASA project involving the 4 Ocean VCs (SST, OST, OCR, OSVW) and GEO projects (MBON, Blue Planet) to enable more widespread use of ocean satellite data in support of applications. An initial phase focused on creating common 25 km global gridded products of 4 Ocean VCs. COVERAGE will serve as a platform for improved and integrated ocean data access utilizing emerging data management and cloud capabilities.

3 NASA Physical Oceanography Program

The following are the recent awarded SST initiatives and proposals:

- National Ocean Partnership Program (NOPP)
    - MISST: Continuing the GHRSST Partnership and Arctic Data (Chelle Gentemann, Earth Space Research)
- ROSES Physical Oceanography 2017
    - Physical Deterministic SST from MODIS and VIIRS Radiances (Prabhat Koner, Univ. of Maryland)
    - Merging Optimal Estimation and Multi-Channel Atmospheric Corrections for Accurate SSTs from MODIS and VIIRS (Peter Minnett, Univ. of Miami)
    - Improved Air-Sea Essential Climate Variables from Aqua AMSR-E and VIIRS (Frank Wentz, Remote Sensing System)

The NASA Physical Oceanography Program also supported the editorial responsibilities and logistics for the online *Remote Sensing Journal: Topical Collection "Sea Surface Temperature Retrievals from Remote Sensing"* with 16 papers published so far and Jorge Vazquez, JPL serving as Guest Editor. See http://www.mdpi.com/journal/remotesensing/special_issues/SST_RS

Acknowledgements

This work was carried out at the NASA Jet Propulsion Laboratory, California Institute of Technology. Government sponsorship acknowledged. Copyright 2018 California Institute of Technology. Government sponsorship acknowledged.

RDAC UPDATE: NAVO (NAVAL OCEANOGRAPHIC OFFICE REGIONAL DATA ASSEMBLY CENTER)

Bruce McKenzie[(1)], Dan Olszewski [(2)], Valinda Kirkland [(3)], Michelle Little [(4)], Doug May [(5)], Dr. Charlie Barron [(6)], Dr. Jean-François Cayula [(7)]

Naval Oceanographic Office, John C. Stennis Space Center, Mississippi, USA,
(1) Email: bruce.mckenzie@navy.mil;(2) Email: daniel.olszewski@navy.mil;
(3) Email: valinda.kirkland@navy.mil;(4) Email: michelle.c.little1@navy.mil;
(5) Email: doug.may@navy.mil;
(6) Naval Research Laboratory Detachment at John C. Stennis Space Center, Mississippi, USA
Email: charlie.barron@nrlssc.navy.mil;
(7) Perspecta Inc., John C. Stennis Space Center, Mississippi, USA
Email: jean-francois.cayula@perspecta.com

1 Introduction

The Naval Oceanographic Office (NAVOCEANO) is a regional data assembly center (RDAC) in the Group for High Resolution Sea Surface Temperature (GHRSST). Several sea surface temperature (SST) products are generated in GHRSST data processing specification (GDS) format and sent to the Jet Propulsion Laboratory (JPL) at the California Institute of Technology. JPL distributes the GHRSST data on its Physical Oceanography Distributed Active Archive Center (PODAAC--https://podaac.jpl.nasa.gov/) to national and international customers. Improvements have been implemented to the SST retrievals that NAVOCEANO generates from Suomi National Polar-orbiting Program (S-NPP) Visible Infrared Imaging Radiometer Suite (VIIRS) sensor data. NAVOCEANO has also discontinued processing SSTs from the National Oceanic and Atmospheric Administration (NOAA) 18 Global Area Coverage (GAC) Advanced Very High Resolution Radiometer (AVHRR) data due to the age of the satellite and the quality of the retrieved SSTs. NAVOCEANO also acquires Meteosat Second Generation (MSG) GHRSST data from JPL for assimilation in the Navy meteorology and oceanography (METOC) analysis.

2 GHRSST Products

The NAVOCEANO RDAC GHRSST products generated operationally and distributed by the JPL PODAAC are listed in Table 1. The L4 product is a gridded analysis at 10 km that will be updated to GDSV2.0 by the end of CY2018.

Table 1: GHRSST Datasets provided by NAVOCEANO RDAC

Level	Satellite/Sensor	Resolution	GDS Version
L2P	NOAA-19 AVHRR GAC	8.8 km	2.0 rev5
L2P	NOAA-19 AVHRR LAC	2.2 km	2.0 rev5
L2P	S-NPP VIIRS	750 m	2.0 rev5
L2P	MetOp-A AVHRR GAC	8.8 km	2.0 rev5
L2P	MetOp-B AVHRR GAC	8.8 km	2.0 rev5
L4	Various	10 km	1.0

NAVOCEANO acquires the GHRSST products listed in Table 2 for ingest by the Navy Coupled Ocean Data Assimilation (NCODA) system that is used as input to the Navy METOC analyses/forecasts.

Table 2: GHRSST Datasets acquired by NAVOCEANO

Level	Satellite/Sensor	Resolution	Data Producer
L2P	Sentinel-3A/SLSTR	1 km at nadir	EUMETSAT
L3C	MSG-1/SEVIRI	0.05 degree	O&SI SAF
L3C	MSG-4/SEVIRI	0.05 degree	O&SI SAF

The MSG L3C data are retrieved from the JPL PODAAC, and the Sentinel-3A L2P data are from NOAA, who receives the Sentinel-3 data via a terrestrial EUMETCAST feed.

3 Main Activities

An update to the VIIRS L2P SST processing (version 3.0) was provided by the Naval Research Laboratory Stennis Space Center (NRL-SSC) and was implemented into operations at NAVOCEANO earlier this year. The two main enhancements were:

1. Contaminant/cloud detection effective resolution is 750 m at nadir instead of 1.5 km in the previous versions.
2. Adherence to standards: Updated compliance is with GHRSST Data Specification (GDS) version 2.0 revision 5, Attribute Convention for Data Discovery (ACDD) version 1.1, and netCDF Climate and Forecast Metadata Conventions (CF) version 1.6.

The contaminant/cloud detection process has been extensively overhauled with the goal of better retaining oceanographic features such as frontal regions and up-welling or diurnal warming events.

- A test on the correlation between thermal and reflective fields replaces the uniformity tests on reflectance and radiance. Unlike the correlation test, the radiance uniformity test removes fronts while the reflectance uniformity by itself can be unreliable.
- Proximity to cloud analysis and clear contiguous regions (segmentation) analysis are added at the end of processing.

After all contaminant/cloud detection steps are completed, to reduce the inherent noise of the SST field, SST values are recomputed.

The other main activity was that NAVOCEANO discontinued processing of the NOAA-18 AVHRR GAC L2P SST. The NOAA-18 satellite was launched in 2005 and the bias and root mean square difference (RMSD) relative to drifting buoys was getting worse, as shown in Figure 1. There were also periods during which minimal nighttime SST retrievals were being generated.

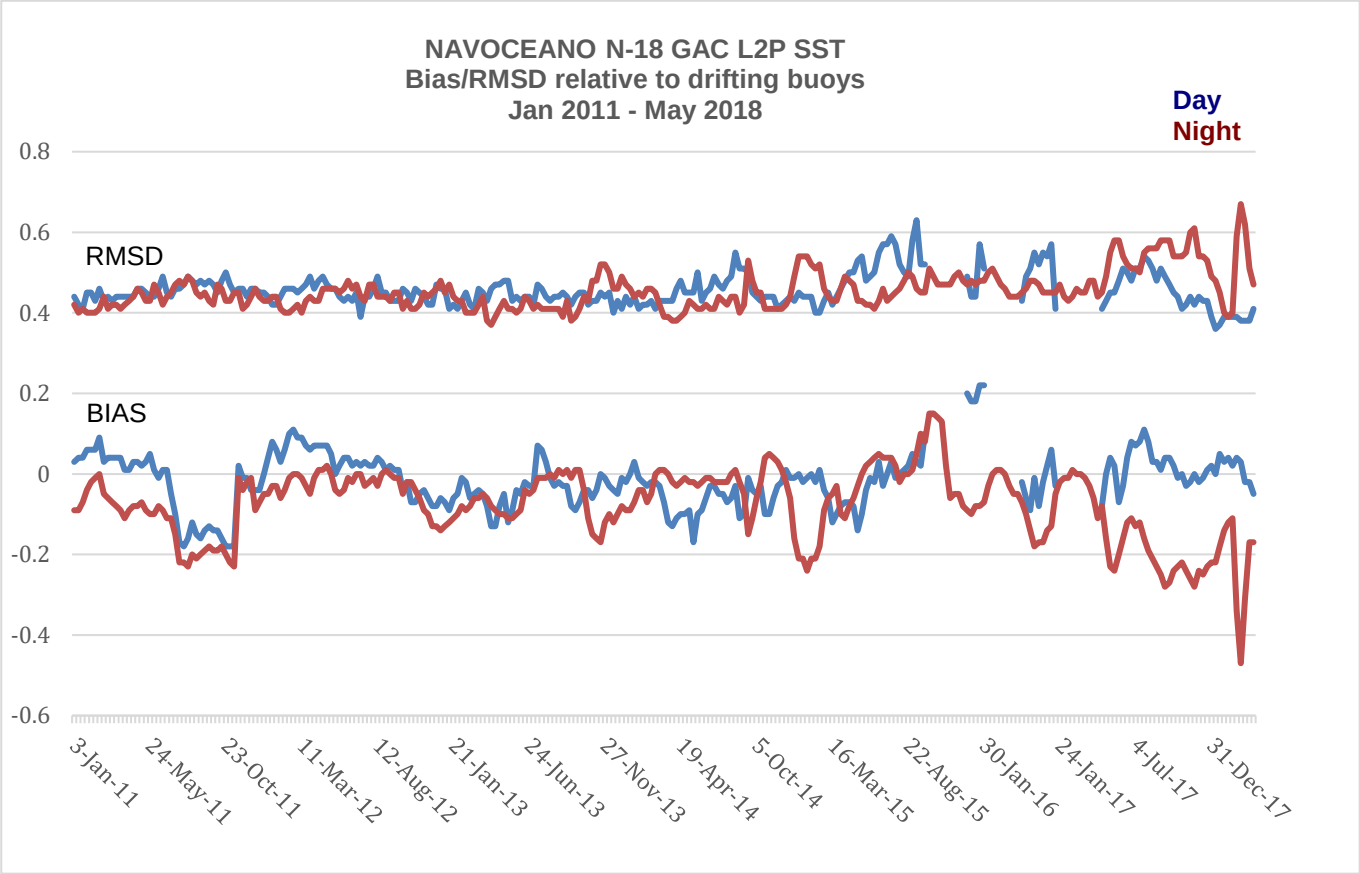

Figure 1: NOAA-18 GAC AVHRR SST Bias/RMSD (Jan 2011 – May 2018)

4 Issues

NAVOCEANO is processing GCOM-W1 (Global Change Observation Mission – Water "Shizuku") AMSR2 (Advanced Microwave Scanning Radiometer 2) data using software provided by Remote Sensing Systems (RSS). This code requires routine calibration updates that NAVOCEANO doesn't have the expertise to provide. There is also AMSR2 SST data on the JPL PODAAC provided by RSS, but it has a high latency, making it unusable as an operational input to NCODA. NAVOCEANO will explore other means to acquire or process AMSR2 SSTs.

5 Conclusion

NAVOCEANO continues to be a contributor and consumer of GHRSST products. Incorporating GHRSST products into operations at NAVOCEANO is done with minimal effort due to the consistent GDS format and the reliability of the data feeds from the operational data providers.

This brief is provided for information only and does not constitute a commitment on behalf of the U.S. Government to provided additional information on the program and/or sale of the equipment or system.

REPORT FROM CMA

Sujuan Wang[(1)], Peng Cui[(2)] , Miao Zhang[(3)] ,

Peng Zhang[(4)] , Caiying Wei[(5)] , Feng Lu[(6)] , Jian Lui[(7)]

National Satellite Meteorological Center, CMA ,Beijing, China,
(1) Email: wangsj@cma.gov.cn, (2) Email: cuipeng@cma.gov.cn, (3) Email: zhangmiao@cma.gov.cn
(4) Email: zhangp@cma.gov.cn, (5) Email: weicy@cma.gov.cn, (6) Email: lufeng@cma.gov.cn, (7) Email: liujian@cma.gov.cn

Abstract

The current status of CMA Fengyun Constellation is introduced. CMA operates GEO and LEO Fengyun satellites. The even number series GEO, and odd number series LEO.

FY4A was launched on 11 Dec. 2016.It has been put into operation since 1 May 2018. NLSST is chosen for the operational SST algorithm. As for validation, We compared SST against L4 CMC SST by a bilinear interpolation approach, and validated SST against in situ with matchup window of within 4KM and 30 minutes,both Buoy and IMOS are compared. The STD is about 0.86K.

FY3D was launched on 15 Nov. 2017, the Post Launch Test phase will be finished by July 2018, it's shown that the 3.8μm band of FY3D MERSI-2 is better than the counterpart of FY3 VIRR.

We also do regional regression and retrieval on FY3C/VIRR. It's shown that solar contamination to mid-infrared band of VIRR is still exit at low latitude in summer. Reprocessing of FY3C/VIRR SST is underway.

CMA would like to increase collaboration with GHRSST Advisory Council in working towards GHRSST specifications.

PLENARY SESSION III: ANALYSIS OF SST

SESSION III REPORT

Chair: Dorina Surcel Colan[(1)] – Rapporteur: Simon Good[(2)]

(1) CMCEP/ECCC, Canada, Email: dorina.surcel-colan@canada.ca
(2) Met Office, UK, Email: simon.good@metoffice.gov.uk

1 Introduction

The plenary session on "Analysis of SST" was held on June 5th 2018 in the morning. The session included three presentations by Xu Li, Helen Beggs and James While, followed by questions and an open floor discussion. This report contains the main points arising from each presentation and the open floor discussion.

2 Sea Surface Temperature Analysis within the NCEP GFS – Xu Li

Summary of presentation:

- A real-time, 6-hourly analysis generated at 50km grid resolution is used as a boundary condition to NWP.
- There are issues with merging indirect observations from different platforms – in some cases there are radiances, in others temperature, there are different observing depths and everything has to be converted to an SST for NWP.
- Analysing SST within the NCEP GFS solves these issues.
- To implement the system, a forward model to simulate radiances is needed, as well as a diurnal cycle model to produce the near-surface sea temperature (NSST) and the Jacobian of the forward model.
- The near-surface temperature is modelled with a foundation SST and warm layer and cool skin models.
- Background error correlation lengths were taken from the RTG analysis system.
- Different satellite and in situ observations have prescribed different SST depths and observation uncertainties.
- Verification is done against observations or against other SST analyses (OSTIA, RTG and NCDC).
- The NCEP analysis is closest to OSTIA than the other analyses.
- OSTIA and NCEP are closest to a time series of a moored buoy.
- Verification suggests NCEP is superior to other analyses.
- Points arising from the questions:
- There is a possibility that it can be disseminated as a GHRSST product in the future.
- The system currently assimilates data from Argo floats.
    - Suggestion to exclude these data, so that they can be used for independent validation.

3 A new Ensemble Optimal Interpolation SST Analysis System at the Bureau of Meteorology – Helen Beggs

Summary of presentation:

- Existing GAMSSA and RAMSSA systems are based on legacy FORTRAN and are difficult to maintain. It is not possible to keep up with the new observation types that are available.
- A new system has therefore been developed using an ensemble Kalman filter framework and an ensemble Optimal Interpolation approach (GSAS).
- The background error covariance matrix comes from OFAM3 (global 0.1 degree ocean model used for ocean forecasts), which was forced by ERA-interim. Through this approach, the background error covariances are anisotropic.
- Code is open source, parallelised and computationally efficient.
- GSAS is near-global, foundation SST. It uses the previous day's analysis as background.
- It currently does not provide SSTs in semi-enclosed coastal regions.
- Comparison to drifting buoys shows CMC to be the best out of it, GSAS and GAMSSA/RAMSSA.
- In study test regions, the version of the products that include VIIRS looks visibly the best. CMC is smoother than the other products. GSAS appears to resolve ocean features most effectively.

Points arising from the questions:

- Argo validation is not available yet but will follow in the future.

4 Variational bias correction of Satellite Sea Surface Temperature observations – James While

Summary of presentation:

- Aim of the work is to improve the current 'offline' bias correction scheme and implement something that would work in historical, sparer data areas.
- There are two ways to estimate observation bias.
- The first is to use a high quality reference data source and estimate the bias from the differences to that reference; if we have a high number of matchups, random errors are averaged out.
- The second is to use differences to model predictions (variational bias correction); again, random errors average out and this works even if a reference sensor is not available.
- In tests using a Lorentz system a combination of these two types of bias estimates gives the best result, followed by variational, then differences; this matches the theoretical result (note that the bias error plot in the presentation shows the discrepancy between the true bias in the data and the estimated bias). If the bias is extremely small, then trying to estimate it actually has a detrimental effect.
- New Met Office system uses a combination of the two methods.
- The system was tested using CCI data and ICOADS. AATSR and drifting buoys were assumed unbiased. A one year run was produced without assimilating AATSR and two years run with AATSR.
- Results were poorest for the one year run without AATSR and using only the observation difference approach because it was not enough information available on biases.
- In "observation minus background" data for AMSRE the variational scheme was shown to be valuable when AASTR was not available. There is however a trade off between using data for bias correction and then not reducing random errors by so much.

- Value of the observation difference bias correction approach can be seen in “observation minus background” statistics for in situ data.

Points arising from the questions:

- Results show a discrepancy between AATSR and in situ (consistent with the ESA SST CCI project’s results).
- Using a high proportion of reference and some of the other data for bias correction reduces the amount available for direct estimation for the SST field.
- New system is being implemented operationally in the future and is an improvement on what we already have.
- If there were high resolution model fields available, would it be used to test the system? Potentially, but it is still necessary to test on real data.

5 Discussion on the future of L4 products given the new requirements for NWP – led by Dorina Surcel Colan

Talks have given examples of sub-daily L4 products and some centers are considering moving to L1/L2/L3 assimilation. Given this, what is the future for L4 analyses?

- Bureau of Meteorology – would like to move towards a semi-coupled (or full-coupled) scheme.
- CMEMS – most forecasting sensors using L3, but still need L4 for users e.g. for validation of model outputs. The strategy is to give people both solutions. Currently L4 tends to perform better than models. CMEMS is moving towards resolving the diurnal cycle in its SST products.
- There is still a need for L4-type data but it could be from a model analysis in the future, potentially.
- We should be moving towards higher temporal resolution as well as higher spatial resolution.
- Should come up with a set of consistent metrics noting that grid resolution does not match the real resolution?
    - Similar what has been done for CDAF.
    - Work done at the Met Office on feature resolution has demonstrated this kind of thing.
- L4 features can be very different even if the mean and RMS against drifters are the same in different analyses.
- It can be possible to mistake noise for features. Only way to really know is by having an experiment with subsampled high resolution model data so that we know the truth. The simulated observations need realistic errors. The ECCO model outputs could be used.
- “Observation minus background” should be preferred over “observations minus analysis” when evaluating systems.

SEA SURFACE TEMPERATURE ANALYSIS WITHIN THE NCEP GFS

Xu Li[(1)], John Derber

(1) EMC/NCEP/NOAA, USA, Email: Xu.Li@noaa.gov

Abstract

In an uncoupled Numerical Weather Prediction (NWP) system, Sea Surface Temperature (SST) is required as an input to prescribe the underlying water surface temperature. Most widely available SST analysis products are produced independent from the NWP system with a univariate analysis scheme. At NCEP since July 2018, the operational NWP system has analyzed the SST together with the atmospheric variables. In the new NCEP approach, the concept of the SST has been extended to the Near Surface Sea Temperature (NSST) profile due to diurnal warming and sub-layer cooling physics with a functional relationship based on a base foundation temperature. The foundation temperature has been incorporated as one of the atmospheric analysis variables within the NCEP GFS.

A series of data assimilation and forecast runs have been performed. The results have shown the SST has been improved in both analysis and prediction mode. The satellite radiance data assimilation also has been improved for the surface sensitive channels. The impact on the weather forecasting is positive in the tropics and neutral in higher latitude areas. In addition, intercomparisons between the new NCEP SST analysis and the other widely available SST analyses are underway and will be presented.

A NEW ENSEMBLE OPTIMAL INTERPOLATION SST ANALYSIS SYSTEM AT THE BUREAU OF METEOROLOGY

Helen Beggs[(1)], Pavel Sakov, Paul Sandery, Gary Brassington

(1) Bureau of Meteorology, Australia, Email: Email: helen.beggs@bom.go

Abstract

A new experimental global, Sea Surface Temperature (SST) analysis system ("GSAS") is presented, based on public, Ensemble Kalman Filter data assimilation C code (EnKF-C) developed by the Bureau of Meteorology (BoM) under the Bluelink Project. The GSAS system uses the Ensemble Optimal Interpolation (EnOI) method. It uses the previous analysis as the background field, and implicitly calculates covariances from a static ensemble of SST fields, based on the operational ocean forecasting system OceanMAPS. The system covers the region 75°S to 75°N, and produces daily SST analyses at approximately 2.5 m depth on a 0.1° x 0.1° rectangular grid, and assimilates various global infrared and microwave satellite SST data streams from S-NPP, Himawari-8, JCOM-W, METOP-A/B and NOAA POES satellites.

The advantages of using the EnOI GSAS system for SST analysis will be outlined, including anisotropic covariance, computational efficiency, use of superobservations to handle different resolution input products, and the ability to account for observation error. The impact of assimilating the various data streams will be presented, and comparisons shown between GSAS and the BoM operational daily, optimal interpolation SST analyses, GAMSSA and RAMSSA.

VARIATIONAL BIAS CORRECTION OF SATELLITE SEA SURFACE TEMPERATURE OBSERVATIONS

James While[(1)], Matthew Martin[(2)]
(1) Met Office, Exeter, UK, Email: james.while@metoffice.gov.co.uk
(2) Met Office, Exeter, UK, Email: matthew.martin@metoffice.gov.co.uk

1. Introduction

Over the last few years the Met Office has been developing a new system for SST bias correction. This work has two aims:

- To improve upon the Met Office's existing bias correction scheme.
- To produce a scheme that will work in the early satellite period when high quality 'unbiased' reference data are less abundant.

To fulfill these criteria, we have developed a variational system that includes 'observations-of-bias' (differences between co-located biased observations and low bias reference observations). Essentially our scheme combines information from observations-of-bias and observation-model differences. The appeal of the scheme is that it should produce realistic bias fields when there are no observations-of-bias but can use observations-of-bias when such data are available.

We have verified our bias correction scheme using both the three variable Lorenz 63 models and a full implementation of the Met Office's ocean modeling system. In both cases four experiments were conducted:

- An experiment with no bias correction.
- An experiment using only observations-of-bias (essentially the Met Office's historic bias correction scheme).
- An experiment using just observation-model differences (i.e. a pure variational scheme).
- Our new scheme that combines observations-of-bias with observation-model differences.

Some results from these experiments are below.

2. Results with the Lorenz 63 system.

The Lorenz 63 system (Lorenz; 1963) is a non-linear three variable (x,y,z) system that is useful for testing ideas in data assimilation. Using Lorenz 63 we conducted a large number of twin experiments where we used one run as the truth, with other runs, subjected to both initial condition and ongoing perturbations, acting as simulations. Noisy observations were assimilated into all three variables of the perturbed runs, but with the x observations deliberately biased.

Figure 1 shows the impact of the level of bias on our Lorenz 63 experiments. As can be seen, doing no bias correction gives the best results when the bias is very small – no information is lost trying to estimate a bias that does not exist – but errors increase rapidly as the bias increases. The observations-of-bias based system is significantly better at larger biases, but still shows increasing error. In contrast, the combined and pure variational systems do not show an increasing error and across most of the graph give the best results. The insensitivity of these algorithms to increasing bias is a highly desirable property, especially in real systems where the bias will be imperfectly known and vary in time. Figure 1 also shows that by including observations-of-bias, the combined

bias correction method reduces the error compared to the pure variational system, although not by much.

The precise shape of the error vs bias graph will depend on the specifics of the system (number of observations-of-bias, observation errors, model errors, etc). In particular, we expect the cross over point at which variational schemes start to give the smallest error will be system dependent. However, we believe the general shape of the curves in Figure 1 to be robust. We have also found that the shape of the graph in Figure 1 agrees well with theoretical predictions for a single variable linear system.

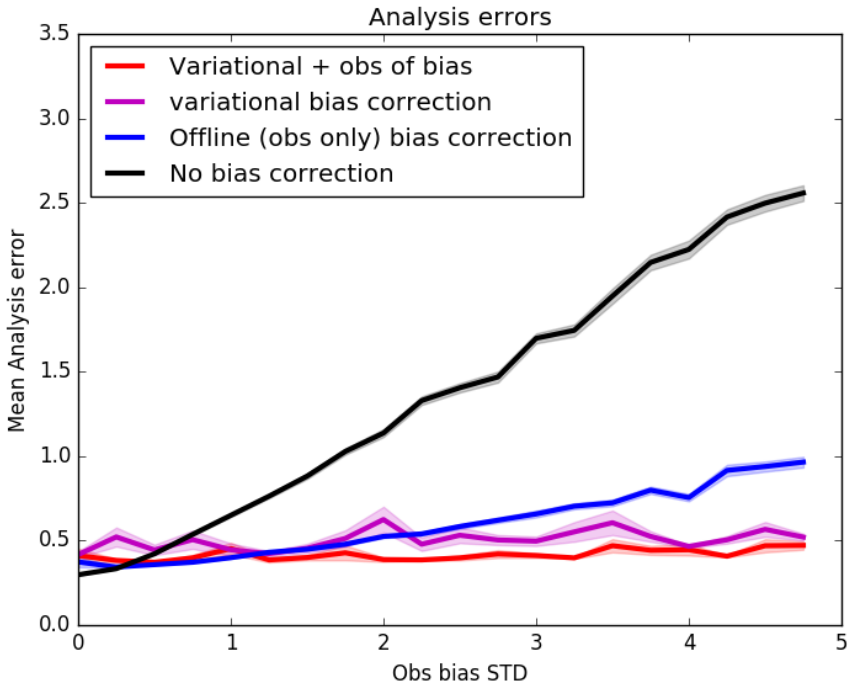

Figure 8: Analysis error verses the bias on x observations for the Lorenz system. The black line is for no bias correction, blue is for observations-of-bias only bias correction; purple is for pure variational bias correction, while red is a combined variational/observations-of-bias system.

3. Results in a full ocean analysis system.

Our bias correction methodology has also been tested using a modified version of the Met Office's Forecasting Ocean Assimilating Model (FOAM; Blockley et al, 2014). In these tests the FOAM system was run from 2008 until 2010 assimilating profile, sea-ice, and altimeter data. Biased satellite data from NOAA-AVHRR-17, NOAA-AVHRR-18, and METOP-AVHRR instruments from the CCI phase 1 project were assimilated. AMSRE data from the Met Office's operational archive were also used. 'Unbiased' reference data were taken from the AATSR satellite instrument and drifting buoys. In order to simulate a lack of reference data, observations from AATSR were withheld from the system in 2009, but were used, both for direct assimilation and for bias correction, in 2008 and 2010.

Figure 2 shows the mean bias fields that were calculated for AMSRE for the three years of the experiments. From this figure, we can see that in 2008 and 2010 all three bias correction schemes

broadly agreed with each other. However, in 2009, when AATSR data were withdrawn, the observations-of-bias scheme was notably different. In particular, the magnitude of the biases was reduced and much of the small-scale structure was lost. This did not occur with the pure variational and combined experiments, which were consistent throughout the three years. These results strongly indicate that variational schemes are far more robust to changes in the observing system than are observation-of-bias based schemes.

Differentiating between the pure variational and the combined experiments is difficult. This is illustrated in Figures 3 and 4, where we show the Global RMS values of the observations minus background for both AATSR and in-situ data. In these figures we see that all of the methods reduced the RMS difference when compared to a control, but there was considerable disagreement between the in-situ and AATSR results. Both variational schemes reported lower RMS values than the observations-of-bias scheme, especially against AATSR. However, against drifting buoys the combined scheme gave the lowest RMS values, while the pure variational scheme gave the lowest RMS against AATSR. It is not currently clear why a pure variational scheme favoured AATSR, while our combined scheme favoured in-situ data.

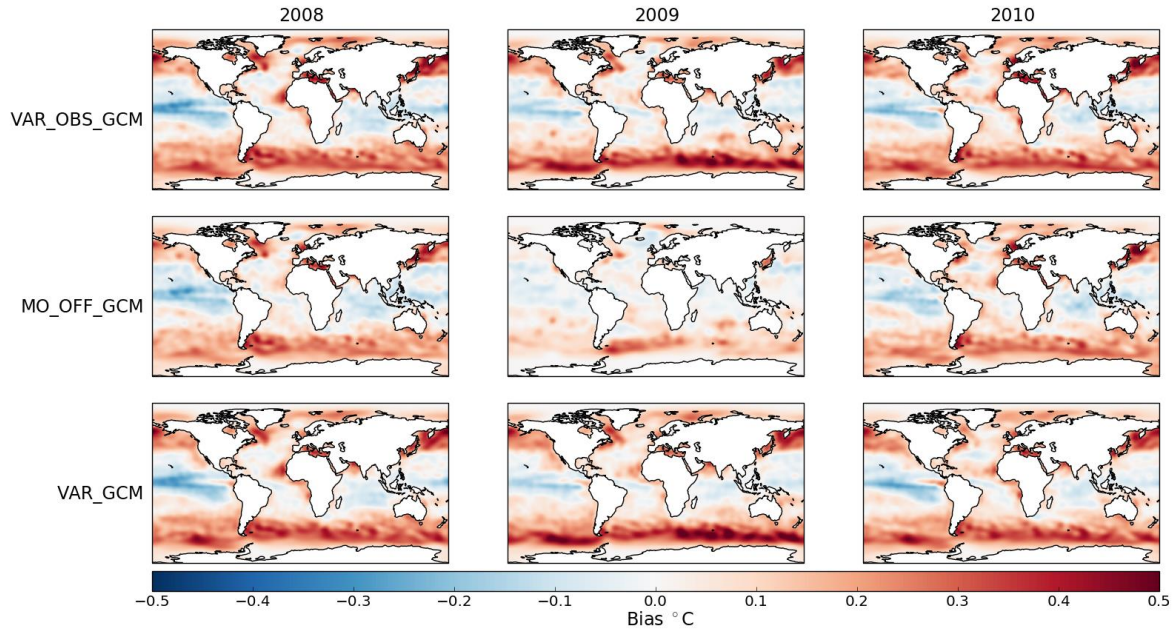

Figure 9: Mean bias fields for AMSRE in our FOAM experiments. Top row is for the combined variational/observations-of-bias experiment, the middle row is for the offline observations-of-bias only experiment, while the bottom row is for the pure variational experiment.

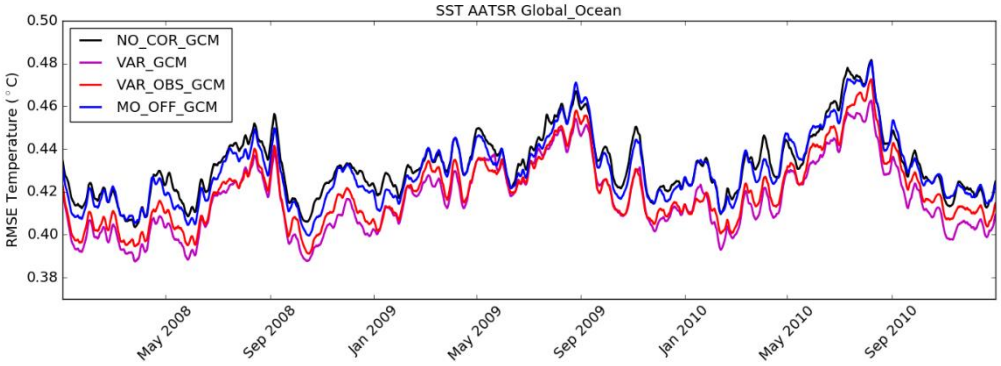

Figure 10: Global RMS differences between AATSR observations and the model background. The black line is for no bias correction, blue is for observations-of-bias only bias correction; purple is for pure variational bias correction, while red is a combined variational/observations-of-bias system.

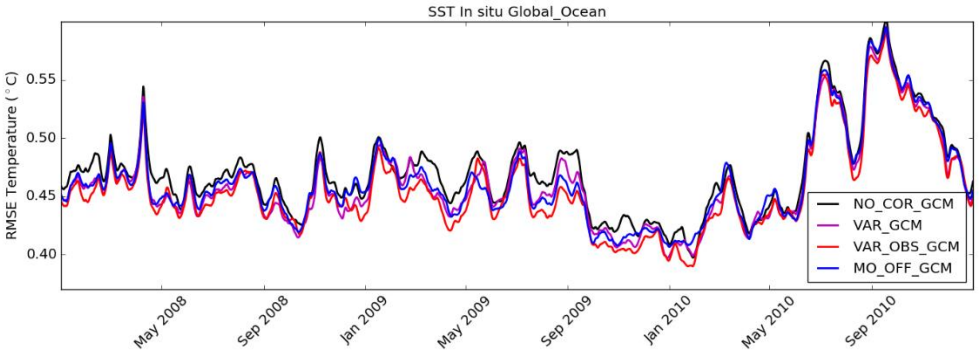

Figure 11: As in Figure 3, but for in-situ drifting buoys.

4. Conclusions

We have developed a new bias correction scheme for observation bias in SST measurements. The scheme combines a variational bias correction method with information from observations-of-bias. For non-trivial biases in the Lorenz 63 system, the new method outperformed both an observations-of-bias only system and a pure variational system. The method was also seen to be robust to changes in the SST bias.

Our method was also tested in a full ocean modelling framework and continued to outperform an observations-of-bias scheme both in terms of RMS statistics, and in the stability of the bias field derived. However, when compared to a pure variational scheme results were mixed, with the pure scheme performing better against AATSR, but the combined scheme giving better results against in-situ data.

5. References

Blockley E. B., M.W. Martin, A.J. McLaren, A.G. Ryan, J. Waters, D.J. Lea, I. Mirouze, K.A. Peterson, A. Sellar, D. Storkey; Recent development of the Met Office operational ocean forecasting system: an overview and assessment of the new global FOAM forecasts, *Geoscientific Model Development.* **7**, 2613-2618, 2014. DOI: 10.5194/gmd-7-2613-2014

Corlett G., C. Atkinson, N. Rayner, S. Good,E. Fielder, A. McLaren, J. Hoeyer, C. Bulgin; Product Validation and Intercomparison Report (PVIR), *ESA CCI SST phase 1 technical report,* 2014, Availible from http:\/\/www.esa-sst-cci.org\/PUG\/documents.htm

Lorenz E. N., Deterministic Nonperiodic Flow , *Journal of the Atmospheric Sciences.* **142**, 130-141, 1963. DOI: 10.1175/1520-0469(1963)020<0130:DNF>2.0.CO;2

PLENARY SESSION IV: APPLICATIONS OF SST

SESSION IV REPORT

Chair: Craig Donlon[(1)] – Rapporteur: Ioanna Karagali[(2)]

(1) ESA, ESTEC, The Netherlands, Email: Craig.Donlon@esa.int
(2) DTU Wind Energy, Roskilde, Denmark, Email: ioka@dtu.dk

1. Introduction

This report summarizes the key points presented and discussed during the plenary session on "Applications of SST". Three presentations took place and 30 minutes of discussion.

2. Summary of presentations

2.1. Skin-subskin SST differences using a collocated nine-year Aqua MODIS/AMSR-E record in support of wave breaking studies (Haifeng Zhang)

Motivation: Infrared signal of breaking waves

Rationale: Establish new method to identify wave breaking probability, severity and thus, global and regional trends.

Data used: MODIS, AMSR-E, iQuam SST, NCEP meteo parameters

Results from validation: For MODIS night-time -.37 K and -0.22 for daytime. For AMSRE, a day-time warm bias was found when the in situ temperature was less than 10 ^{0}C.

Finally, it was decided to filter the datasets such that water vapour was in the range 12-50 kg/m2 and SST was between 10 and 30 ^{0}C.

Overall MODIS vs AMSRE bias for day-time was -.19 and -.29 for night-time. In addition, a latent heat flux dependence was identified such that a day-time negative LHFX resulted in positive differences. A positive air-sea temperature difference in the daytime could also lead to positive IR-MW differences. InfraRed minus Microwave biases larger than -.5 were identified in specific regions such as the Tropical Warm Pool (TWP) and the Tropical Atlantic.

2.2. A new synergetic approach for the determination of the sea-surface currents in the Mediterranean Sea (Daniele Ciani)

Motivation: Altimeter-derived circulation cannot fully describe surface motion in the Mediterranean Sea but only the geostrophic component (scales from 100 km up to the basin scale).

Rationale: Optimal currents (OC) through the use of low resolution geostrophic altimeter velocities as background and apply to successive SST images. From numerical simulations it was found that using this approach, the altimeter derived currents are improved by 35%.

Datasets used included the SSALTO/DUACS surface currents, CNR L4 SST, MERCATOR global operational model, HF Radar CALYPSO, MFS model, In Situ derived currents.

When comparing the OC product to the HF Radar Calypso, the former was found to have the lowest RMS Bias. AIS-ship-derived currents also exhibited satisfactory RMS and Bias for V component (but negative bias for U component) and they will constitute an interesting in-situ

dataset for validation (due to high coverage in the Mediterranean). The Optimal Currents method showed overall improvement compared to altimetry when using drifter derived currents. In addition, it was found that the retrieval of small scale geostrophic and ageostrophic motions was possible.

As a future outlook, OC could be computed at very high resolution (1km spatial and 1hr temporal). Additionally, the validation period should be extended while the possibility to merge OC with other tracers, such as ChlA should be evaluated.

Finally, while most of the improvement is to be expected at coastal regions (where the altimeter estimation tends to be degraded), further analyses showed that the improvements also depend on the intensity of the SST spatial gradients. A case study showed an improvement of the main meanders and eddies of the Gulf Stream when applying the Optimal Currents method.

2.3. Exploring Internal Wave signature on remote sensing infrared SST observations (Cristina González-Haro)

Motivation: Internal waves (IW) contribute to sea level variability for scales less 100 km and fast motions complicate retrieval of ocean currents from altimeters. Although some IW are tidal and stationary, and therefore can be predicted and removed from altimeter data, some have lost their phase relationship to astronomical forcing and are hard to detect.

Rationale: Since there is a synergy between SST and SSH, it is possible to disentangle IW

and balanced signatures in SSH using the quasi-geostrophic framework and assuming that the IW signature on SST is weak. The objective here is to quantify the IW signature on SST and validate its weakness. The assumption is that IW currents periodically advect SST fronts and cause SST fluctuations.

Datasets: Baroclinic and Barotropic sea level atlases at 1/20 and 1/16 degree resolution, correspondingly along with METOP/VIIRS/MODIS L2 SST and climatology of max SST gradients.

The focus was on areas where strong thermal SST gradients along with a significant IW signature was present. Advection of fine scale SST fronts causes IW signature which is weak compared to SST variations over short (tidal) windows but maybe compared to absolute accuracies of SST products. The wave length of semidiurnal internal tidal waves is approximately 100 km thus SAR derived internal waves are not of relevant scales.

3. Discussion

There was an extensive discussion about signals of wave breaking on microwave and infrared triggered by the first talk. The concept that SST products could be used to identify wave breaking was not strongly supported as it was highlighted that differences between MW and IR observations retrieved with the existing algorithms will mostly show instrument differences rather than physical ocean features. Nonetheless, it was highlighted that upcoming missions and instruments can support resolving wave signatures in the future, especially coupled with some IR measurements (maybe airborne).

Regarding the potential of retrieving surface currents by gradients in SST it was discussed, from a user perspective, that maintaining flagged data is important and it would be valuable to provide metrics on position of frontal structures in L3, L4 products.

From the data producers perspective, it was mentioned that a previous survey for gradients on what to report and how, did not receive many responses thus this topic is still considered unresolved.

Finally, it was summarized that depending on the application, different metrics are relevant but overall the proper location and intensity of the gradient are very important.

SKIN-SUBSKIN SST DIFFERENCES USING A COLLOCATED NINE-YEAR AQUA MODIS/AMSR-E RECORD IN SUPPORT OF WAVE BREAKING STUDIES

Haifeng Zhang[(1)], Alexander Babanin, Alexander Ignatov

(1) The University of Melbourne, Australia, Email: helen.beggs@bom.go

Abstract

The cool skin effect can be potentially used in wave breaking studies. Normally, the skin SST, measured by infrared (IR) sensors and representative of the upper 10-20 μm layer, is a few tenths of a degree cooler than the subskin SST, measured by microwave (MW) sensors effectively in the top ~ 1 mm layer. When a wave breaks, this skin layer is disrupted, resulting in closer IR and MW SSTs. Therefore, theoretically wave breaking information, such as probability (based on the temperature differences) and severity (based on the duration for which the skin layer is disrupted), may be linked to the collocated IR and MW SST records, on a global scale. Both MW and IR SSTs are sensitive to different factors affecting radiation formation in the ocean-atmosphere system, and retrieval physics. Thus, wave breaking information may be obtained by statistical processing of large volumes of IR and MW SSTs and suppressing random and independent errors.

As a first step we explore the IR-MW differences. The AQUA satellite, carrying both MODIS and AMSR-E, is well suited to measure both skin and subskin SST simultaneously, providing an excellent opportunity to investigate the differences between IR and MW SSTs. This study explores nine years (Oct. 2002-Sep. 2011) of MODIS (processed by the NASA Ocean Biology Processing Group Data Centre) and AMSR-E SSTs (acquired from the Remote Sensing System). Focus is on IR-MW biases, and their dependencies on the environmental (wind speed, SST etc) and retrieval (view zenith angle, etc) conditions.

A NEW SYNERGETIC APPROACH FOR THE DETERMINATION OF THE SEA-SURFACE CURRENTS IN THE MEDITERRANEAN SEA

Daniele Ciani[(1)], Marie-Hélène Rio[(2)], Rosalia Santoleri[(1)], Salvatore Marullo[(3)]

(1) Consiglio Nazionale delle Ricerche, Istituto di Scienze dell'Atmosfera e del Clima, Rome, Italy
Email: d.ciani@isac.cnr.it, r.santoleri@isac.cnr.it
(2) Collecte Localisation Satellites, Ramonville St-Agne, France. Email: mrio@cls.fr
(3) Ente per le Nuove Tecnologie, l'Energia e l'Ambiente, Frascati (Rome), Italy
Email: salvatore.marullo@enea.it

1. Introduction

The synoptic retrieval of the sea-surface currents is a major challenge in observational oceanography. Its applications in scientific and socio-economic fields include studies on climate change, air-sea interaction, transport of oceanic tracers and suspended matter (e.g. salt, nutrients, plastics, oil spills, etc.), fishery, marine safety&rescue activities and the optimization of the ship routing. All these activities have three requirements in common: high spatial coverage, high temporal repetitiveness and high spatial resolution of the sea-surface observations, which are generally achieved using observations derived from satellite-sensors. Nowadays, no satellite mission provides a direct measurement of the sea-surface currents and their global-to-regional scale monitoring is provided by satellite altimetry. Being based on the observation of the sea-surface height (SSH), satellite altimetry reconstructs the large-scale geostrophic component of the surface motions at an operational level. Indeed, the altimeter-derived currents have spatio-temporal spectral responses from the mesoscale to the basin-scale range [Pujol et al. (2012)], corresponding to temporal scales ranging from some weeks to several hundred years.

The Mediterranean Sea is a basin where the improvement of the synoptic sea-surface currents retrieval is crucial from a geophysical, commercial and environmental point of view. In fact, the Mediterranean is characterized by Rossby deformation radii around 10-20 km, hence, its typical mesoscale features (O(10-100 km)) are only partially captured by classical satellite altimetry [Malanotte-Rizzoli (2011)]. Moreover, this region (and in particular the Sicily Channel area) represents the main ship route between the Indian Ocean and the main harbours of the European Union and hosts 25% of the world oil trade, with a consequent presence of illegal oil spills of the order of 600 Kt per year [Pisano et al. (2016)]. This makes high-resolution surface currents a necessary tool for monitoring the Mediterranean and improving the knowledge of its surface dynamics.

In our study, the retrieval of the Mediterranean surface motion is obtained from the combination of altimetric and thermal-band satellite observations. The approach is based on the results of Rio et al. 2016 and Rio and Santoleri 2018. These recent studies showed that it is possible to combine observations of sea-surface temperature and sea-surface currents in order to obtain global-scale improved currents both in terms of temporal and spatial resolution. We will focus on the Sicilly Channel area and we will assess the quality of the currents retrieval via comparison with High-Frequency Radar-derived currents in the Malta-Sicily Channel during the year 2016.

2. Method and Results

Following Piterbarg (2009), Mercatini et al. (2010), Rio et al. (2016) and Rio and Santoleri (2018), we derive the surface circulation in the Mediterranean Sea combining the DUACS geostrophic velocities (daily data with resolution of ~10 km) and the CNR-Sea Surface temperatures (daily data with resolution of ~5 km) for the year 2016. Both of these Mediterranean regional datasets are distributed by the Copernicus Marine and Environmental Monitoring Service. The optimal merging of these two datasets is based on the inversion of the heat conservation equation (1) for the estimation of the surface flow (in the zonal and meridional directions):

$$\partial_t \mathrm{SST} + u\partial_x \mathrm{SST} + v\partial_y \mathrm{SST} = F \quad (1)$$

where (u,v) are respectively the zonal and meridional component of the surface currents, (x,y) are the zonal and the meridional directions and F is the forcing term, containing the source and sink terms for the conservation equation. The expressions for the optimized merged velocity (u_{opt}, v_{opt}) are the following:

$$u_{opt} = u_g + u_{cor}$$
$$v_{opt} = v_g + v_{cor} \quad (2)$$

where (u_g,v_g) are the geostrophic currents and u_{cor},v_{cor} are the correction factors appearing in the optimal merging method of Piterbarg (2009). Such factors depend on the spatial and temporal gradients of the SST observations, expressing the synergy between the altimetric and the thermal band observations.

An example of the Optimal Current performances is given in Figure 1. The figure shows the surface circulation as seen by the altimeter and after the merging with SST data during a summertime upwelling event in the Sicily Channel area (July 2016).

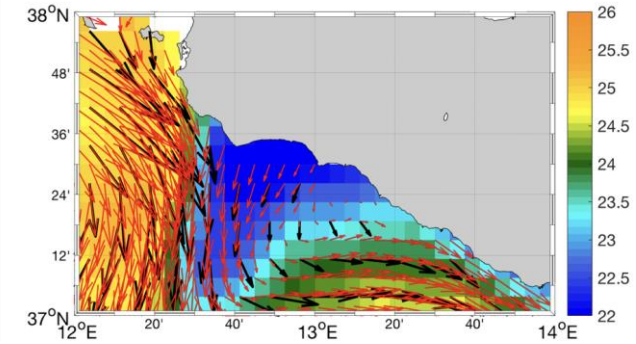

Figure 1: Optimal Currents (red arrows) and Altimeter Currents (black arrows) over SST (°C). Sicily Channel – July 23rd 2016.

In this area, during summertime, the upwelling events are quite frequent and they constitute an interesting testbed for assessing our reconstruction method. The upwelling systems are generally associated with an offshore-directed circulation, perpendicular with respect to the coastline (Piccioni et al). In our case (Figure 1), the upwelling is evidenced by the cold filament where the SST reaches 22°C. In correspondence of the filament the altimeter-derived currents exhibit a cross thermal-gradient circulation that remains mostly parallel to the coast (see in particular the circulation patterns around 12.5° E, 37.5° N). On the other hand, the Optimal estimation reduces significantly this effect and is more in agreement with the physics of the upwelling dynamics.

A quantitative validation of the Optimal currents was also performed. As a benchmark, we used the High-Frequency (HF) Radar currents of the Calypso platform in the Malta-Sicily channel area. Such data, with respective temporal and spatial resolutions of 1 hour and 1/37°, are available via the EMODNET physics service.

Year 2016	**BIAS (cm/s)**	**RMSE (cm/s)**
OPTIMAL	U=3.60 V=1.40	U=10.12 V=9.00
DUACS (geostrophic)	U=4.39 V=1.30	U=11.23 V=9.12

Table 1. Mean Bias and RMS errors between the Optimal (upper line), the DUACS altimeter-derived currents (lower line) and the high frequency radar-derived currents in the Malta-Sicily Channel (Year 2016).

During the whole year 2016, we computed the mean bias and root mean square error (RMSE) between the Altimeter, the Optimal currents and the HF Radar currents in the Malta-Sicily Channel. The results are shown in Table 1. According to this table, the Optimal Currents exhibit a better performance in retrieving the surface motion. Indeed, if compared to the DUACS geostrophic currents, they exhibit lower zonal bias and lower RMS for both the components of the motion. The main message of the qualitative and quantitative results shown in this section is that bringing the SST spatio-temporal variability inside the large scale geostrophic observations, it is actually possible to improve the remotely sensed surface motions at regional scale.

3. Conclusions and Perspectives

In order to improve the spatio-temporal resolution of the sea-surface currents in the Mediterranean Basin, we relied on the synergy between multiple satellite observations. We used a method firstly developed in a theoretical and numerical framework (see Piterbarg 2009 and Mercatini 2010) and recently applied with success to global-scale oceanographic datasets of altimeter-derived geostrophic currents and sea-surface temperature (see Rio et al 2016 and Rio and Santoleri 2018). For the moment, our results are focused on a restricted area of the Mediterranean Basin: the Sicily Channel. Such an area is an interesting testbed for assessing the method performances. Indeed, during summertime it is often characterized by ageostrophic circulation, e.g. during the upwelling events. Merging the information contained in the large scale geostrophic circulation with the one of a higher resolution sea-surface temperature, we improved the altimeter estimations, obtaining a surface field which is more comparable to the HF radar observations in the area. Quite interestingly, the method allowed to improve both the geostrophic and the ageostophic component of the surface motion. In the near future we plan to further improve the spatial and temporal resolution of the Mediterranean Sea Surface currents retrieval using 1 km resolution and hourly SST data. The robustness of the method will also be assessed via comparison with interannual drifters-derived surface currents at the basin scale.

4. References

Malanotte-Rizzoli, P. (2011, November). the Pan-Med Group, 2012. In *Physical forcing and physical/biochemical variability of the Mediterranean Sea: A review of unresolved issues and directions of future research. Report of the Workshop "Variability of the Eastern and Western Mediterranean circulation and thermohaline properties: similarities and differences", Rome* (p. 48)

Mercatini A., A. Griffa, L Piterbarg, E. Zambianchi, M. Magaldi, 2010 : Estimating surface velocities from satellite tracer data and numerical models: implementation and testing of a new simple method, Ocean Modelling, 33, 190-203;

Piccioni, A., Gabriele, M., Salusti, E., and Zambianchi, E. (1988). Wind-induced upwellings off the southern coast of sicily. *Oceanologica Acta*, 11(4):309–314.

Pisano A, De Dominicis M, Biamino W, Bignami F, Gherardi S, Colao F, Coppini G, Marullo S, Sprovieri M, Trivero R, Zambianchi E, Santoleri R (2016). An oceanographic survey for oil spill monitoring and model forecasting validation using remote sensing and in situ data in the Mediterranean Sea. DEEP-SEA RESEARCH. PART 2. TOPICAL STUDIES IN OCEANOGRAPHY, vol. 133, p. 132-145;

Piterbarg, L. I. (2009). A simple method for computing velocities from tracer observations and a model output. *Applied Mathematical Modelling*, *33*(9), 3693-3704;

Pujol, M., G. Dibarboure, P. Le Traon, and P. Klein, 2012: Using high resolution altimetry to observe mesoscale signals. J. Atmos. Oceanic Technol. doi:10.1175/JTECH-D-12-00032.1;

Rio, M. H., Santoleri, R., Bourdalle-Badie, R., Griffa, A., Piterbarg, L., & Taburet, G. (2016). Improving the Altimeter-Derived Surface Currents Using High-Resolution Sea Surface Temperature Data: A Feasability Study Based on Model Outputs. *Journal of Atmospheric and Oceanic Technology*, *33*(12), 2769-2784

Rio and Santoleri (in press). Improved global surface currents from the merging of altimetry and Sea Surface Temperature data, Remote Sensing of Environment;

EXPLORING INTERNAL WAVE SIGNATURE ON REMOTE SENSING INFRARED SST OBSERVATIONS

Cristina González-Haro[(1)] , Aurélien Ponte[(1)] , Emmanuelle Autret[(1)]

(1) Ifremer, CNRS, Univ. Brest, IRD, Laboratoire d'Oceanographie Physique et Spatiale (LOPS), IUEM, Brest, France

Emails: cristina.gonzalez.haro@ifremer.fr, aurelien.ponte@ifremer.fr, emmanuelle.autret@ifremer.fr

1. Introduction

Internal waves (IW) have recently been shown to significantly contribute to sea level variability at scales lower than about 100km [Richman et al. , 2012 , Rocha et al. , 2016 , Savage et al. , 2017]. The contamination of IW at theses scales limits our ability to predict ocean currents from altimetric data because IW currents are not related to sea level via geostrophy unlike slower/mesoscale balanced structures [Arbic et al. , 2015]. Some IW are of tidal origin and stationary with respect to tidal forcings such that the signatures of these waves on altimetric data can be predicted and can eventually be removed from altimetric data [Ray and Zaron , 2016]. Unfortunately most IW are either 1) from tidal origin but have lost their phase relationship with tidal forcing after interaction with the slower oceanic turbulence (nonstationary internal tides, Zaron [2016]) or 2) from non tidal origin (e.g. wind-forced, lee-waves). In both cases, it is difficult to these waves nowadays.

A direction of research that has been poorly explored yet deals with the signature of IW on

satellite data of non-altimetric nature (e.g. sea surface temperature (SST), color) and potential synergies in order to disentangle IW and balanced signatures in altimetric data. We recently proposed in an idealized context a tentative method in order to carry such synergies [Ponte et al. , 2017]. While it is highly premature to attempt to apply such method to real data, the objective is here to determine the amplitude of IW signature on SST and verify its smallness compared to mesoscale/submesoscale signatures. This can be achieved given an a priori knowledge of IW currents (available for stationary internal tides from existing numerical model predictions and/or from existing harmonic analyses of altimetric datasets) and maps of the SST field.

In this work, we will show a first attempt to quantify the tidal signature on SST fields through two different case studies that use infrared SST images captured by orbiting satellites (Metop and Viirs).

2. Method

The objective is to determine the amplitude of IW signature on SST and verify its smallness compared to mesoscale/submesoscale signatures. This can be achieved given a priori knowledge of tidal currents and SST observations captured by Infrared sensors. Tidal currents are indeed expected to periodically advect SST fronts and result in SST fluctuations:

$$\partial_t T_w = -u_w \partial_x T_s - v_w \partial_y T_s \quad (1)$$

where $T_w$is the variation of SST due to IW, $u_w$and v_w are the zonal and meridional components of the IW currents, respectively, and T_s stands for the SST. Assuming that $u_w = \Re(u_c e^{-iwt})$ where $u_c = u_r + iu_i$ and w is the IW frequency, equation (1) can be rewritten as:

$$\Re(-iwT_w e^{-iwt}) = -\Re(e^{-iwt}[u_c \partial_x T_s + v_c \partial_y T_s]) \quad (2)$$

Thus, the amplitude of IW signature on SST can be estimated as:

$$T_w = \frac{u_c \partial_x T_s + v_c \partial_y T_s}{iw} \quad (3)$$

The quantification of the IW signature on SST can be splited in three steps:

- Compute *gradient of SST*: The Sobel gradient of SST is computed from free cloud infrared SST observations.
- *IW current amplitudes*: the IW current amplitudes are first derived from the sea level output model and then interpolated into the grid of SST observations.
- IW signature on SST: The final step consists in evaluating expression (3) using the SST gradients and the amplitude of IW currents computed in the two previous steps.

3. Data Sources

We use infrared GHRSST SST images captured by several orbiting satellites, particularly, we explored the data archive available at LOPS servers for AVHRR-METOP-A (OSISAF), VIIRS and MODIS. We have explore the L2 data archive from 1st January 2014 to 31st December 2016 for AVHRR-METOP, VIIRS and MODIS. Additionally, IW current amplitudes are derived from the sea level output of the High Resolution Empirical Tide (HRET) Model (courtesy of Ed Zaron, Portland State University http://web.cecs.pdx.edu/~zaron/pub/HRET.html.) and the FES2014 for the barotropic currents (https://www.aviso.altimetry.fr/en/data/products/auxiliary-products/global-tide-fes.html).

4. Preliminary Results

Figure 1 illustrates the quantification of the signature of the semidiurnal M2 IW on SST for a case study region, in the South of Madagascar. We first compute the sobel gradient of the SST field, then we retrieve the M2 baroclinic current for regions deeper than 1000m from HRET numerical simulations. Finally, the amplitude of IW signature on SST estimated for this particular case is lower than 0.1 ºC.

In order to compare the estimated signature of IW on the SST with other variations associated to mesoscale/submesoscale, diurnal cycles, we computed the variation of SST between two consecutive passes within an interval time of 12 hours (see Figure 2). . The two SST images considered correspond to the ascending and descending passes of METOP on the 5th June 2014. The temporal variability shown here is dominated by the slow balanced flow.

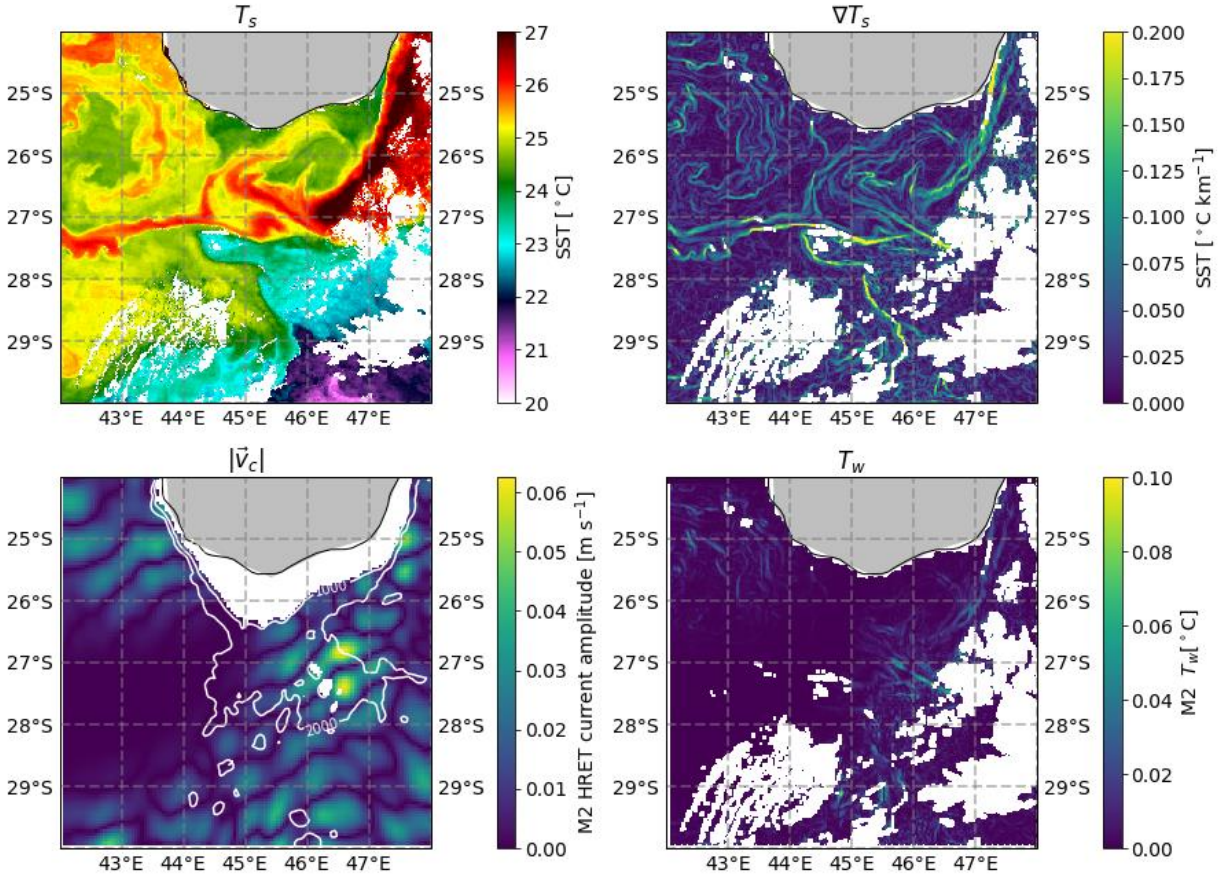

Figure 1: (Top left) SST captured by metop on the 5 June 2014. (Top right) Sobel gradient of SST. (Bottom left) M2 baroclinic HRET amplitude current for areas with a bathymetry deeper than 1000m. White contour lines correspond to the bathymetry. (bottom right) Estimation of the amplitude of M2 IW signature on SST.

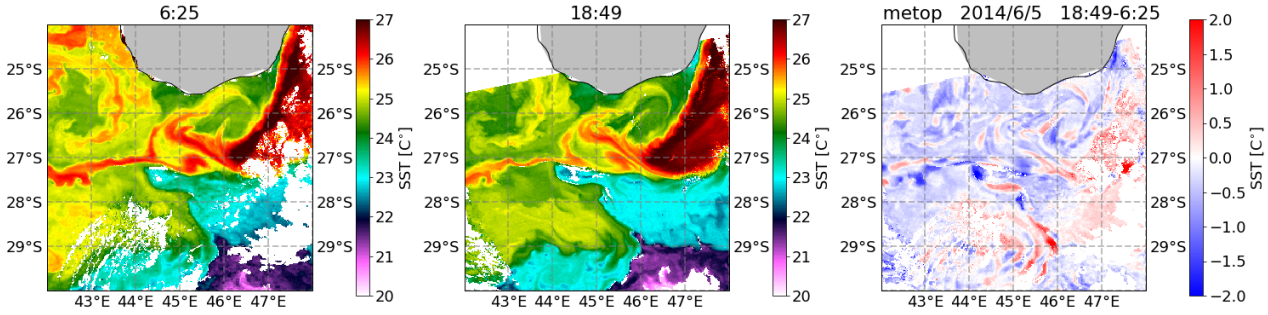

Figure 2: (left) SST captured by metop on the 5 June 2014 at 6:25. (middle) SST captured by metop on the 5 June 2014 at 18:49 (right) Difference between SST captured at 18:49 (middle) and the one captured at 6:25 (left).

5. Summary

- We present here a first ***attempt*** to quantify the signature of IW on SST observations provided by orbiting satellites.
- This signature is related to the advection of fine scale SST fronts. It is thus also fine-scale and confined to the front location. It is also proportional to the product of the SST frontal gradient and tidal currents.
- SST fluctuations due to internal tides motions are lower than 0.1 K.
- Such signatures appears to be weak compared to SST variations over short (tidal) temporal windows associated to: mesoscale/submesoscale; diurnal cycles (even though spatial structure is large scale for the latter).
- These amplitudes may be compared to the absolute accuracy of SST products (0.3 K) [Ocarroll et al. 2012, Wu et al. 2017] and to the instrument pix noise (presumably weaker than the former).

6. References

B. K. Arbic, F. Lyard, A. Ponte, R. Ray, J. G. Richman, J. F. Shriver, E. Zaron, and Z. Zhao.

Tides and the swot mission: Transition from science definition team to science team. Technical report, CNES-NASA, 2015.

A. L. Ponte, P. Klein, M. Dunphy, and S. Le Gentil. Low-mode internal tides and balanced

dynamics disentanglement in altimetric observations: Synergy with surface density observations. J. Geophys. Res., Oceans , 2017. ISSN 2169-9291. doi: 10.1002/2016JC012214. URL http://dx.doi.org/10.1002/2016JC012214 .

R. D. Ray and E. D. Zaron. M2 internal tides and their observed wavenumber spectra from satellite altimetry. J. Phys. Oceanogr. , 46:3–22, 2016.

James G. Richman, Brian K. Arbic, Jay F. Shriver, and E. Joseph Metzger. Inferring dynamics from the wavenumber spectra of an eddying global ocean model with embedded tides. J. Geophys. Res. , 117(C12012), 2012. doi: 10.1029/2012JC008364.

Cesar B Rocha, Sarah T Gille, Teresa K Chereskin, and Dimitris Menemenlis. Seasonality of submesoscale dynamics in the kuroshio extension. Geophys. Res. Lett. , 2016.

A. G. O'Carroll, T. August, P. Le Borgne, and A. Marsouin. The accuracy of SST retrievals from Metop-A IASI and AVHRR using the EUMETSAT OSI-SAF matchup dataset. Remote Sensing of Environment , 126:184–194, November 2012. doi: 10.1016/j.rse.2012.08.006.

F. Wu, P. Cornillon, L. Guan, and L. Li. Evaluation of the precision in level-2 avhrr sea surface temperature fields. In 2017 IEEE International Geoscience and Remote Sensing Symposium (IGARSS), pages 2954–2957, July 2017. doi:10.1109/IGARSS.2017.8127618.

PLENARY SESSION V: AIR-SEA INTERACTION

SESSION V REPORT

Chair: Rosalia Santoleri[(1)] – Rapporteur: Peter Minnett[(2)]

(1) CNR - Institute of Atmospheric Sciences and Climate, Italy, Email: rosalia.santoleri@artov.isac.cnr.it

(2) Rosenstiel School Rosenstiel School of Marine and Atmospheric Science, University of Miami, Miami, FL 33149, USA Email: pminnett@rsmas,miami.edu

1. Introduction

The coupling of the ocean and atmosphere is a fundamental characteristic of the Earth's climate system and, on shorter time scales, a major influence on global weather patterns. There are five primary components of air-sea interactions: the radiative fluxes comprising the shortwave energy from the sun and the longwave emission from the atmosphere, sun and ocean surface; the turbulent heat fluxes through surface evaporation (latent heat) and heat loss by the ocean because it is nearly everywhere warmer than the overlying atmosphere (sensible heat flux); and the water gain by the ocean through rainfall, which also introduces a heat flux as the raindrops are generally cooler than the ocean surface. The turbulent fluxes and the infrared emission from the sea surface are directly related to the sea surface temperature.

There were three presentaions in this session which was chaired by Dr Rosalia Santoleri:

- *Ioanna Karagali* - Improved diurnal variability forecast of ocean surface temperature through community model development.
- *Salvatore Marullo* - The Lampedusa Cal/Val site: assessing heat fluxes and high frequency SST estimates in the Mediterranean Sea.
- *Hiroyuki Tomita* - Ensemble SST and air-sea heat flux estimate.

Additional research was reported in the interactive sessions.

2. Improved diurnal variability forecast of ocean surface temperature through community model development

Dr. Karagali of the Technical University of Denmark (DTU) opened the session with a summary presentation of research on diurnal heating and cooling characteristics of the waters around Denmark and the western Baltic Sea. Time series of SEVIRI SSTs reveal strong diurnal signals of several degrees in this area, especially in June and July. None of the established models of diurnal temperature variability are able to replicate these signals to a satisfactory level, generally giving too large heating in areas where the SEVIRI data show small heating amplitudes, and producing too small signals in cases where SEVIRI data indicate large heating. Also the spatial extent and duration of large amplitude (≥ 2K) heating in the SEVIRI SSTs are poorly represented in the models. Using the General Ocean Turbulence Model (GOTM) driven by surface variables measured in situ at the Arkona Becken moored buoy, and taken from the ECMWF analysis fields, produced reasonable corresponded with the SEVIRI SSTs, and with the subsurface temperatures measured at discrete depths on the mooring, but had discrepancies of several tenths of a Kelvin in SST, and over a Kelvin at depths to 50 m.

These results indicate a need to improve model representations of diurnal heating in this area if the intended capability to forecast high temporal and spatial resolution SST is to be realized. A new collaborative research project between DTU and the Danish Meteorological Institute, called Diurnal Variability of the Ocean Surface Temperature for Community Modelling (DIVOST-COM) is being initiated to develop and integrate a diurnal variability model in the Baltic Monitoring Forecasting Centre 3-D physical-biological model and the SST TAC level 4 analysis to improve the CMEMS modelling and satellite products for the Baltic Sea. The main objectives are to:

- Better describe the ocean biogeochemical parameters.
- Provide consistent ocean-atmosphere products.
- Contribute to a better monitoring and description of the ocean state and its variability.

The initial focus will be the Baltic Sea but in the future, if successful, it could be extended to the global oceans. The forecasting horizon for CMEMS is seven days.

3. The Lampedusa Cal/Val site: assessing heat fluxes and high frequency SST estimates in the Mediterranean Sea

Dr. Marullo of ENEA, the Italian National Agency for New Technologies, Energy and Sustainable Economic Development, introduced the climate observatory on the island of Lampedusa, to the south of Sicily and to the east of Tunisia, and on a nearby mooring. The instrument suite is extensive and many variables are measured to support the study of the surface heat budget and to assess errors and uncertainties in satellite derived estimates of the components of the heat fluxes. A time series of hourly, near-surface sea temperatures measured on the mooring reveals diurnal heating and cooling signals throughout the year.

Focussing on the period of June 3rd to October 31st, 2017, incident surface radiation measurements at the mooring were compared to retrievals from SEVIRI and derived from simple parameterizations based on standard meteorological measurements. The SEVIRI shortwave retrievals had a mean error of 5.8 Wm^{-2} and RMS of 68 Wm^{-2} compared to the measurements taken on the surface float of the mooring, whereas the corresponding values derived from the parameterization were 9.0 Wm^{-2} and 91 Wm^{-2}. In the longwave, the SEVIRI retrievals had a mean error of 11.4 Wm^{-2} and an RMS of 19.4 Wm^{-2} compared to the measurements from the mooring; the values for the parameterized estimates were -7.14 Wm^{-2} and 21.2 Wm^{-2} when the parameterization was based on meteorological measurements taken from the mooring, and -11.5 Wm^{-2} and 22.5 Wm^{-2} when the parameterization used variables taken from ECMWF fields. The mean differences between the SEVIRI retrievals of the incoming infrared fluxes and the mooring measurements were much less sensitive to variability in the surface humidity and cloud cover than were the parameterized values. A major source of error in the satellite and parameterized estimated of both short- and longwave fluxes is the effect of small clouds. Using ECMWF surface fields, parameterized estimates of the turbulent latent heat flux differed by 2.3 Wm^{-2} in the mean when compared to estimates obtained from measurements at the mooring, which had a mean value of -97.2 Wm^{-2}, and 0.1 Wm^{-2} for sensible heat flux with a mean value of -5.2 Wm^{-2}. It should be noted that these are not mean errors in estimates of the heat fluxes, but the differences in estimates derived using different input variables to the same parameterization.

Two case studies of the seasonal development of surface and subsurface temperatures derived using the GOTM showed good correspondence between modelled and temperatures measured at the mooring when GOTM was driven by measurements taken at the mooring, but significant deviations, >1 K, in the temperature at 1 m depth when the model was driven with surface radiative

fluxes derived from SEVIRI, which over-estimates the shortwave radiation and the longwave sky irradiance for a total of more than 15 Wm^{-2}.

4. Ensemble SST and air-sea heat flux estimate

Dr. Tomita from Nagoya University in Japan, reported on research to improve global estimates of air-sea fluxes in the ice-free oceans in a research endeavour called Japanese Ocean Flux Data Sets with Use of Remote Sensing Observations (J-OFURO). Faced with the problem of selecting the best global SST field derived from satellites, a new ensemble field has been generated from L3 and L4 SSTs from 12 sources. The average spread (standard deviation) of the ensemble is 0.45 K for 1988-2015. Calculating turbulent heat fluxes using the maximum and minimum SSTs from the ensemble results in differences of 60 Wm^{-2} over much of the world's oceans, but reaching 120 Wm^{-2} over western boundary currents.

5. Conclusion

While global, accurate determination of the surface air-sea fluxes is a long-standing target of remote sensing researchers, the prospect of reaching the target accuracies required to generate Climate Data Records is still elusive. The CEOS objectives for surface heat fluxes are:

Latent Heat Flux:

- Frequency: Hourly to monthly
- Resolution: 1-25 km
- Required Measurement uncertainty: 10-15 Wm^{-2}
- Stability (per decade unless otherwise specified: 1-2 Wm^{-2}

Sensible Heat Flux:

- Frequency: Hourly to monthly
- Resolution: 1-25 km
- Required Measurement uncertainty: 10-15 Wm^{-2}
- Stability (per decade unless otherwise specified: 1-2 Wm^{-2}

Surface net longwave;

- Frequency: Monthly (resolving diurnal cycle)
- Resolution: 100 km
- Required Measurement uncertainty (Requirements on global mean): 1 Wm^{-2}
- Stability: 0.2 Wm^{-2}/decade

Surface net shortwave:

- Frequency: Monthly (resolving diurnal cycle)
- Resolution: 100 km
- Required Measurement uncertainty (Requirements on global mean): 1 W/m^2
- Stability: 0.2 W/m^2 /decade

The discussion of this session included concerns about attempting to derive near surface atmospheric variables by remote sensing as the closer to the surface the weighting function of a satellite radiometer spectral channel becomes, the larger the proportion of the signal originates at the surface and therefore the air-sea differences in temperature and humidity, needed to estimate the turbulent heat fluxes, are based on correlations between the surface and the lower atmosphere and not on independent measurements. This may be acceptable in some cases, but it will not identify situations that depart from normal.

In summarising the session, Dr. Santoleri commented that there are clearly many researchers in the GHRSST community working on improving remote sensing of surface fluxes, but that current estimates have large errors and uncertainties and that these have important, but, negative, consequences on our ability to understand air-sea exchanges and to make meaningful forecasts.

IMPROVED DIURNAL VARIABILITY FORECAST OF OCEAN SURFACE TEMPERATURE THROUGH COMMUNITY MODEL DEVELOPMENT

Ioanna Karagali[(1)], Jun She[(2)], Jacob L Høyer[(2)]

(1) DTU Wind Energy, Frederiksborgvej 399, Roskilde DK-4000 Email: ioka@dtu.dk
(2) Danish Meteorological Institute, Copenhagen Ø DK-2100, Email: js@dmi.dk,jlh@dmi.dk

1. Introduction

During daytime, under low winds and due to solar heating, the skin and sub-skin temperatures, typically measured by satellites can increase by several degrees compared to the foundation temperature. Diurnal variability has been observed in the Mediterranean [5], western North Atlantic [1] and the global ocean [2,3] from in situ and satellite observations. Diurnal heating has been reported at higher latitudes [4] and an extended study to characterise the regional patterns of diurnal SST variability over the Atlantic Ocean and the European Seas [5], showed frequent occurrences of diurnal warming events reaching several degrees, in the Baltic Sea.

Nonetheless, diurnal SST variability it is not fully resolved by ocean and coupled ocean-atmosphere models. Although some of the important diurnal variability and cool skin effects [6] have been shown to be reproducible [7], the vertical grid resolution of the models is of meter-scale. In addition, regional CMEMS ocean forecasting systems only assimilate a single SST field per day, representative of night-time conditions when the water column is well mixed and thus, no diurnal signal is present. Such simplification of the SST has been reported to cause biases in the estimated surface fluxes [8,9]. The implications associated with the lack of a properly resolved SST daily cycle in atmospheric, oceanic and climate models have been quantified in terms of heat budget errors mostly in the Tropics. Heat flux errors associated with the warm layer development were reported in [9] to range between 10 and 50 Wm^{-2}. In regions with diurnal warm layer formation, [10] reported an annual mean surface flux out of the ocean that reached up to 9 Wm^{-2}. In addition, strong SST diurnal signals can complicate the assimilation of SST fields in ocean and atmospheric models, the derivation of atmospheric correction algorithms for satellite radiometers and the merging of satellite SST from different sensors [11]. Not accounting for the daily SST variability can cause biases in the prediction and modelling of algal blooms, especially as cyanobacteria blooms in the Baltic Sea are promoted by high SST values [12] - and the estimated net flux of CO_2, as the outflux of oceanic CO_2 is positively correlated with the increase of SST [13].

Various models exist for the description of the diurnal cycle and their complexity varies from empirical parameterisations, based on various input parameters such as the surface winds and heat fluxes, to turbulent closure models. Parameterisation models are typically developed based on observational evidence at specific locations and depths, thus carry the uncertainty of their parameters and forcing fields, typically from Numerical Weather Prediction (NWP) models not resolving the SST diurnal cycle. Such parameterisations were compared to SEVIRI SST derived signals in the North Sea and the Baltic Sea [14] with moderate results. More sophisticated models such as turbulence closure models can resolve the vertical extend of the diurnal signal but are computationally expensive. The one-dimensional General Ocean Turbulence Model [15] was shown in [16] to perform very well in reproducing the vertical temperature structure as described by satellite SST and buoy measurements. The success of such modelling attempts highly depends on the accuracy of the input fields, typically obtained from atmospheric models. Consequently, there is a need to evaluate the impact of properly resolving the daily variability of SST in atmospheric models as well. When examining very strong diurnal warming cases, it was found that updating the

SST every 6hours in the meso-scale model WRF, as opposed to using one daily value, resulted in average day-time differences of up to 20% for the 10 m winds and up to 40% for the surface heat flux [17].

The "Improved Diurnal Variability Forecast of Ocean Surface Temperature through Community Model development (DIVOST-COM)" project will "improve the representation of diurnal variability and cool skin layer in forced ocean and coupled ocean-atmosphere models" and the aim of this report is to provide an overview of the project. Section 2 describes the project methodology, section 3 describes the background and expected outcomes while the main conclusions are presented in Section 4.

2. Methodology

The project will use the Baltic (BAL) Monitoring & Forecasting Centre (MFC) domain as an example for the implementation and experiments. Relevant input fields for the initialisation of GOTM describing the state of the lower atmosphere will be retrieved from DMI's operational modelling chain (DMI-HARMONIE 54h forecast), thus creating the infrastructure for a future operational application of GOTM. The model vertical grid permits the fine discretization of layers, thus allowing a direct comparison with the operational BAL MFC model, i.e. currently the HIROMB-BOOS Model (HBM), to quantifying the latter's ability to resolve the upper ocean thermal structure (in WP1). In addition, direct comparisons with the SST TAC L4 product for the North Sea and the Baltic Sea will be performed in order to establish the reference depth of the foundation temperature. This will allow the identification of the relevant depths at which the L4 product can be assimilated with optimal results for the HBM system. Furthermore, after the initial impact assessment in WP1, sensitivity tests (in WP2) will aim at i) optimising the bottom boundary conditions in GOTM by using HBM forecasts and ii) optimising the GOTM model in terms of the used light absorption scheme to account for the biological factors, such as chlorophyll [18]. The optimized version of GOTM will be implemented as an add-on model to the HBM system for an updated run over the entire domain for a full year, and the impact for using the GOTM water temperature to improve the L4 SST production, heat flux assessment and Baltic Sea ocean forecast will be assessed in WP3. Finally, recommendations for further use of this research for CMEMS will be provided in WP4.

3. Rationale and expected outcome

A typical diurnal warming event in the region around Denmark was identified from SEVIRI observations (Figure 1), when day-time temperatures increased by as much as 5.5 degrees.

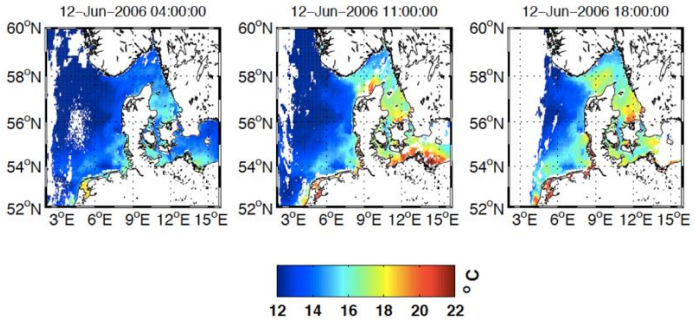

Figure 1: Example of SEVIRI SST changing during the course of a day.

The spatial patterns and characteristics of the diurnal cycle in the North Sea and the Baltic Sea have been characterised in [5]. The monthly averaged daily cycle, computed from hourly averaging

grid cells with dSST of 0.5 K or more at least once during a day is shown in the left panel of Figure 2 while the right panel shows the monthly distribution of dSST greater or equal to 1, 2 and 3 K for the period 2006-2011, normalised over the total number of quality 5 SEVIRI retrievals. Modelling of the measured signals using simple parameterisations in [14], showed that the spatial patterns derived by observations are difficult to reproduce, e.g. Figure 3. Using the 1-d GOTM system, in [16] it was found that isolated warming events could be reproduced both at the surface but also along the depth of the water column. Figure 4 (left) shows an example of modelled temperatures at the Arkona Becken station located in the Baltic Sea, for the first GOTM layer at approximately 1.5 cm depth, using different combinations of meteorological forcing and initial temperature profiles along with SEVIRI sub-skin retrievals. The right panel of Figure 4 shows a vertical profile from the insitu measurements (circles) along with GOTM profiles using different forcing combinations. Based on the existing findings, DIVOST-COM aims at producing GOTM model outputs for the entire domain of interest (Figure 3). The final outcome of DIVOST-COM is expected to expand previous findings. Evaluating GOTM at an entire domain will allow direct comparisons to the BAL MFC operational outputs (currently, the HBM model).

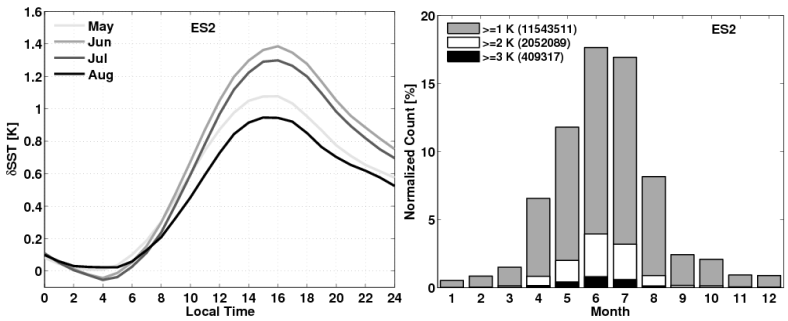

Figure 2: Monthly averaged daily cycle (left) and monthly distribution of anomalies larger than 1, 2 and 3 degrees for the North Sea-Baltic Sea.

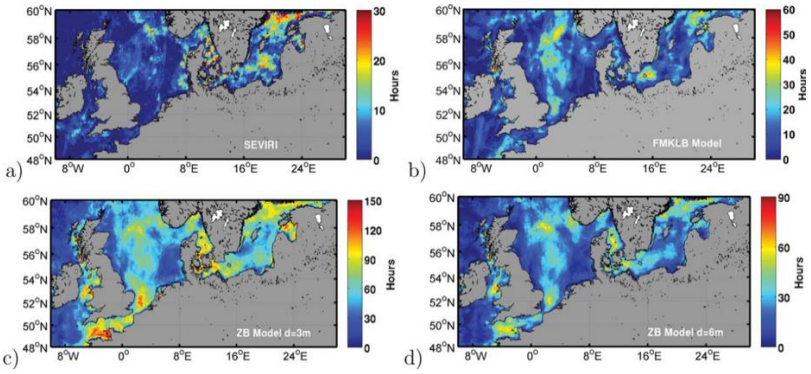

Figure 3: Spatial extent of warming exceeding 2 K from February 2009 to January 2010 from (a) SEVIRI and 3 models (b-d).

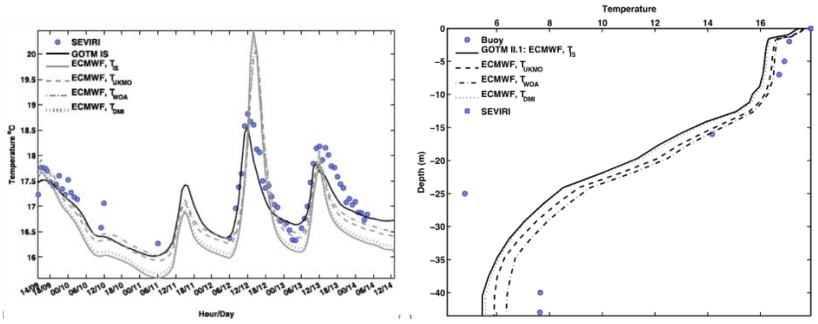

Figure 4: GOTM top layer temperature (solid), with in situ (black) or ECMWF (grey) forcing fields and SEVIRI (circles) sub-skin SST, 9-14 July 2013 (left). Vertical temperature from the measurements (circles), GOTM with ECMWF forcing fields (lines) and SEVIRI on 13 July 2013, 13:00 (right).

4. Conclusion

Diurnal variability in the North Sea and the Baltic Sea has been studied and characterised from SEVIRI SST retrievals. Attempts to model the spatial and statistical patterns of diurnal warming resulted in a candidate model to resolve the temperature profile in the upper few meters of the ocean, where thermal stratification is strong. This will be used within DIVOST-COM and the results are expected to provide insights regarding i) the MFCs' operational system skill to resolve the upper ocean thermal structure and potential weaknesses to be improved, ii) the depth where L4 SST foundation temperature products can be considered representative leading to their optimal assimilation from the MFC model systems and iii) the future ability of SST Thematic Assembly Centre (TAC) to improve the blended L4 products by adding a diurnal variability "layer" to the foundation SST. As demonstrated in [4] and [5], the Baltic Sea is prone to the diurnal variability of the upper ocean, which also has a direct impact on modelling and forecasting the events of algal blooms occurring in this semi-enclosed basin. The proposed project is also expected to support an improved reproduction of biological processes with a diurnal component, in all MFCs.

5. References

1. Deschamps P.Y., and Frouin R., Large Diurnal Heating of the Sea Surface Observed by the HCMR Experiment, *J. Phys. Ocean.* **14**, 177-184, 1984.
2. Cornillon, P., and Stramma, L., The distribution of diurnal sea surface temperature events in the western Sargasso Sea. J. Geophys. Res., **90** (C6), 11811-11815, 1985.
3. Otobe, H., and Asai, T., Heat balance of the upper ocean under a land and sea breeze in Sagami Bay in summer, *J. Ocean.,* **41** (5), 299-306, 1985.
4. Stuart-Menteth, A.C., Robinson, I.S., and Challenor, P.G., A global study of diurnal warming using satellite-derived sea surface temperature, *J. Geophys. Res.*, 108, C5, 3155, 2003.
5. Karagali, I., Høyer, J.L., and Hasager, C.B., SST diurnal variability in the North Sea and the Baltic Sea. *Rem. Sens. Env.,* 121, 159-170, 2012.
6. Karagali, I., and Høyer, J.L., Characterisation and quantification of regional diurnal SST cycles from SEVIRI. *Ocean Sci. Discuss.,* **11**, 1093-1128, 2014.
7. Fairall, C.W., Bradley, E.F., Godfrey, J.S., Wick, G.A., Edson, J.B., and Young, G.S., Cool-skin and warm-layer effects on sea surface temperature, *J. Geophys. Res. C Oceans,* **101** (1), 1295-1308, 1996.

8. Fallmann, J., Lewis, H., Castillo, J.M., Arnold, A., and Ramsdale, S., Impact of sea surface temperature on stratiform cloud formation over the North Sea, *Geophys. Res. Lett.*, **44**, 4296-4303, 2017.
9. Webster, P.J., Clayson, C.A., and Curry, J.A., Clouds, radiation, and the diurnal cycle of sea surface temperature in the Tropical Western Pacific. *J. Climate,* **9**, 1712-1730, 1996.
10. Ward, B., Near-surface ocean temperature. *J. Geophys. Res.,* **111**, C02004, 2006.
11. Bellenger, H., and Duvel, J.P., An analysis of ocean diurnal warm layers over tropical oceans. *J. Climate,* **22***,* 3629-3646, 2009.
12. Donlon, C., Robinson, I., Casey, K.S., Vazquez-Cuervo, J., Armstrong, E., Arino, O., et al., The Global Ocean Data Assimilation Experiment High-resolution Sea Surface Temperature Pilot Project. *Bull. Am. Met. Soc.*, **88** (8), 1197-1213, 2007.
13. Lips, I., and Lips, U., Abiotic factors influencing cyanobacterial bloom development in the Gulf of Finland (Baltic Sea). *Hydrobiologia,* **641** (1),133-140, 2008.
14. Takahashi, T., Sutherland, S.C., Sweeney, C., et al., Global sea-air CO 2 flux based on climatological surface ocean pCO_2 and seasonal biological and temperature effects. *Deep-Sea Research Part II-Topical Studies in Oceanography,* **49**, 1601, 2002.
15. Karagali, I., and Høyer, J.L., Observations and modeling of the diurnal SST cycle in the North and Baltic Seas*. J. Geophys. Res.-Oceans,* **118** (9), 4488, 2013.
16. Burchard, H., Bolding, K., and Villarreal, M.R., GOTM - A general ocean turbulence model. Theory, applications and test cases, Tech.Rep. EUR 18745 EN, 1999, Eur. Comm. Brussels, Belgium.
17. Karagali, I., Høyer, J.L., and Donlon, C.J., Using a 1-D model to reproduce the diurnal variability of SST. *J. Geophys. Resea.-Oceans,* **122** (4), 2945-2959, 2017.
18. Karagali, I., ESA STSE “SST Diurnal Variability: Regional Extend - Implications in Atmospheric Modelling”. Poster at ESA Living Planet Symposium 2016, Prague, Czech Republic, 2016.
19. Pimentel, S., Haines, K., and Nichols, N.K., Modeling the diurnal variability of sea surface temperatures*, J. Geophys. Res.,* **113**, C11004, 2008.

THE LAMPEDUSA CAL/VAL SITE: ASSESSING HEAT FLUCSES AND HIGH FREQUENCY SST ESTIMATES IN THE MEDITERRANEAN SEA

Salvatore Marullo(1), Alcide Di Sarra, Rosalia Santoleri, Daniele Ciani, Vincenzo Artale, Carlo Bommarito

(1*) ENEA, Italy, Email: salvatore.marullo@enea.it*

ABSTRACT

Estimates of air-sea radiative fluxes derived either from satellite or applying bulk formulae to meteorological parameters have been compared with direct measurements made at the ENEA Station for Climate Observations on the island of Lampedusa, in the central Mediterranean Sea. This climate observations station is a research facility dedicated to measurements of climatic parameters. Lampedusa is an integrated atmospheric/oceanic observatory composed by two sections: a ground-based laboratory operating since 1997, dedicated to the investigation of changes in atmospheric composition and structure and their effects on the surface radiation, and an oceanic buoy operating since 2015, dedicated to the investigation of air-sea interactions and to ground-truth of satellite observations. The instruments installed on the buoy include a Vaisala MAWS401 meteorological station and Kipp and Zonen CMP21 and CGR4 radiometers for shortwave and longwave irradiances. Water temperature is measured at 1 and 2 meters depth using two SBE 39 plus sensors acquiring with a frequency of 1 minute. The data collected at Lampedusa gave us the chance to evaluate various bulk formulae used to estimate turbulent and radiative heat fluxes, and various satellite products. The determination of radiation components have been investigated in particular showing an overestimation of the surface solar irradiance estimated from SEVIRI data and by bulk formulae currently used in Mediterranean GCM. The impact of these determinations on 1D numerical simulations of the upper ocean temperature vertical structure evolution have been also investigated and further demonstrated importance of using correct fluxes in reproducing sea surface and vertical temperature evolution.

ENSEMBLE SST AND AIR-SEA HEAT FLUX ESTIMATE

Hiroyuki Tomita

Institute for Space-Earth Environmental Research (ISEE)
Nagoya University, Japan, Email: tomita@isee.nagoya-u.ac.jp

1. Introduction

Sea surface temperature (SST) is an essential variable for determining surface turbulent heat fluxes. It is also used to estimate upward long-wave radiation flux from the surface. We here introduce ensemble median SST approach in a third-generation air-sea heat flux data set of the Japanese Ocean Flux Data Set with Use of Remote-Sensing Observations (J-OFURO3). Currently, there are many kinds of global SST products being used in numerous applications, including the estimation of surface heat flux. Moreover, each product has different spatial resolution and representative depth of SST. It is unclear which data set is most accurate or appropriate for air-sea flux estimation. J-OFURO3 adopts an ensemble median SST (EMSST) approach using data obtained from various global SST products.

2. Overview of J-OFURO3 satellite-derived air-sea flux estimates

J-OFURO3, satellite-derived air-sea flux data set, was constructed for 1988–2013 (Tomita et al. 2018, submitted). General feature of data set are summarized in Table 1. One of signature feature of J-OFURO3 is use of multi-satellite observations. Multi-micro wave radiometers and scatterometers were used to calculate daily air-sea turbulent heat flux. J-OFURO3 data are freely available from our web site: (https://j-ofuro.scc.u-tokai.ac.jp).

Table 1. Overview of J-OFURO3 satellite-derive air-sea flux data set

		J-OFURO3
Time period, temporal average		1988-2013, daily mean
Spatial grid size		0.25° x 0.25°
Sea surface temperature		Ensemble median product
Surface specific humidity	Algorithm	New algorithm (Tomita et al. 2018)
	Satellite sensor	SSMIs, SSMISs, AMSR-E, TMI, AMSR2
Surface wind speed	Satellite sensor	SSMIs, SSMISs, AMSR-E, TMI, WindSat, AMSR2, ERS-1&2, QuikSCAT, ASCAT-A/B, OSCAT
Flux data availability*		LHF, SHF, LWR, SWR, NHF, TAUX, TAUY, FWF

* LHF: latent heat flux, SHF: sensible heat flux, LWR: longwave radiation, SWR: shortwave radiation, NHF: net heat flux, TAUX/Y: zonal/meridional components of momentum flux, FWF: freshwater flux

3. J-OFURO3 ensemble SST product

J-OFURO3 SST was constructed by calculating ensemble statistics between 12 kinds of multi global SST data sets. The source products are listed in Table 2. Most of L4 data were obtained from the GHRSST framework. Since they have different spatial grid size, that was unified into the common 0.25 x 0.25 degree regular spatial grid system by linear interpolation method before the calculation. For the single microwave radiometer L3 products, twice-daily (ascending and descending) data are available. Therefore, we calculate the daily mean from them. The daily ensemble median value was used in calculation of J-OFURO3 turbulent heat flux. The ensemble statistics: average, spread (as standard deviation), minimum, maximum and number of product were also stored for the present study. As a result, we obtained 26-years (1988-2013) daily ensemble SST data set.

Figure 1 shows long-term mean of J-OFURO3 EMSST and ensemble spread. The overall features in global SST distribution are well; the large ensemble spread (> 1.0K) was found in the western boundary current (WBC) regions in the mid-latitude. This will be related to differences in spatial resolution among source data sets. In the sub-tropics to tropics, the spread is smaller than those in mild-latitude. In the high-wind regions, the spread is quite small. On the other hand, right wind region, the spread is relatively large. This looks reasonable because right-wind atmospheric condition may induce large differences of temperature among surface layer. Along the zonal lines near the 40N/S, there are artificial differences. This corresponds the region of TMI's observations. Global averaged daily spread is about 0.45K.

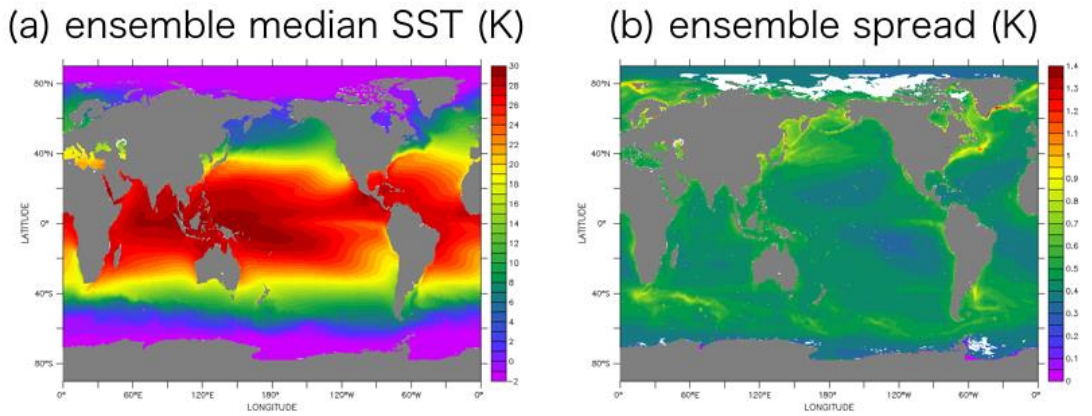

Figure 1. J-OFURO3 long-term mean (a) ensemble median SST and (b) daily spread.

4. Impact on turbulent heat flux

Figure 2 shows the maximum difference among the source products and its potential impact on turbulent heat flux. These were evaluated in the calculation of J-OFURO3 turbulent heat flux. The large differences were found in WBC regions, with the difference between the maximum and minimum estimate is about 120W/m^2. This implies that selection of SST product has large impact on flux estimation.

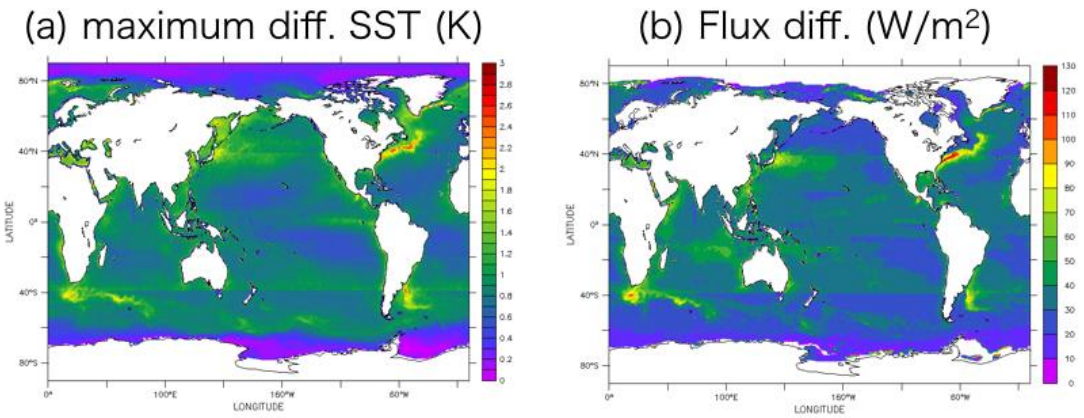

Figure 2: the maximum difference among source SST products (K) and its potential impact on turbulent heat flux (W/m^2).

Table 2 Source global SST products

Product name	Provider	Spatial grid size (°)	Level	Reference
MGDSST	JMA	0.25	L4	Kurihara et al. 2006
OSTIA-NRT	UKMO	0.05	L4	Donlon et al. 2012
OSTIA-RA	UKMO	0.05	L4	Robert-Jones et al. 2012
AMSR-E	RSS	0.25	L3	Wentz et al. 2014a
Microwave OI SST	RSS	0.25	L4	-
OISST (AVHRR)	NOAA	0.25	L4	Banzon et al. 2016; Reynolds et al. 2007
OISST(AVHRR+ AMSR)	NOAA	0.25	L4	
WindSAT	RSS	0.25	L3	Wentz et al. 2013
TMI	RSS	0.25	L3	Wentz et al. 2015
Global Tohoku SST	TOHOKU UNIV.	0.1	L4	-
AMSR2	JAXA	0.25	L3	-
AMSR2	RSS	0.25	L3	Wentz et al. 2014b

5. Summary

Ensemble SST from multi global products was adopted for global satellite-based air-sea heat flux estimation in J-OFURO3. Median and spread were calculated form 12 kinds of ensemble members for 1988–2013. Averaged daily spread is about 0.45 K. In the WBC regions, the spread is large. The impact of selection of SST product on air-sea flux estimation is quite large, with a maximum

difference of 120 W/m^2 in WBC regions. Comparison with in situ buoy observations, our ensemble approach provides more robust estimate of SST and Flux compared with use of single product.

6. References

Banzon V, Smith TM, Chin TM, Liu CY, Hankins W (2016) A long-term record of blended satellite and in situ sea-surface temperature for climate monitoring, modeling and environmental studies. Earth Syst Sci Data 8:165-176. doi:10.5194/essd-8-165-2016.

Donlon CJ, Martin M, Stark J, Roberts-Jones J, Fiedler E, Wimmer W (2012) The Operational Sea Surface Temperature and Sea Ice Analysis (OSTIA) system. Remote Sens Environ 116:140-158. doi: 10.1016/j.rse.2010.10.017.

Kurihara Y, Sakurai T, Kuragano T (2006) Global daily sea surface temperature analysis using data from satellite microwave radiometer, satellite infrared radiometer and in-situ observations. Weather Bull 73(special issue): 1-18 (in Japanese).

Reynolds RW, Smith TM, Liu C, Chelton DB, Casey KS, Schlax MG (2007) Daily high-resolution-blended analyses for sea surface temperature. J Clim 20(22). doi:10.1175/2007jcli1824.1.

Roberts-Jones J, Fiedler EK, Martin MJ (2012) Daily, global, high-resolution sst and sea ice reanalysis for 1985-2007 using the OSTIA system. J Clim 25(18). doi:10.1175/jcli-d-11-00648.1.

Tomita H, Hihara T, Kubota M (2018) Improved satellite estimation of near-surface humidity using vertical water vapor profile information. Geophys Res Lett, 45, doi: 10.1002/2017GL076384

Tomita H, Hihara T, Kako S, Kubota M, and Kutsuwada K, An Introduction to J-OFURO3, a Third-Generation Japanese Ocean Flux Data Set Using Remote-Sensing Observations, Journal of Oceanography (in revision)

Wentz FJ, Meissner T, Gentemann C, Brewer M (2014a) Remote Sensing Systems AQUA AMSR-E Daily Environmental Suite on 0.25 deg grid, Version 7.0 SST, WSPD, and VAPOR. Remote Sensing Systems, Santa Rosa, CA. Available online at www.remss.com/missions/amsre.

Wentz FJ, Ricciardulli L, Gentemann C, Meissner T, Hilburn KA, Scott J (2013) Remote Sensing Systems Coriolis WindSat Daily Environmental Suite on 0.25 deg grid, Version 7.0.1, SST, WSPD, VAPOR, and WDIR. Remote Sensing Systems, Santa Rosa, CA. Available online at www.remss.com/missions/windsat

Wentz FJ, Gentemann C, Hilburn KA (2015) Remote Sensing Systems TRMM TMI Daily Environmental Suite on 0.25 deg grid, Version 7.1, SST, WSPD and VAPOR. Remote Sensing Systems, Santa Rosa, CA. Available online at www.remss.com/missions/tmi.

Wentz FJ, Meissner T, Gentemann C, Brewer M (2014a) Remote Sensing Systems AQUA AMSR-E Daily Environmental Suite on 0.25 deg grid, Version 7.0 SST, WSPD, and VAPOR. Remote Sensing Systems, Santa Rosa, CA. Available online at www.remss.com/missions/amsre.

PLENARY SESSION VI: CALIBRATION/VALIDATION

INTER-CALIBRATION OF HY-1B/COCTS THERMAL INFRARED CHANNELS WITH METOP-A/IASI

Mingkun Liu [(1)], Christopher Merchant [(2)], Lei Guan [(3)], and Jonathan Mittaz [(4)]

(1) Department of Marine Technology, Ocean University of China, Qingdao, China
Department of Meteorology, University of Reading, Reading, UK
Email: liumingkun_ouc@126.com
(2) Department of Meteorology, University of Reading, Reading, UK
Email: c.j.merchant@reading.ac.uk
(3) Department of Marine Technology, Ocean University of China, Qingdao, China
Email: leiguan@ouc.edu.cn
(4) Department of Meteorology, University of Reading, Reading, UK
Email: j.mittaz@reading.ac.uk

1. Introduction

The Haiyang-1B (HY-1B) satellite, operated by the National Ocean Satellite Application Center (NSOAS) of the State Oceanic Administration (SOA) of China, was launched in April 2007. The main payloads on board HY-1B were the Chinese Ocean Color and Temperature Scanner (COCTS) and Coastal Zone Imager (CZI). The COCTS has 8 visible near infrared bands, named channel 1-8 (0.402-0.422 μm, 0.433-0.453 μm, 0.480-0.500 μm, 0.510-0.530 μm, 0.555-0.575 μm, 0.660-0.680 μm, 0.730-0.770 μm, 0.845-0.885 μm) for ocean color observations and 2 thermal infrared bands, named channel 9 (10.30-11.40 μm) and channel 10 (11.40-12.50 μm) used for measuring SST, with a spatial resolution of 1.1 km at nadir [1]. The Infrared Atmospheric Sounding Interferometer (IASI) is one of the payloads on board MetOp series satellites, mainly providing atmospheric emission spectra to derive humidity and temperature profiles, as well as SST, clouds, atmospheric trace constituents and land measurements [2]. IASI is a whiskbroom scanning instruments with scan angles of ±48.3°, including 30 effective fields of view (EFOV) in total. Each EFOV consists of a 2x2 matrix of instantaneous fields of view (IFOV), each IFOV having a spatial resolution of 12 km near nadir [2]. IASI measures the spectral radiance in 8461 channels, covering the spectrum from 3.63 μm (2760 cm^{-1}) to 15.5 μm (645 cm^{-1}) with a spectral binning of 0.25 cm -1 [2-3]. The IASI calibration has been proven to be accurate and stable Due to its hyperspectral nature and high-quality radiance measurements, IASI can serve as the reference for in-orbit re-calibration of other instruments.

In this study, we use IASI radiance as the reference to evaluate and correct HY-1B COCTS radiance of thermal infrared channels from 2009 to 2011in the region of 0°-48°N and 100°E-148°E. The data we used include the COCTS Level 1B (L1B) radiance data provided by NSOAS and IASI Level 1C (L1C) radiance data provided by EUMETSAT. The IASI L1C products are the geolocated, calibrated and apodized radiances, consisting of 8461 spectral samples every 0.25 cm^{-1} [5-8].

2. Inter-calibration method

IASI L1C radiance data include 8461 spectral samples in every pixel with a fixed spectral binning of 0.25 cm-1. The spectral ranges of COCTS thermal infrared spectral response functions (SRF)

for channel 9 and channel 10 are 9.50-12.50 μm and 10.50-13.50 μm respectively, both with a bin size of 0.002 μm. Due to the spectral resolution difference between IASI spectral radiance and COCTS SRFs, linear interpolation is used to generate COCTS spectral response value at each IASI radiance samples. Then, the IASI-convolved radiance corresponding to COCTS SRFs could be calculated using equation (1) as follows, where subscript i indicates COCTS thermal infrared channel number, $L(\lambda)$ is the IASI spectral radiance, $S_i(\lambda)$ is the COCTS spectral response, and λ_1 and λ_2 are COCTS bandpass boundary values. According to the COCTS and IASI spatial resolution of 1 km and 12 km near nadir respectively, COCTS and IASI-convolved radiance are projected to equal-angle maps in the research region (0°-48°N and 100°E-148°E) with the grid size of 0.01° and 0.12° respectively. The collocations of COCTS and IASI radiance data are generated with a spatial window of 0.12°, a temporal window of 0.5 h and an atmospheric path tolerance of 3%. We use the relative standard deviation, that is the standard deviation/mean of the COCTS valid pixels inside each IASI IFOV, to quantify the homogeneity. We also use a perimeter region outside the central collocation area to reduce the likelihood of time variable components such as errors caused by differences in the cloud and/or clear distributions in a similar way.

$$L_i = \frac{\int_{\lambda_1}^{\lambda_2} L(\lambda) S_i(\lambda) d\lambda}{\int_{\lambda_1}^{\lambda_2} S_i(\lambda) d\lambda} \quad (1)$$

3. Comparison of COCTS radiance with IASI

Based on these 13353 filtered matchups presented in Section 2, COCTS radiance from channel 9 and channel 10 are compared with IASI. The overall statistics of COCTS with IASI radiance indicate large cold biases of -6.35 mW m^{-2} cm sr^{-1} and -7.56 mW m^{-2} cm sr^{-1}, with the corresponding standard deviations of 0.96 mW m^{-2} cm $sr^{-1}$and 0.63 mW m^{-2} cm sr^{-1}. For COCTS channel 9 and channel 10, both radiance differences represent approximately linear dependence on radiance. The difference for COCTS channel 9 more obviously depends on scene radiance than for channel 10. For channel 9, the mean value of radiance difference is about -3.3 mW m^{-2} cm sr^{-1} when radiance is around 70 mW m^{-2} cm sr^{-1}, becoming around -7.4 mW m^{-2} cm sr^{-1} when the IASI radiance is about 110 mW m^{-2} cm sr^{-1}. The radiance difference of channel 10 has a less-strong dependence on IASI radiance, spanning roughly -7 mW m^{-2} cm sr^{-1} to -8 mW m^{-2} cm sr^{-1} over the matchup range.

There is distinct striped noise with a pattern approximately repeating every four scan lines in COCTS radiance image, due to the inconsistency between four parallel detectors. To estimate the measurement difference between different detectors, the COCTS pixels inside each IASI IFOV measured by individual detectors are averaged separately. Then, the COCTS radiance from four detectors (called detector 1, detector 2, detector 3, and detector 4 thereafter) are compared with IASI separately. Figure 1 represents the comparisons of COCTS radiance measured by four individual detectors with IASI radiance. For channel 9, the comparison results show smaller difference between adjacent detectors with the maximum difference of 0.22 mW m^{-2} cm sr^{-1} corresponding to detector 3 and detector 4. However, for channel 10, both the variation plots and the statistics results indicate the difference between adjacent detectors are larger than channel 9 in the whole radiance range, that is consistent with more obvious striped noise shown in COCTS channel 10 radiance image.

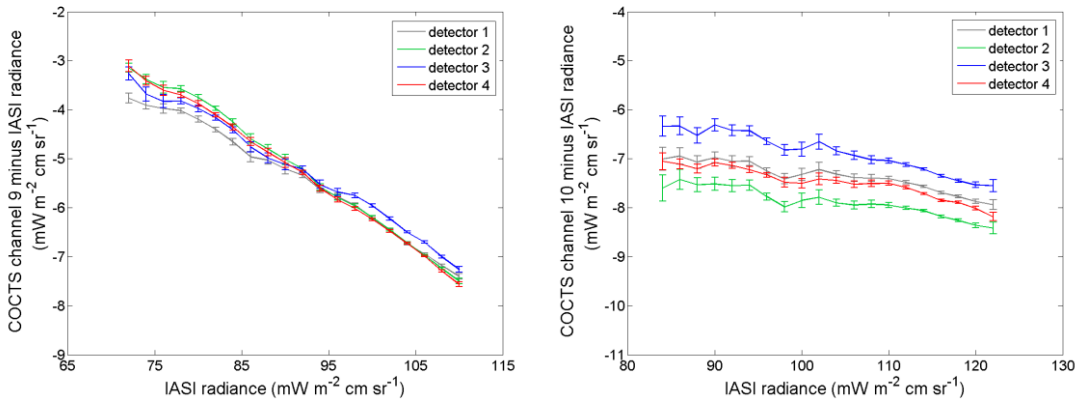

(a) (b)

Figure 1. The variations of COCTS channel 9 (a) and channel 10 (b) radiance measured by four detectors (gray line: detector 1; green line: detector 2; blue line: detector 3; red line: detector 4) minus IASI radiance difference against IASI radiance

4. Calculation of coefficients for COCTS radiance correction

The coefficients of COCTS radiance correction are obtained based on the filtered matchups of COCTS with IASI radiance. We use the robust linear regression to obtain the slope a and offset b of the relationship between COCTS minus IASI radiance difference and IASI radiance, represented as the equation (2) as follows:

$$L_{COCTS} - L_{IASI} = a \times L_{IASI} + b \quad (2)$$

$$L_{COCTS'} = \frac{L_{COCTS} - b}{a+1} \quad (3)$$

where theL_{COCTS} and L_{IASI} represent the IASI and COCTS source radiance respectively. The corrected COCTS radiance $L_{COCTS'}$ could be calculated using equation (3). A randomly selected subset, 2/3 of the whole matchup dataset, is used for regression and the remaining 1/3 are used for validation.

5. Validation of COCST corrected radiance

The comparison results of COCTS channel 9 and channel 10 corrected radiance with IASI are shown as figure 2. The large biases between COCTS source radiance and IASI radiance are removed after correction, with the value of -0.02 mW m^{-2} cm sr^{-1} and -0.01 mW m^{-2} cm sr^{-1} for channel 9 and channel 10 respectively. For channel 9, the significant radiance-dependent pattern of radiance difference is corrected, with the reduced overall standard deviation from 0.95 mW m^{-2} cm sr^{-1} to 0.51 mW m^{-2} cm sr^{-1}. A reduction in the bias and standard deviation between the COCTS and IASI is also seen for channel 10. In addition, after the correction of COCTS source radiance using individual coefficients for four detector measurements, the striped noise shown in corrected COCTS radiance images is reduced, with smoother variations along track, demonstrating that the inter-calibration method in this study is useful in some extent for COCTS striped noise elimination. After inter-calibration, the noise level in both channels are decreased, and the improvement of channel 10 is greater than channel 9, mainly due to the much distinguishable difference between neighbor detectors of channel 10. The radiance inter-calibration does not fully eliminate apparent

striping, presumably because of residual error or temporal evolution of the calibration differing between detectors. Nonetheless, the improvements of COCTS radiance accuracy after inter-calibration are essential for improved SST retrieval from COCTS, which will be the topic of future work.

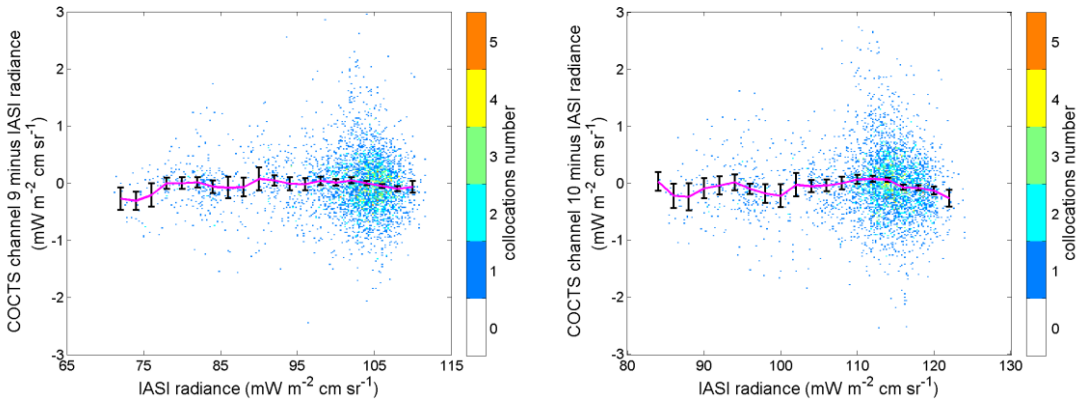

(a) (b)

Figure 2. The variation of COCTS channel 9 and channel 10 minus IASI radiance against IASI radiance after correction

6. Conclusion

In this study, the COCTS radiances from thermal infrared channels are inter-calibrated with IASI in the northwest Pacific region during the period from 2009 to 2011. The comparison results indicate that the mean values of COCTS channel 9 and channel 10 radiance minus IASI radiance difference are -6.35 mW m^{-2} cm sr^{-1} and -7.56 mW m^{-2} cm sr^{-1}, with the corresponding standard deviations of 0.96 mW m^{-2} cm sr^{-1} and 0.63 mW m^{-2} cm sr^{-1} respectively. In addition, the radiance difference between COCTS and IASI is radiance-dependent for both channel 9 and channel 10 with a stronger dependence in the channel 9 radiance difference with IASI radiance than channel 10.

The inter-calibration coefficients are obtained using linear robust regression for COCTS individual detectors separately. After correction, the mean values of COCTS minus IASI radiance difference are -0.02 mW m^{-2} cm sr^{-1} and -0.01 mW m^{-2} cm sr^{-1} respectively, with the corresponding standard deviations of 0.51 mW m^{-2} cm sr^{-1} and 0.57 mW m^{-2} cm sr^{-1}. Both mean values of COCTS channel 9 and channel 10 corrected BTs minus IASI are -0.01 K, with the corresponding standard deviations of 0.33 K and 0.35 K respectively. Compared with COCTS source radiance statistic results, the biases are removed and the standard deviations are reduced, and the dependence of radiance difference on IASI radiance is disappeared after correction. The significant striped noise of COCTS source radiance is reduced, which is evident in imagery and distributions of local standard deviation. In conclusion, several strands of evidence indicate the calibration accuracy of COCTS is improved after the correction. In a future study, the COCTS corrected radiance will be applied to SST retrieval in the expectation that this will improve the COCTS SST accuracy.

7. References:

[1] Pan, D. Future-generation satellites of Chinese ocean remote sensing. Proc. SPIE Sensors, Systems, and Next-Generation Satellites VIII. 2004, 5570, 228-233, DOI: 10.1117/12.563894.

[2] EUMETSAT. IASI Level 1: Product Guide; EUMETSAT: Darmstadt, Germany, 2017; EUM/OPS-EPS/MAN/04/0032, v4D

[3] Hilton, F.; Armante, R.; August, T.; Barnet, C.; Bouchard, A.; Camy-Peyret, C.; Capelle, V.; Clarisse, L.; Clerbaux, C.; Coheur, P.F.; Collard, A.; et al. Hyperspectral Earth observation from IASI: Five years of accomplishments. Bull. Am. Meteorol. Soc. 2012, 93, 347-370, DOI: 10.1175/BAMS-D-11-00027.1.

[4] Hewison, T.J.; Wu, X.; Yu, F.; Tahara, Y.; Hu, X.; Kim, D.; Koenig, M. GSICS inter-calibration of infrared channels of geostationary imagers using Metop/IASI. IEEE Trans. Geosci. Remote Sens. 2013, 51, 1160-1170, DOI: 10.1109/TGRS.2013.2238544.

[5] Blumstein, D.; Chalon, G.; Carlier, T.; Buil, C.; Hebert, P.; Maciaszek, T.; Ponce, G.; Phulpin, T.; Tournier, B.; Simeoni, D.; Astruc, P.; et al. IASI instrument: Technical overview and measured performances. In Infrared Spaceborne Remote Sensing XII. 2004, 5543, 196-208, DOI: 10.1117/12.560907.

[6] Blumstein, D.; Tournier, B.; Cayla, F.R.; Phulpin, T.; Fjortoft, R.; Buil, C.; Ponce, G. In-flight performance of the Infrared Atmospheric Sounding Interferometer (IASI) on METOP-A. In Atmospheric and Environmental Remote Sensing Data Processing and Utilization III: Readiness for GEOSS. 2007, 6684, DOI: 10.1117/12.734162.

[7] Blumstein, D.; Pequignot, E.; Buffet, L.; Buil, C.; Hebert, P.; Larigauderie C.; Phulpin, T.; Camy-Peyret, C.; Simeonii, D. 2009. The IASI instrument. Proc. ECMWF/EUMETSAT Workshop on The Assimilation of IASI in NWP. Available online: https://www.ecmwf.int/sites/default/files/elibrary/2009/8249-iasi-instrument.pdf.

[8] Wang, L.; Goldberg, M.; Wu, X.; Cao, C.; Iacovazzi, R.A.; Yu, F.; Li, Y. Consistency assessment of Atmospheric Infrared Sounder and Infrared Atmospheric Sounding Interferometer radiances: Double differences versus simultaneous nadir overpasses. J. Geophys. Res.: Atmospheres. 2011, 116(D11), DOI: 10.1029/2010JD014988.

USING SAILDRONE AUTONOMOUS IN SITU DATA FOR SATELLITE VALIDATION AND RESEARCH INTO UPPER OCEAN PHYSICS

Chelle Gentemann[(1)], Peter Minnett, Peter Cornillon, Richard Jenkins

(1*) Earth & Space Research, USA, Email: leiguan@ouc.edu.cn*

Abstract

The objective of this work is to determine the utility of Saildrone measurements for satellite SST validation. There are currently only 2 research
instruments regularly retrieving skin SST for satellite skin SST validation, ISAR (Donlon et al., 2008) and (Marine-Atmosphere Emitted Radiance Interferometer) M-AERI (Minnett, et al., 2001). While these provide extremely valuable observations, they are mostly limited to ships-of-opportunity and semi-permanent deployments on repeat cruise track ships. Saildrone provides the opportunity to measure skin SST at a lower cost with sampling of a broader range of environmental conditions. Saildrone measurements of skin SST, bulk SST, and wind speed will be used to for validation of GOES-R, VIIRS, MODIS, GMI, and AMSR-2 satellite SSTs. Satellite SSTs will be collocated with Saildrone measurements to determine how satellite SST uncertainty depends on environmental conditions. Using multiple sensors in a triple collocation analysis will provide a valuable estimate of both the accuracy of Saildrone and satellite observations (Gentemann, 2014). Five annual Arctic cruises are planned for 2019 - 2022, specifically oriented towards satellite validation. Initial results from a 60-day deployment in Spring 2018 will be presented.

INFERENCE FROM DISTRIBUTIONS OF DIFFERENCE IN SEA SURFACE TEMPERATURE VALIDATION DATAA

Christopher Merchant

University of Reading, UK, Email: c.j.merchant@reading.ac.uk

Abstract

Distributions of difference between satellite sea surface temperature (SST) and in situ SST measurements are used to assess the bias and precision of satellite SSTs, and also to validate uncertainty estimates. Difference distributions are generally not normally distributed, with supra-gaussian tails, both warm and cold. Heavy cold tails are often interpreted as a symptom of residual cloud contamination and/or biassing of SST retrievals by unaccounted-for atmospheric aerosols. Standard statistics (mean and standard deviation) and outlier-robust statistics (median and scaled median-absolute-deviation) are often calculated as part of validation. The standard and robust statistics would be identical for a normal distribution, and disagreement between standard and robust statistics give an indirect measure of the degree to which cold and/or warm tails are present in the difference distribution. It is shown that an alternative approach is to fit a six-parameter model to the validation data, comprising two parameters quantifying the centre and spread of the main distribution, and two parameters quantifying the relative weight and scale of each tail, warm and cold. The fitting can be practically achieved by Markov chain Monte Carlo methods. The tail parameters more directly describe the importance of large differences to the overall distribution. Coherent interpretations of the cold tail parameters in particular can be made in terms of the relative rates of residual cloud and aerosol contamination in different SST products. This offers a means, for example, to quantify more objectively the impact of improved cloud screening on SST products.

PLENARY SESSION VII: SLSTR

THE SENTINEL-3 TANDEM MISSION

Craig Donlon

ESA, The Netherlands, Email: craig.donlon@esa.int

Abstract

Recognising that, even though S3A and S3B are identical in design, it is expected that differences in performance of payload instruments will exist due to subtle differences and tolerances of materials, manufacture and pre-flight characterisation. A clear and justified scientific basis to fly a limited duration Sentinel-3A and Sentinel-3B (and furthermore Sentinel-3C and Sentinel-3D) "Tandem Mission" during the Phase-E1 commissioning has been developed:

- To increase knowledge of Sentinel-3 constellation payload differences
- To reduce uncertainties when comparing data from different satellite missions within the constellation
- To homogenise differences within the Sentinel-3 constellation payload by defining appropriate adjustments

The S3 Tandem Phase has a duration of 4-6 months has been implemented during which Sentinel-3A and 3B will be separated by 30s in time. This approach limits uncertainty due to ocean geophysical and atmospheric/ionospheric space and time variability: both issues introduce uncertainty into the direct inter-calibration of S3A and S3B. However, by flying S3A and S3B in tandem separated by ~30 seconds on the same ground track (±1 km) the correlation between these uncertainties is maximised. This presents a near ideal situation where:

- Optical instruments can view the same area, almost simultaneously, allowing direct comparisons of the data from the two satellites.
- A statistically significant set of data will be available in a short period of time over many surfaces.
- Instruments can be operated in different modes (eg. altimeter SAR and LRM) at the same time.

This presentation will review the basis, implementation and progress of the S3 tandem mission.

MONITORING AND EVALUATION OF SST PRODUCTS IN THE EUMETSAT METIS FRAMEWORK: A YEAR OF S3A SLSTR DATA AND PREPARATION FOR S3B

Prasanjit Dash(1), Anne O'Carroll, Igor Tomazic, Jean-Francois Piolle, Gary Corlett, Craig Donlon

(1*) NOAA NESDIS STAR, GST Inc., and affiliate CSU CIRA, Email: prasanjit.dash@noaa.gov*

Abstract

Modern dual-viewing-sensors provide an enhanced potential over traditional nadir-viewing-sensors for SST-retrievals by *Design* and *Physics*. The dual-viewing-ability comes from conical radiometers, a flagship European design since the ERS-1/ATSR. The latest in this line-of-sensors, an SLSTR, flies onboard the Copernicus Sentinel-3A and will be complemented soon by Sentinel-3B. Sensor design is a major engineering challenge. Scientific challenges include *inverse-algorithm*, *cloud-detection* and *routine product-evaluation*. SLSTR SST-products at native-resolution were released operationally by EUMETSAT on 5-July-2017. *In-situ* matches are generated employing the Felyx system. These products undergo incremental improvements by EUMETSAT/partners and include future additions, *e.g.*, Bayesian-cloud-mask. Similar activities are foreseen for S3B. The final distribution-type is called as Water-Surface-Temperature (WST) in GHRSST L2P-format, an agglomerate of five different internal-products that optimize the use of combining different channels and view-angles: Nadir-2-channel, Nadir-3-channel, Nadir-3-channel aerosol robust, Dual-View-2-channel and Dual-view-3-channel. Agglomeration is based on a conditional ranking to find the best WST combination. To routinely evaluate WST/WCT products and assess processor-changes, the Monitoring and Evaluation of Thematic Information from Space (METIS) system was set up: one *public* and one *internal*. The public METIS-SST monitors SSTs from S3A-SLSTR and Metop-B IASI/AVHRR: *http://metis.eumetsat.int/sst/*. The concept was motivated by NOAA-SQUAM but focusses on EUMETSAT-products and offers 15 additional RoIs in addition to global diagnostics. The internal METIS-SST monitors WCT/WST products, jointly, stratified by QFs and using/ignoring of SSES bias in the global domain. Results of METIS-SST diagnostics and evolution of S3A-SSTs approximately during the past one year will be highlighted. Also, extension *plans* for S3B will be briefed.

AN OPEN-SOURCE CAL/VAL ENVIRONMENT AND ITS APPLICATION TO SENTINEL-3A SLSTR

Jean-François Piollé[(1)], Igor Tomazic, Anne O'Caroll

(1) *Ifremer, France, Email: jfpiolle@ifremer.fr*

Abstract

To support the Sentinel-3 mission cal/val, a dedicated platform has been implemented at Eumetsat, to which users can remotely connect to analyse the data from all Sentinel-3A instruments (SLSTR, OLCI and SRAL). A framework was designed and deployed onto this platform to enable the Cal/Val activities, based on complete open-source solutions. The work was mainly focused on the SLSTR instrument, but the framework was prepared as a multi-sensor and multi-mission framework from its inception. It addresses, through different open-source off-the-shelf tools, functions such as:

- The management of the platform configuration itself, software deployment, source control and processing environments (using ansible, gitlab).
- The management and control of automatic dataflows (collecting the necessary input data, as well as required reference or complementary datasets) and workflows (automated background operations) (using airflow).
- The interactive remote processing of data through tools like Jupyter, or distributed processing over several virtual machines (using celery).
- The generation of satellite to in situ match-up databases and satellite to satellite cross-overs (using indexing tools felyx and naiad) based on third party "big data" technologies (using ElasticSearch).
- the production of monitoring products and diagnostics

This presentation will give a brief overview of the various technologies used here and their practical application to the assessment and monitoring of SLSTR data.

INDEPENDENT VALIDATION OF SENTINEL 3A SLSTR SEA SURFACE TEMPERATURE PRODUCTS

Gary Corlett

University of Leicester, UK, *Email: gkc1@leicester.ac.uk*

Abstract

Sea surface temperature (SST) estimation from space-borne infrared (IR) radiometers provides essential data for operational weather and ocean forecasting as well as long-term climate change assessment. The first Sea and Land Surface Temperature Radiometer (SLSTR) was launched in February 2016 on the European Commission's Copernicus Sentinel 3A satellite. The SLSTR instrument is a highly-stable self-calibrating, IR, near-infrared and visible, dual-view radiometer, designed to provide accurate global SST measurements with an accuracy of better than 0.3 K (one sigma).

The data collected from the SLSTR instrument is routinely processed by EUMETSAT as part of the Copernicus ground segment. SLSTR skin SSTs are estimated using retrieval coefficients derived from a linear regression of SST to modelled brightness temperatures (BTs) in three spectral bands with nominal band centres at 3.7 µm, 11 µm and 12 µm.

An intensive SST validation programme is in operation that involves validating retrieved SLSTR SSTs against independent measurements taken in situ from drifting buoys, moored buoys and Argo profiling floats. In addition, SLSTR has been routinely compared to operational SST analyses and measurements of SST from other satellite sensors.

This presentation will summarise SLSTR SST validation activities so far and will show that SLSTR is currently meeting its objective to determine accurate global SST measurements to within 0.3 K (one sigma). The requirement of having multiple long-term validation data sets is emphasised to avoid incorrect conclusions on product accuracy.

SENTINEL 3A SLSTR SST VALIDATION USING A FIDUCIAL REFERENCE MEASUREMENT (FRM) SERVICE

Werenfrid Wimmer[(1)], Tim Nightingale, Jacob Høyer, Jean-Francois Piolle, Hugh Kelliher, Steffen Dransfeld

(1) *University of Southampton, UK, Email: w.wimmer@soton.ac.uk*

Abstract

Building on the International Shipborne Radiometer Network (ISRN) and FRM4STS, ESA has established a validation service, the International SST FRM Radiometer Network (ISFRN), to provide fiducial reference measurements to the SST community. The ISFRN includes partners from the UK (University of Southampton, Rutherford Appleton Laboratory, Space ConneXions), Denmark (Danish Meteorological Institute) and France (Ifremer) and will not only collect Shipborne radiometer data but also use the data to validate SLSTR and other satellite SST products with the Felyx MDB tool. Included in the service is a long term data archive of the FRM datasets at Ifremer where the data will be stored in the ISFRN netCDF L2R format. We will show examples of the ISRFN data and demonstrate its use with SLSTR validation results in the ISFRN network regions.

ASSESSMENT OF SLSTR L2P SST DATA AS INPUT TO THE CMEMS MED L3S/L4 MULTISENSOR OPERATIONAL SYSTEM

Rosalia Santoleri[(1)], Andrea Pisano, Bruno Buongiorno Nardelli, Cristina Tronconi

(1) *CNR-ISAC Roma, Italy, Email: rosalia.santoleri@artov.isac.cnr.it*

Abstract

Since the launch of Sentinel-3A, continuous effort has been dedicated to the assessment of SLSTR data in order to improve ocean surface temperature estimates. The latest version of the L2P SST product (v.2.18) has been integrated in the CMEMS CNR processing chain to build daily (nighttime) merged multi-sensor (L3S) and interpolated (L4) SST fields for the Mediterranean Sea. A first analysis, performed on SLSTR L2P product alone, evidenced a noticeable and persistent bias at the edges of the oblique-view, thus requiring to split the SLSTR dual and nadir view *SST* estimates. In addition, since the SST variable is representative of the skin temperature, SLSTR L2P SST data are corrected to the foundation temperature by adding 0.2 °C. Then, a careful assessment through inter-comparison exercises with different dual- and nadir-view configurations in the operational chain has been carried out and results validated against co-located surface drifting buoy measurements. The validation covers 9 months, from July 2017, beginning of SLSTR L2P data availability, to March 2018. Preliminary results show that the best accuracy (bias and root-mean-square error) of the output L3S/L4 SST products is achieved by using the dual-view as reference and the nadir-view as last (in the sensor hierarchy). Further assessment will be carried as soon as the improved SLSTR L2P SST product with the Bayesian cloud mask will be available.

PLENARY SESSION VIII: SST PRODUCTS

SESSION VIII REPORT

Chair: Helen Beggs[(1)] – Rapporteur: Jacob Høyer[(2)]

(1) Bureau of Meteorology, Australia, Email: helen.beggs@bom.gov.au
(2) Danish Meteorological Institut, Denmark, Email: jlh@dmi.dk

Minutes from presentations and discussions

Title: OSI SAF Sea Surface Temperature reprocessing of MSG/SEVIRI archive.

Presenter: Stéphane Saux Picart:

- Reprocessed the SEVIRI/MSG archive for 2004 - 2012
- Used the nonlinear algorithm using OSTIA derived climatology
- Cloud mask from CM SAF
- Process 15 minutes slots and aggregate into hourly
- Sensitivity High in most of domain, some areas with low or too high sensitivity
- Saharan Dust Index (SDI) used from Merchant et al. (2006) and added a term in the night time retrieval
- Standard algorithm shows regional biases so they have used the bias correction algorithm from Leborgne et al. (2011)

- Assessment:
  a) Use the ERA climatology dataset (2014)
  b) QL 345: Bias almost zero and stddev consistently below 0.5 degrees
  c) Temporal stats: stable and homogeneous in time.
  d) Assessment following the CDAF framework:
     i) Global median of SAT-in situ
     ii) Geographical effects: STD of median computed for spatial scales of 1000 km
     iii) These above show the bias correction to be working very well.
     iv) Stability: used moored buoys from GTMBA: about 4 mk/year, but limited number of moored buoys
  e) Diurnal warming events: also captured in the data set
  f) L3C available on Ifremer FTP server (see http://osi-saf.eumetsat.int) and L2P on demand. Matchup dataset can be shared.

Question (Sasha Ignatov): Do you see any discontinuities in Diurnal cycle due to different algorithms?

Answer (Stephane Saux Picart)**:** No, we are using same algorithm day and night

Sasha: What is the fraction of clear sky pixels ?

Answer (Stephane)**:** I do not know

Question (Sasha): Have you looked at the sharpness of the image ? How well are the gradients represented ?

Answer: (Stephane): No we have not. As they are very difficult to evaluate

Question (Chris Merchant): 4 mk/year longterm trend: Very small, where does it come from ?

Answer (Stephane): I do not know, it may be dust

Question (Chris): What about the 3.9 channel ?

Answer: (Stephane): We do not use the 3.9 time channel as it is sensitive to various contamination: solar, and sensor ice.

Title: ACSPO hourly SST Products from GOES-R/ABI & Himawari-8/AHI

Presenter: Irina Gladkova:

- Motivation: New generation geostationary satellites provide many data, so users want collated product.
- Several options to composite and collate: temporal/spatial subsampling.
- Here: Hourly "L2C" is produced from all L2P files
- Coverage increase: about 40 % for the ABI.
- Cloud masking issues:
  a) Current ASCPO has cloud leakage and false alarms
  b) Collated product reduces these effects

- Main steps of L2C approach:
  a) Initial cloud mask as 1st guess
  b) Remove residual cloud leakages based on temporal information
  c) Estimate diurnal resolved information.
  d) Used slowly varying curve in time to screen out data
  e) Additional cloud screening forward and backward screening works very well.
  f) Cloud screening also removes the “warm clouds”, which are probably a retrieval artefact.

- Compared with L2P, the L2C has better coverage and higher spatial resolution features
- Examples show good performance: better coverage and less cloud leakages.

The performance is monitored in SQUAM (https://www.star.nesdis.noaa.gov/sod/sst/squam/), showing good performance with lower standard deviations than for L2P.

- Collated from brightness temperatures, which is better than collation from L2P SSTs.
- Hourly L2C maps are now available in ARMS (https://www.star.nesdis.noaa.gov/sod/sst/arms/geo.php) for selected highly dynamic regions.

Question (Chris Merchant): Nice to see the temporal resolution: The examples with warm clouds is interesting. Is it diurnal warming you are removing?

Answer (Irina): Not in this particular case, as I have looked into it.

Title: Consistent Line of ACSPO L3U SST Products

Presenter: Matthew Pennybacker

- Initial L2P product, but a lot of data and users asked for L3U
- L3U: 0.02 degrees and only 0.45 GB per day, compared to 26 GB/day
- Current operational version running is using BOM code to get L3U
- ASCPO 2.6: (will be implemented in near future)
  a. Like the VIIRS product, L3U at 0.02 degrees
  b. Uniform across all algorithms/sensors
  c. Include a feature preserving up-sampling for coarse resolution sensors with native resolution lower than 0.02 degree grid.
- L3U: all product sizes are decreased with L3, compared to original L2P.
- Algorithm (Bilateral filtering): Each pixel is a weighting of the neghboring pixels, with weighting determined by sensor noise levels sensor resolution and empirical to minimize frontal displacements.
- Each sensor has its own parameters for the bilateral filtering
- L2P QL, flags, SSES bias and SSES standard deviations are also preserved in the gridding.
- Metop down-scaled "GAC" AVHRR L3U compares well with FRAC AVHRR L3U data
- Examples comparing the old and new L3U products show good improvements.
- Sample imagery: Show consistent SST products across all sensors for example in Baja ,California
- Mean is comparable and stddev is reduced for L3U compared to L2P (for all sensors.
- Satellites: MODIS, Metop FRAC A+B, AHI, ABI, NOAA 18 + 19.
- Reanalysis: In the process of generating reanalysis for all
- Future: Explore 0.01 degree regional L3U, L3C and L3S products, as well as 0.02 degree L3C/L3S.

Question: (Peter Cornillon): Have you considered the spatial sprectrum of the reconstructed fields?

Answer (Matthew): No, focus has been on the validation statistics against in situ observations and not the quantitative assessment yet.

Question (Chris Merchant): Why are you doing upscaling ? is there a risk that the users misuse the product?

Answer (Sasha Ignatov): Users want consistent products that are easy to use with same spatial resolution.

Question (Helen Beggs): I am surprised that you are regridding the AVHRR GAC observations to higher resolution. We have done this for HRPT AVHRR products because users want the gridded products. You have to be a bit careful. Maybe keep them in-house and put them into an L3S product.

Answer (Sasha Ignatov): I was personally very skeptical about this upscaling product, but we are doing samples which appear to work well.

Question (Craig Donlon): Interesting discussion. Understand why you are doing this, but I will agree with Chris. Is there not a double interpolation (collation) going on here?

Answer (Ignatov): We are producing the L3U because the users want reduced data volumes.

Question (Donlon): Should the space agencies stop producing these high-resolution data?

Answer (Chelle): No because of the improved cloud information.

Answer (Irina): Reply to Chris: Users take MUR and apply their frontal analysis on this products. So we have many users. We have had a lot of debate within group whether to show this to users or not. We decided to be fully transparent.

Question (Alexey Kaplan): Are there uncertainties coming together with this L3U? and are they adequate ?

Answer (Ignatov): There is a community that wants high resolution products (1 km) so we are considering a 0.01 degree product. We do not say that one size fits all. We have been focusing upon L4 producers but fisheries and coastal managers have other requirements.

Answer (Irina) We do provide the uncertainties as SSES stddev.

Comment (Andy Harris): We have had this discussion before. Issue with upsampling is that one pixel can be turned into 8 pixels. It needs thinking about how you do this correctly. This should be an actitivity within the GHRSST.

ACTION: consider a task team to look at the L3 collation

OSI SAF SEA SURFACE TEMPRATURE REPROCESSING OF MSG/SEVIRI ARCHIVE

Stéphane Saux Picart[(1)], Anne Marsouin, Gérard Legendre, Sonia Péré, Hervé Roquet

(1) Météo-France, Email: stephane.sauxpicart@meteo.fr

Abstract

The Ocean and Sea-Ice Satellite Application Facility (OSI-SAF) of the European Organisation for the Exploitation of Meteorological Satellites (EUMETSAT) has performed a reprocessing of Sea Surface Temperature (SST) from Spinning Enhanced Visible and Infrared Imager/Meteosat Second Generation (SEVIRI/MSG) archive (2004-2012).

The retrieval method consists in a non-linear split-window algorithm and the algorithm correction scheme developed by Le Borgne et al. (2011). The algorithm correction relies on simulations of infrared brightness temperatures performed using Numerical Weather Prediction model atmospheric profiles of water vapour and temperature, and RTTOV radiative transfer model.

The cloud mask used is the Climate SAF reprocessing of the MSG/SEVIRI archive. It is consistent over the period considered.

Atmospheric Saharan dusts have a strong impact on the retrieved SST in the Atlantic and Mediterranean regions, they are taken into consideration through the computation of the Saharan Dust Index (Merchant et al., 2006) which is then used to determine an empirical correction applied to SST.

The reprocessing has benefited from experiences of the OSI SAF team in operational near real time processing of MSG/SEVIRI data, and the methods have been improved to provide a higher quality SST. The MSG/SEVIRI SST reprocessing dataset consist in hourly level 3 composite of sub-skin temperature projected onto a regular 0.05° grid over the region 60N,60S and 60W,60E. It has been thoroughly validated against drifting buoys and moored buoys using the ERA Clim dataset.

This presentation gives an overview of the data and methods used for the reprocessing, and some of the validation results obtained.

ACSPO HOURLY SST PRODUCTS FROM GOES-R/ABI & HIMAWARI-8/AHI

Irina Gladkova[1,2,3], Alexander Ignatov[1], Matthew Pennybacker[1,3], Olafur Jonasson[1,3], Yury Kihai[1,3]

(1) NOAA/STAR, College Park, USA Email: irina.gladkova@gmail.com
(2) City College of New York, New York, USA
(3) Global Science and Technology Inc., College Park, USA

1. Introduction

Frequent looks at the same ocean domain from the new generation geostationary sensors, ABI and AHI (every 10/15 min), makes temporal consistency analyses a more efficient and accurate way to differentiate slowly changing ocean features from faster-moving clouds. A new algorithm has been implemented in the NOAA Advanced Clear-Sky Processor for Ocean (ACSPO) v2.60, based on a combination of various time-space windows, to improve clear-sky identification. Despite the obvious advantages of more frequent looks, many SST users do not need and often cannot afford the huge volume of SST data with the native temporal resolution. For many applications that require diurnally resolved SST observations, a product with a lower time resolution (e.g., hourly) is often sufficient. In response to users' needs, the NOAA SST team has developed an hourly "collated" SST product that improves spatial coverage and temporal consistency, reduces cloud leakages and false alarms, and suppresses spatial-temporal noise in the data, while preserving the native spatial feature resolution and temporal information content.

2. Approach

The algorithm uses the current ACSPO L2P clear-sky mask as a first guess and performs additional screening of remaining cloud leakages using temporal information. Next, a diurnally-resolving reference is estimated at locations, where clear-sky observations were available during the considered period of time and is used to modify the L2P clear sky domain. Then, a high-resolution diurnally-resolved proxy is estimated and used together with clear-sky SST values to iteratively estimate the collated SST value at hourly increments. This aggregation procedure takes into consideration that identified clear-sky SST values can still be contaminated by cloud. The resulting hourly SST product has reduced residual cloud contamination, increased spatial coverage, and reduced noise compared to the native temporal resolution L2P data.

2.1. Cloud screening

The idea of using the space-time-spectral domain for improved clear sky detection is not new (e.g., Rossow 1993). Major clear/cloud discrimination approaches and tests are based on i) spatial contrast/uniformity test (applied to individual IR or reflectance images); ii) radiance thresholds (both IR and reflectance images); iii) accumulation of space/time statistics (both IR and VIS images); iv) comparing to clear-sky SST composites (typically, using available L4 SST fields); v) time contrast test (consecutive IR images at constant diurnal phase), which is underutilized by current operational SST cloud screening algorithms.

Until recently, the NOAA ACSPO clear-sky identification procedure did not use any temporal information. It relied mostly on a spatial uniformity test, L4 clear-sky composite and accumulation of spatial statistics (Petrenko 2010). This heritage mask performed very well globally but had limitations on a regional scale, being subject to false alarms (wrongly screened clear pixels) and cloud leakages (residual cloud). An example of a typical cloud leakage is shown in Fig.1.

Additional cloud screening implemented in ACSPO 2.60 employs temporal information as the following tests:

- 1-step forward and backward difference, using 2 consecutive in time observations (1x1x2 window)
- Deviation from average (1x1x3 window)
- Cold drop-out test (1x1x6 window, set for detecting short-term cold dips)
- Local min test (1x1x3, detects and removes local minimums prior to low-res reference estimation)
- Space-time BT consistency (PCA) test (3x3x3 window, 4 spectral bands).

Figure 1 shows a time series of SST values at a particular location, illustrating typical small cloud drop-outs, which are challenging to detect in a 2D SST imagery, but can be identified using temporal information.

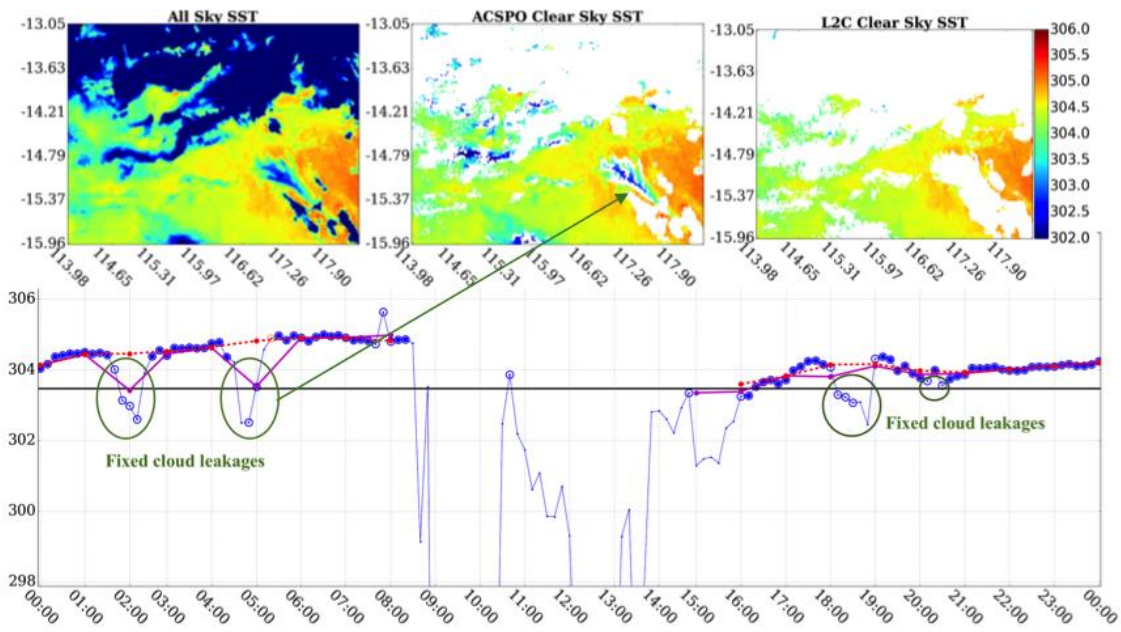

Figure 1: Example of cold clouds missed by the current ACSPO mask. Magenta: hourly collated SST without additional could screening. Red: collated SST with cloud screening using temporal filters and robust collation.

2.2. Main Steps of the Algorithm

The main steps of the algorithm are illustrated in Figure 2, which shows a dynamic portion of the Gulf of Mexico (panels a-d, f) and time series corresponding to a 6-hour window at one pixel (panel e):

- Initialize with current ACSPO clear-sky mask as a first guess, assuming that it may be (and often, it is) subject to occasional cloud leakages and false alarms (Fig. 2a)
- Remove residual cloud leakages based on temporal information (shown in Fig. 1 for different scene)

- Estimate low-resolution diurnally-resolved reference (for locations with clear-sky observations available during the considered period of time) (Fig. 2b and magenta line in Fig. 2e)
- Fit low-res model to clear-sky observation, in each pixel (Fig. 2c and green line in Fig. 2e)
- Use the computed reference to identify false alarms and return wrongly screened-out pixels back to clear-sky domain (not shown in Fig. 2 due to space limitation)
- Aggregate the new clear-sky SSTs and high-resolution proxy to estimate collated SST values at 1 hour increments (Fig. 2f and black marker in Fig. 2e)

The main idea is to use a time-varying reference, estimated from the actual observations, rather than a L4 analysis from the previous day. Such diurnally-resolved reference is then used for refining the clear-sky domain and for “guidance” in the collation process, during which the clear sky values can still be cloud contaminated even after additional time-based cloud screening.

2.3. Implementation Considerations

Several adjustments have been made to the initial design, resulting in more robust and faster performance:

Near-Real-Time trade-off. The original approach was developed with daily chunks in mind, but given that memory usage is approximately 1 GB/L2P granule + overhead, the decision was made to shorten the time interval. Testing found that global statistics and coverage were degraded using fewer than 25 granules, resulting in a NRT version of the code which now processes 6-hour chunks with 5 hours of history for ABI (3 hours for AHI) and 1 hour of future data. The current implementation takes ~6 min on our development systems, making L2C product for N:00 UTC available 6 min after the (N+1):00 UTC L2P granule is obtained.

Collation/Retrieval order. Two options were considered: 1) Collating L2P SST values; 2) Collating brightness temperatures (BTs) and retrieving SST from the collated BTs.

Option 2 allows estimation of SSES bias and standard deviation, while the first version (Option-1) only provided L2C SST and brightness temperatures computed independently. Retrieving SST from collated BT’s required a new set of coefficients, which were calculated using 3 months of *in* situ match-ups and are now used to produce L2C SST.

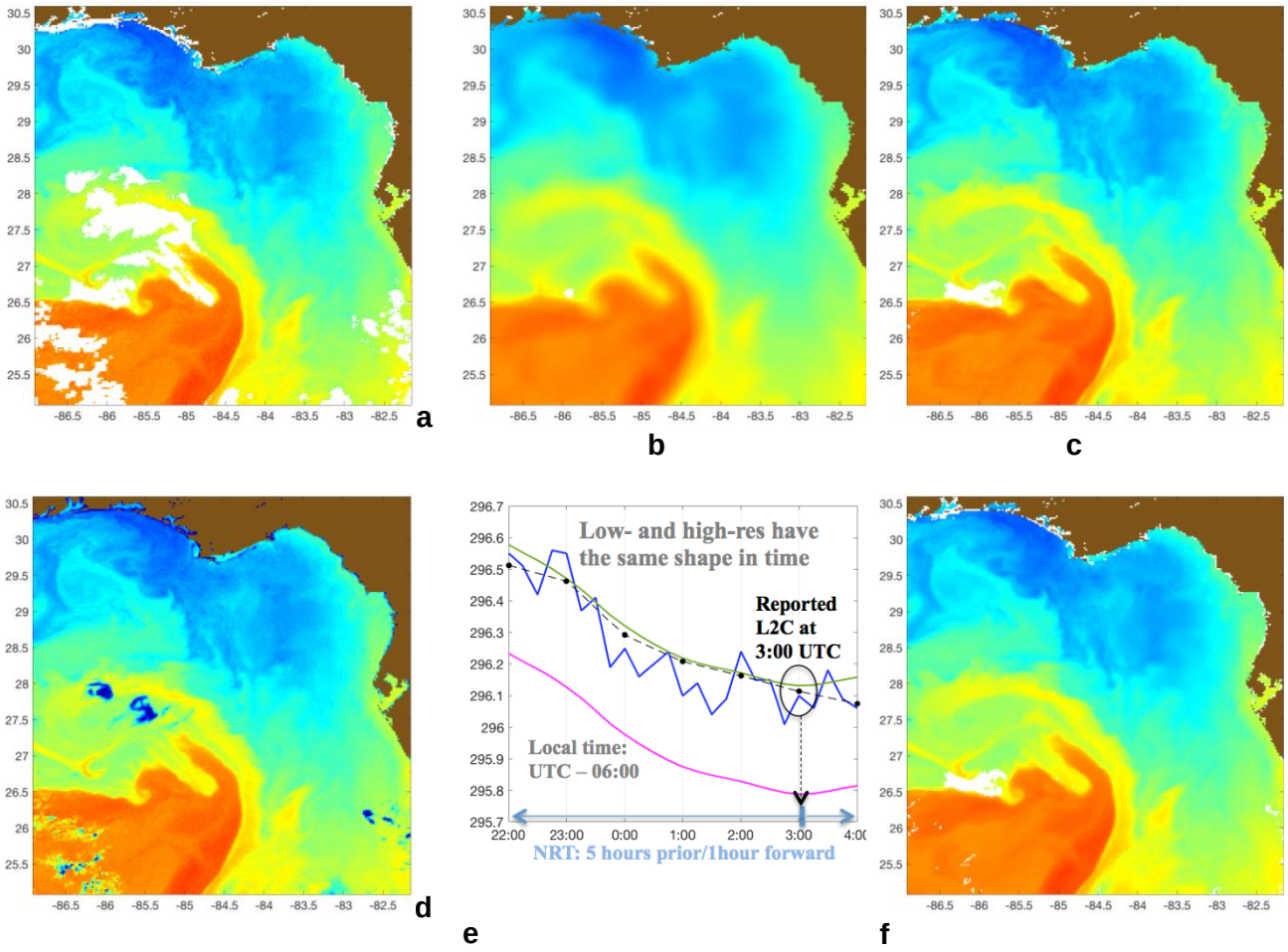

Figure 2: a) L2P with ACSPO mask; b) Low-resolution estimate; c) High-resolution estimate; d) All sky L2P (for visual reference); e) Time series for one selected pixel in this scene; f) final hourly collated SST at 03:00 UTC (21:00 LT).

3. Evaluation and Monitoring

Collated products (from both G16 and H08) have been monitored and validated using the NOAA SQUAM (SST Quality Monitor) and ARMS (ACSPO Regional Monitor for SST) systems. Evaluations in SQUAM against L4 analysis (CMC) and *in situ* measurements (drifters, tropical mooring buoys, ARGO floats) show the superior performance of the collated product compared to the original L2P (cf. Figure 4). Evaluations in ARMS show improved image quality and increased and more consistent in time coverage.

4. Conclusion and Future Work

A new geo collation algorithm has been developed and implemented in ACSPO v2.60, employing a combination of various time-space windows. This allows it to better discriminate clear sky from cloud-obscured observations and to more accurately estimate SST values at hourly increments from 10/15 min observations. The resulting collated SST product has larger spatial coverage, reduced residual cloud contamination and reduced noise (caused by radiometric and other random errors, e.g. from the ACSPO atmospheric correction algorithm) compared to the native temporal resolution L2P data.

The generated collated product has been added to NOAA monitoring systems and performs consistently better than L2P.

Future work will be focused on improved initialization of the algorithm. Massive false alarms (large clear sky regions, screened out by the current ACSPO L2P mask) take place in dynamic/coastal regions. These false alarms are mainly due to threshold-based decisions in the heritage ACSPO mask, based on comparisons with daily L4s. Although the collation algorithm has the capability to restore over-screened clear sky domain, the large lost areas cannot be fully restored without modification of the initial mask.

5. Acknowledgement

We would like to thank other NOAA SST team members for their contribution in the development and testing of geo collated product. Specifically, Yanni Ding for monitoring geo L2/3C in ARMS, Xinjia Zhou and Kai He for providing *i*Quam *in situ* data and monitoring in SQUAM, Maxim Kramar for routine geo ACSPO testing/processing in STAR, Boris Petrenko for recalculating NLSST coefficients and SSES LUT's for L2C, and Andrew Fitzgerald for rewriting prototype MatLab code into initial C++ implementation. This work is supported by the NOAA GOES-R and ORS Programs. The views, opinions, and findings in this report are those of the authors and should not be construed as an official NOAA or U.S. government position or policy.

6. References

Gladkova, I., A. Fitzgerald, A. Ignatov, Exploring Temporal Information in new generation geo sensors for improved SST. *NOAA Satellite Conference*, New York, CCNY, July 2017.

Petrenko, B., A. Ignatov, Y. Kihai, et al. Clear-Sky Mask for the Advanced Clear-Sky Processor over Ocean, *JTECH*, **27**(*10*), 1609, 2010.

Rossow, W., and L. Garder. Cloud detection using satellite measurements of infrared and visible radiances for ISCCP. *J. Climate*, **6**, 2341, 1993.

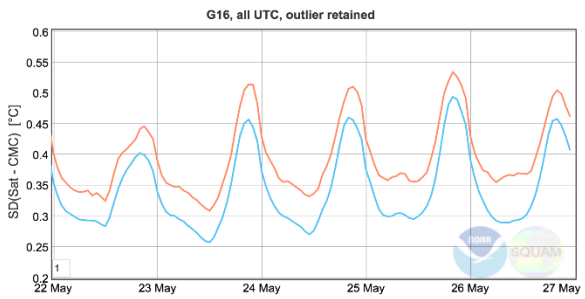

a

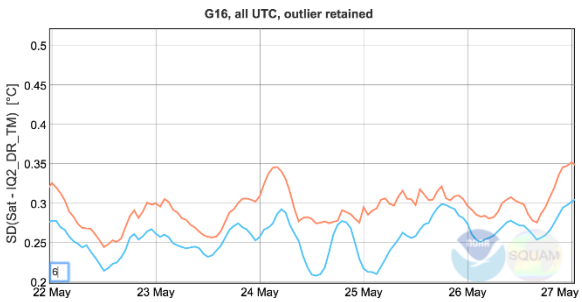

b

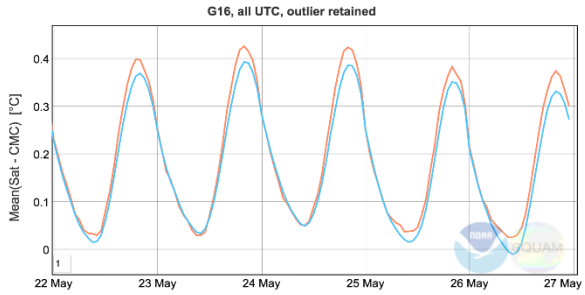

c

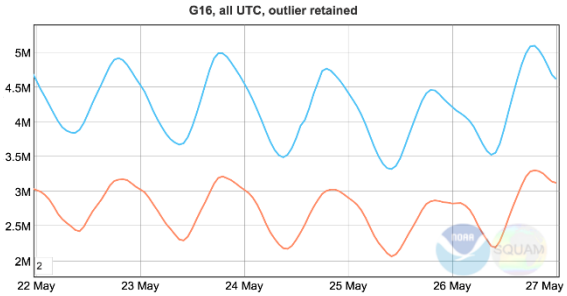

d

Figure 4: Standard deviations wrt L4 CMC (a) and in situ measurements: drifters + tropical moorings (b) are consistently lower for hourly collated (orange) than L2P subsampled at the hour UTC (blue). Mean difference (c) with respect to reference L4 CMC retain the same diurnal shape as original L2P data. The coverage (d) is ~40% larger than for L2P.

CONSISTENT LINE OF ACSPO L3U SST PRODUCTS

Matthew Pennybacker[(1)], Irina Gladkova[(2)] , Alexander Ignatov[(3)], Yury Kihai[(4)]

(1) NOAA/STAR and GST, Inc., USA, Email: matthew.pennybacker@noaa.gov
(2) NOAA/STAR, GST, Inc., and City College of New York, USA, Email: irina.gladkova@gmail.com
(3) NOAA/STAR, USA, Email: alex.ignatov@noaa.gov
(4) NOAA/STAR and GST, Inc., USA, Email: yury.kihai@noaa.gov

1. Introduction

At the 2016 and 2017 GHRSST science team meetings, the Advanced Clear-Sky Processor for Ocean (ACSPO) Level 3 Uncollated (L3U) products were introduced from S-NPP VIIRS and Metop-A/B AVHRR FRAC, which consist of remapped L2P data at 0.02º resolution. L3U for these platforms is reported in GHRSST GDS2 format as 10-min granules, with daily L3U data volumes being significantly smaller than the corresponding L2P, as demonstrated in Table 1. Another L3U product from NOAA-20 VIIRS, launched in November 2017, is now being generated experimentally at NOAA.

With the release of ACSPO v2.60, the L3U code has been updated to additionally generate 0.02º gridded products from the heritage polar sensors, AVHRR GAC and MODIS, and hourly products from the new generation of geostationary sensors: ABI on GOES-16 and GOES-17, and AHI on Himawari-8. Although they use largely the same algorithm, the geostationary products are called L3C, since the L2P which it is generated from is based on hourly collated brightness temperatures. L3U products continue to be generated for VIIRS and AVHRR FRAC exactly as before.

In developing the ACSPO L3U products, consistency between L3U and L2P for different platforms and sensors is a primary concern. Spatial patterns are well preserved in all L3U products, with no degradation. Validation against *in situ* data, data coverage and image quality yield the same result: in all respects, the ACSPO L3U products are comparable, or even improved, compared to the original L2P.

Having generated a consistent line of L3U products, the next step is to generate a unique line of collated and super-collated ACSPO L3C/S. These will address the needs of many users, who find it challenging to deal with multiple platform/sensor-specific individual L3U products, and requested (super-)collated gridded products that have the best data coverage, while preserving the high-resolution features from the original data.

	GDS2 L2P (GB/day)	GDS2 L3U (GB/day)	Factor
VIIRS (S-NPP/N20)	26	0.45	~58x
MODIS (Aqua/Terra)	7.1	0.45	~16x
AVHRR FRAC (MetOp-A/B)	7.5	0.4	~19x
AVHRR GAC (MetOp-A/B/N18/N19)	0.7	0.3	~2.5x
ABI (G16/G17, Hourly)	6.2	0.6	~10x
AHI (H08/H09, Hourly)	6.5	0.6	~11x

Table 1: Average daily volume of ACSPO L2P and L3U data from 1-7 March 2018.

2. L3U Algorithm

The algorithm implemented in ACSPO v2.60 is largely the same as the one presented at previous GHRSST science team meetings (Ignatov, *et al.* 2017). In contrast to nearest neighbor assignment or simple spatial weighting, the bilateral weighting employed by ACSPO L3U can help to mitigate sensor noise and residual cloud while preserving features contained in the original L2P data.

2.1. Bilateral Weighting

The first step of the algorithm is to determine the nearest neighbors from the L2P input of each L3U output pixel. For each L3U pixel i, call these L2P neighbors collectively $N(i)$. The number of pixels in $N(i)$ is limited to 11 for computational efficiency, and the maximum distance of any neighbor is at most 3 L3U pixels in any direction.

Most quality flags are assigned by majority voting: if more than half of the nearest neighbors from $N(i)$ are flagged, that flag is set for the corresponding pixel i in the L3U output. The only flag that is assigned in a different way is the ocean/land flag, which is assigned based on a fixed land mask.

Continuous variables (*e.g.* SST) are assigned by computing

$$f(i) = \frac{1}{w(i)} \sum_{j \in N(i)} f(j) \cdot g_s(d(i,j)) \cdot g_v(|f(j) - \tilde{f}(i)|)$$

where $f(i)$ is the value of the variable at pixel i in the L3U output, $f(j)$ is the value of the variable at pixel j in the L2P input, $d(i,j)$ is the geographic distance between pixels i and j, and $\tilde{f}(i)$ is the median of the variable in the neighborhood $N(i)$. The sum is taken over only clear-sky pixels in $N(i)$. Within the sum, the first weight g_s is spatial weighting and the second weight g_v is “intensity” weighting, which helps reduce noise and eliminate residual cloud.

The functions g_s and g_v are gaussian weights, with standard deviations σ_s and σ_v respectively, and $w(i)$ is the sum of the weights over the neighborhood $N(i)$. The parameter σ_s roughly corresponds to the sensor resolution, and σ_v roughly corresponds to the sensor noise level. For the geostationary sensors ABI and AHI, the spatial scale σ_s is made to increase as view zenith angle

increases. An additional parameter ΔT helps preserve the positions of fronts: if the nearest neighbor is less than ΔT from the result of bilateral weighting, then the nearest neighbor value is used. Current parameter values are listed in Table 2.

	σ_s	σ_v	ΔT
VIIRS (S-NPP/N20)	1.0	0.100	0.350
MODIS (Aqua/Terra)	1.5	0.200/0.250	0.475
AVHRR FRAC (MetOp-A/B)	2.0	0.215/0.175	0.575/0.550
AVHRR GAC (MetOp-A/B/N18/N19)	5.0	0.200	0
ABI (G16/G17) & AHI (H08/H09)	1.0 (at nadir)	0.100	0.350

Table 2: Current parameter values for the ACSPO L3U bilateral weighting algorithm.

An intuitive way to think about bilateral weighting is as a generalization of other re-gridding algorithms. In the limit $\sigma_v \to \infty$, the formula above becomes gaussian weighting by distance. Taking both $\sigma_v \to \infty$ and $\sigma_s \to \infty$ yields simple arithmetic averaging; taking $\sigma_v \to \infty$ and $\sigma_s \to 0$ yields nearest-neighbor assignment; taking $\sigma_v \to 0$ and $\sigma_s \to \infty$ yields the neighborhood median. By selecting the parameters appropriately, it is possible to exploit the benefits of each method.

2.2. AVHRR GAC Upsampling

In order to create a fully consistent line of L3U products, 0.02º L3U is now generated from AVHRR GAC on MetOp-A/B and NOAA-18/19. It has also been generated for the ACSPO RAN1 GAC reanalysis, which covers 2002-2018 using MetOp-A/B and NOAA-15/16/17/18/19. These data are available from NOAA CoastWatch (https://coastwatch.noaa.gov/cw_html/sst_avhrr_gac.html). The goal of the GAC L3U products is to maintain global consistency with the original L2P data while providing improved regional imagery.

The original bilateral algorithm alone is not sufficient to re-grid the lower resolution GAC data without creating visual artifacts. This occurs because the neighborhood of L2P pixels $N(i)$ used in the bilateral algorithm often contains only a few pixels, if any, as a result of the distance restriction on neighbors. Easing this restriction increases the runtime of the algorithm significantly, thus L3U becomes computationally infeasible. As a result, it is necessary to add an additional processing step during which the L2P data are upsampled in their original swath projection. The upsampling uses only gaussian spatial weights, with the distance measured in terms of L2P pixels, rather than as geographical distances. This automatically takes into account the changing footprint of the pixel with respect to view zenith angle. The resulting upsampled image is then passed into the bilateral algorithm.

An example comparing FRAC L3U with the corresponding GAC L3U generated by ACSPO v2.60 can be seen in Figure 1. GAC L2P data for MetOp-A are generated on the ground by NOAA/OPSO using the same aggregation scheme as onboard legacy AVHRR sensors, decreasing the along-scan resolution by a factor of five. Remarkably, the GAC L3U image contains nearly all the

features of the FRAC image, without noticeable visual artifacts. Note that the upsampling step is being performed **only** for AVHRR GAC at this time.

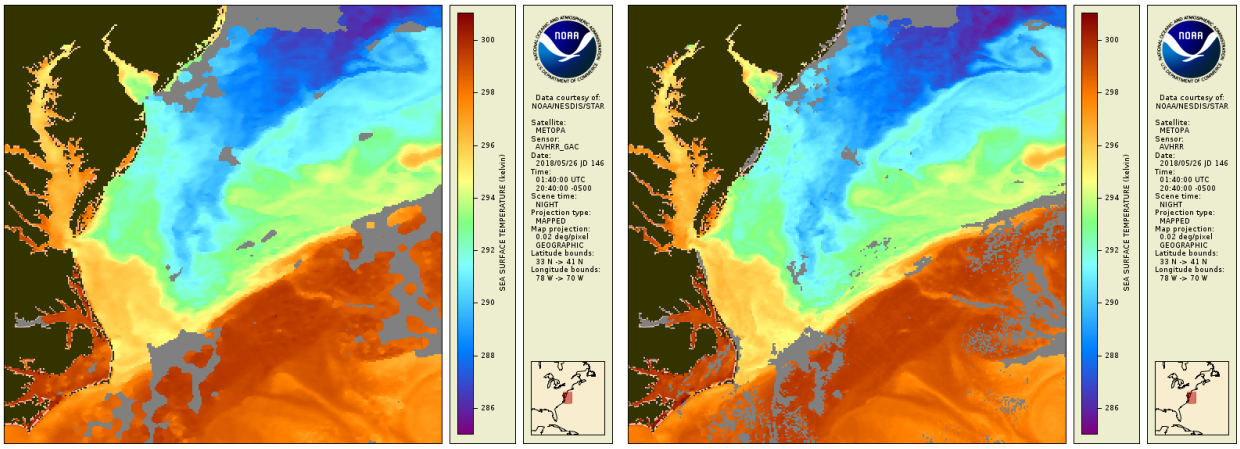

Figure 12: Example of the GAC upsampling algorithm from MetOp-A at 0140 UTC on 26 May 2018. The GAC L3U is on the left, and the corresponding FRAC L3U is on the right.

3. Validation

Ongoing analysis and numerous case studies, performed using data from the NOAA *in situ* Quality Monitor (*i*Quam, https://www.star.nesdis.noaa.gov/sod/sst/iquam/), confirm that all ACSPO L3U products are comparable in terms of global statistics with the L2P products from which they are derived. A sample of these validation exercises is presented in Table 3. The matchups are performed for all night-time clear-sky pixels with drifting buoys and tropical moorings.

In most cases, the mean difference is slightly elevated and the standard deviation slightly reduced in the L3U data compared to the L2P. This can be attributed to the L3U algorithm reducing noise and eliminating residual cloud that are present in the L2P data. Note also that the number of matchups is significantly increased in the GAC product after conversion to L3U due to the upsampling step, although it does not appear to degrade the global statistics.

	L2P			**L3U/C**		
	# Matchups	**Mean**	**Std. Dev.**	**# Matchups**	**Mean**	**Std. Dev.**
VIIRS S-NPP	336402	-0.03	0.29	64140	-0.02	0.29
MODIS Aqua	100222	-0.03	0.29	45194	-0.02	0.28
FRAC MetOp-B	211287	-0.01	0.34	62729	-0.02	0.31
GAC N19	9815	-0.00	0.36	62909	0.01	0.32
ABI G16	29118	-0.01	0.24	42768	-0.03	0.25

Table 3: Night-time comparison with in situ data (drifting buoys and tropical moorings) from iQuam over the period 6-12 May 2018 for VIIRS/MODIS/AVHRR and 6 May 2018 only for ABI.

Results from comparable sensors on other platforms reflect similar performance characteristics to the ones presented here. Routine monitoring of all ACSPO L2P and L3U products will be available in the NOAA SST Quality Monitor (SQUAM, https://www.star.nesdis.noaa.gov/sod/sst/squam/) system once v2.60 has been implemented operationally later this year. Experimental L3U imagery is available now in the ACSPO Regional Monitor for SST (ARMS, https://www.star.nesdis.noaa.gov/sod/sst/arms/).

4. Conclusion and Future Work

As all the imagery and statistics so far indicate, the ACSPO L3U products are comparable, or even improved, compared to the original L2P. A primary purpose for the evolution of our L3U products in ACSPO v2.60 to include all available sensors at a consistent 0.02º spatial resolution is to work toward collated and super-collated polar L3C/S. Once we have sufficiently resolved the remaining intra- and inter-sensor biases, we plan to generate US regional VIIRS L3C/S products which may eventually be generalized to global coverage.

Along similar lines, and in response to user requests, we plan to improve our implementation of the ACSPO L3U algorithm to allow for generation of regional 0.01º L3U/C/S products, since the current implementation is neither flexible nor efficient enough for this task. We also plan to generalize the L3U algorithm to enable alternative geolocation grids (*e.g.* polar stereographic projection).

5. Acknowledgements

Thank you to the rest of the NOAA SST team for their contribution in the development and testing of the ACSPO L3U product. Specifically, Yanni Ding has maintained the L3U code and developed many of the updates for v2.60, and Xinjia Zhou and Kai He have provided *i*Quam *in situ* data and monitoring in SQUAM. This work is supported by the NOAA JPSS and GOES-R Programs. The views, opinions, and findings in this report are those of the authors and should not be construed as an official NOAA or U.S. government position or policy.

6. References

Ignatov, A., I. Gladkova, Y. Ding, F. Shahriar, Y. Kihai, and X. Zhou. JPSS VIIRS level 3 uncollated sea surface temperature product at NOAA, *J. Appl. Remote Sens.* **11** (3), 2017.

PLENARY SESSION IX: TOOLS AND SERVICES

SESSION IX REPORT

Chair: Jean-François Piollé[(1)] – Rapporteur: Stéphane Saux Picart[(2)]

(1) Ifremer, France, Email: jfpiolle@ifremer.fr
(2) Météo-France, France, Email: stephane.sauxpicart@meteo.fr

Abstract:

This session is about tools and services related to SST products. Such tolos may be used by data producers only in order to diagnose problems or search through data sets, it is the case of the ARM regional monitoring of ACSPO. Other tools are intended for the user community and Open source.

Progress with the NOAA ACSPO Regional Monitor for SST (ARMS) System (Alexander Ignatov)

ARMS regional monitoring of ACSPO SST and cloud mask. Presents new evolutions brought to the version 2.1. Tool mostly used internally to pinpoint some specific problems such as cloud masking.

Q: Helen: tool used at the BoM. In polar page GEO SST: display the closest GEO in time.

Q: Jean-François: Do you plan something more interactive in the future. Answer: No

Ocean Science Data Analytics using Apache Science Data Analytics Platform (Thomas Huang)

Presents a new way of processing data: by splitting the data into little chunks processed in a distributed environment, it is possible to speed up the process enormously.

Powerful interactive tool for quick analysis, multi-dimensional and multi-variate analysis (for instance climatic analysis). Able to export results and share them.

Make links between datasets. On the fly in-situ matchups. Everything free and open source software.

We need to think beyond the archive/download/process for scientific application because the data volume is becoming to large to be handled efficiently.

Q: Chelle: Very powerful to do all this in Open Source environment to be able to share the codes and run it in other places. Also need to have more communication with the science community.

Q: Jeff: how do users trust the data they are getting from the system? A: It depends on the users and their objectives.

Improving search relevancy for oceanographic data discovery (Ed Armstrong)

Bring 4 different technologies together to have an efficient data discovery tool for ocean data. One question was what features of the data are most relevant to data search and how can the datasets be ranked? The solution adopted in MUDROD is based on a Machine learning algorithm to rank the datasets. MUDROD search is much better than the PODAAC search.

MUDROD will be infused into PODAAC eventually.

Discussion:

Igor: How easy are the platform to transfer and maintain? ACSPO's platform is not Open Source and difficult to transfer.

Thomas: different deployment options, it is possible to deploy on little clusters or simple computer.

PROGRESS WITH THE NOAA ACSPO REGIONAL MONITOR FOR SST (ARMS) SYSTEM

Alexander Ignatov(1), Kai He, Yanni Ding

(1) NOAA STAR, USA, Email: Alex.Ignatov@noaa.gov

Abstract

The NOAA Advanced Clear-Sky Processor for Ocean (ACSPO) Regional Monitor for SST (ARMS; www.star.nesdis.noaa.gov/sod/sst/arms/) system focuses on areas of interest to SST users (e.g., coastal/internal waters, high-latitudes, dynamic or cloudy regions), which are often challenging for SST producers, too (e.g., dynamic ocean is often masked out as “cloud”; SST algorithms subject to large errors in the high-latitudes, etc.). So far, the ARMS monitoring has mainly focused on polar ACSPO products, with geo products available in a “comparison mode”.

Since GHRSST-18, ARMS has been updated to version 2.1. Several new targets have been added, per users’ requests. With the launch of Himawari-8 (H8) and GOES-16/17 (G16/17), users expressed more interest in geo imagery, especially in the hourly SST evolution. Two modules, polar and geostationary, have been established. Users can check the hourly Level 2 collated (L2C) hourly data, and the corresponding L3C SSTs from ABI onboard G16/17 and from AHI onboard H8. Two L3 super-collated (L3S) SST products from the Australian BoM are now monitored. The number of L4 SST data (available in a “comparison mode”), has increased to five (four global – CMC, OSTIA, NOAA geo-polar blended, and MUR, and one regional - BoM RAMSSA). SSES bias corrected SSTs and ΔSSTs (SST minus CMC SST) are now available.

This presentation discusses the updates of ARMS, compares SSTs from different platforms and data levels, and provides some preliminary results of validating the ACSPO SSTs in the high latitudes and coastal and dynamic regions.

OCEAN SCIENCE DATA ANALYTICS USING APACHE SCIENCE DATA ANALYTICS PLATFORM

Thomas Huang(1), Edward Armstrong, Frank Greguska, Joseph Jacob, Nga Quach, Lewis McGibbney

(1) NASA Jet Propulsion Laboratory, USA, Email: thomas.huang@jpl.nasa.gov

Abstract

An Integrated Science Data Analytics Platform is an environment that enables the confluence of resources for scientific investigation. It harmonizes data, tools and computational resources which subsequently enable the research community to focus on the investigation rather than spending time on security, data preparation, management, etc. OceanWorks is a NASA technology integration project to establish an Integrated Ocean Science Data Analytics Platform at NASA's Physical Oceanography Distributed Active Archive Center (PO.DAAC) for big ocean science. OceanWorks is developed collaboratively between the NASA Jet Propulsion Laboratory (JPL), Center for Ocean-Atmospheric Prediction Studies (COAPS) at Florida State University, National Center for Atmospheric Research (NCAR), and George Mason University (GMU). It focuses on technology integration, advancement and maturity by bringing together several NASA open-source, big data projects. It includes cloud-based technologies for on-the-fly time-series analysis, oceanographic anomaly detection, in situ to satellite data match up, quality-screened subsetting, search relevancy and discovery, and web-based visualization.

In 2017, the OceanWorks project team has donated all of the project's source code to the Apache Software Foundation and established the official Science Data Analytics Platform (SDAP) project (http://sdap.incubator.apache.org) for community-driven and development of data access and analysis platform for the cloud environment. The OceanWorks project team is now develop in the open. This presentation will provide the current progress on the OceanWorks activity with demonstrations on some of the cloud-based analysis this platform enables using SST data and discuss how the GHRSST community can leverage and support SDAP.

IMPROVING SEARCH RELEVANCY FOR OCEANOGRAPHIC DATA DISCOVERY

Ed Armstrong(1), Chaowei Yang, Thomas Huang, David Moroni, Lewis Mcggibney, Frank Greguska

(1) NASA Jet Propulsion Laboratory, USA, Email: edward.m.armstrong@jpl.nasa.gov

Abstract

Free text data searching of earth science datasets has been implemented with varying degrees of success and completeness across the spectrum of satellite data distribution centers. At the JPL Physical Oceanography Distributed Active Archive Center (PO.DAAC) the search engine has been developed around the Solr/Lucene platform. Others have chosen other popular enterprise search platforms like Elasticsearch. Regardless, the default implementations of these search engines leveraging factors such as dataset popularity, term frequency and inverse document term frequency do not fully meet the needs of precise relevancy and ranking of earth science search results. Recently, the PO.DAAC has teamed with an effort led by George Mason University to improve the improve the search and relevancy ranking of oceanographic data via a simple search interface and powerful backend services called MUDROD (Mining and Utilizing Dataset Relevancy from Oceanographic Datasets to Improve Data Discovery) funded by the NASA AIST program. MUDROD has mined and utilized the combination of PO.DAAC earth science dataset metadata, usage metrics, and user feedback and search history to objectively extract relevance for improved data discovery and access. In addition to improved dataset relevance and ranking, the MUDROD search engine also returns recommendations to related datasets and related user queries. This presentation will report on use cases that drove the architecture and development, and the success metrics and improvements in search precision and recall for GHRSST datasets and other oceanographic products that MUDROD has demonstrated over the existing PO.DAAC search interfaces

PLENARY SESSION X: RETRIEVAL OF SST

SESSION X REPORT

Chair: Andy Harris[(1)] – Rapporteur: Sandra Castro[(2)]

(1) NOAA-CICS, University of Maryland, United States, Email: andy.harris@noaa.gov
(2) University of Colorado, United States, Email: sandrac@colorado.edu

09:00 – 09:20: Bingkun Luo and Peter Minnett: Improving Satellite Retrieved Infrared Sea Surface Temperatures in Aerosol Contaminated Regions

Asks: How are SST errors dependent on aerosol properties? How to improve aerosol-contaminated SST retrievals?

Study based on MODIS SST quality level 0,1,2 and buoy matchups (10 km, 30 min). The distribution of MODIS SST errors relative to buoy matchups shows cold/negative biases in SST for the Saharan dust region. The MODIS SST error (satellite –buoy) exhibits correlations with the MODIS Aerosol Optical Depth (AOD), with CALIPSO top and base layer altitudes, and with satellite zenith angle.

Proposes a MODIS dust correction algorithm based on the Dust-introduced SST Difference Index (DSDI). The DSDI is a quadratic equation for the SST error as a function of the brightness temperature (BT) differences: (BT3.8 - BT12), (BT3.8 – BT8.9), (BT11-B12) and $(BT11-B12)^2$.

DERIVATION: Uses RTTOV simulations with MERRA2 (includes aerosol mixing ratios at each layer) to simulate BT differences with AOD. The RTTOV simulations use MAERI SST data from AEROSE and atmospheric profiles from the CALIPSO Lidar satellite.

The coefficients of the DSDI parameterization are derived by regressing the MODIS-buoy SST differences on the RTTOV-MERRA2 simulated BT differences.

Uses 80% of satellite-buoy matchups to derive the DSDI coefficients and 20% for validation.

MODIS DSDI-based correction: MODIS SST – buoy SST = -1.7 DSDI +0.891

Next, they introduce the dust correction into the nighttime MODIS SST algorithm. Validations with buoy differences are shown before (SD: 0.76K) and after correction (SD: 0.65K) for small Sahara area.

Impact of correction is much more beneficial for MODIS SST QL2 suggesting that much of these data may be aerosol contaminated – don't need to throw out – can correct.

For future –look at day; add more calypso data to look at different heights; look at different types of aerosols (e.g. smoke)

Questions:

Chris Merchant: For the derivation of the DSDI – did you use the simulated brightness temperatures from MERRA or observations? Used simulated BTs to determine the DSDI equation form; then derived the coefficients from observations with situ buoy matchups.

What is the source of the big errors for such small aerosol concentrations – needs to look into that.

Sasha Ignatov: Right now – night with 3.9? Answer: yes. The statistics before and after correction, SD = 0.76K vs. SD = 0.65K, are they global or regional statistics? Answer: Regional.

The SD for nighttime MODIS dust-corrected SSTs is still pretty poor after correction. What kind of in situ data did you use? Are you doing any quality control on the in situ data? Used buoy data from iquam and ship data from MAERI.

Andy Harris: Any work on physical retrieval? Answer: No.

09:20 – 09:40: Prabhat Koner: Use of 3.9 micron channel for daytime sea surface temperature retrieval

Shows data/methods used: Truncated (TTLS) and Modified total least squares (MTLS).

Why the 3.9-channel is important: for ~40% of measurements in the 11 micron, the fundamental assumptions of the split window don't apply, whereas TOA 3.9 micron measurements always hold surface information. Gets 40% number from SST Jacobian at 11 microns – Jacobian is proportional to transmission. Planck function at 3.9 is steeper than at 11 micron.

Proposes experimental cloud filter based on the 3.9-micron channel and concludes that the use of 3.9 micron for daytime retrievals using physical models is "undisputable": CRTM calculates specular reflection satisfactorily. BRDF, however, needs improvement in CRTM. Need to discard pixels with deficiency of CRTM, but can still use ~20% of measurements after rejection, which is better than considering measurements with quality index 5 only (~7%). The result is daytime SSTs with STD comparable to nighttime retrievals.

Next proposes regression-based retrievals including additional terms with specular reflection angle and (BT3.9 –BT11) and compares with GOES-13 daytime SST retrieval. Concludes that SWIR is a must for unambiguous SST retrievals. Results published in 2016 in RSE.

Daytime retrievals using 3.9 has been successfully implemented operationally with geo-sensors. For polar orbiters, daytime regression algorithms including additional terms based on the (BT3.9 – BT11) and (BT3.7 – BT11) differences are proposed.

Questions:

B. Luo: what about the term *sec(theta -1*)? Replies that, yes there is a typo there.

Question as to why the 3.9 helps physically? Responds 3.9 has bigger Jacobian – better transmission – less ambiguity – better to get surface – less absorption in atmosphere.

C.Merchant: Question about statement of need to improve BRDF in CRTM – is it Cox/Munk? What is source? Prabhat thinks atmospheric bit is incomplete in BRDF. Scattering of aerosols not computed correctly in CRTM.

B. Luo: Would the 3.9 retrievals give more bias in dust areas? Answer: Aerosol correction is included in physical retrievals and no bias is observed in dust areas.

09:40 – 10:00: Pia Nielsen-Englyst: Optimal Estimation of SST from AMSR-E

Motivation: Limited European activity with PMW, but good value seeing through clouds and small response to aerosols.

Optimal Estimation (OE) provides pixel level information on retrieval quality. OE also being used with sea ice within ESA CCI (The ESA SICCI). A new PMW sensor (CIMR) is candidate for the Copernicus expansion mission.

Multi-sensor Matchup Dataset for OE algorithm development based on AMSR-E L2A BTs from RSS (NSIDC). Period: 2002-2011. includes array of AMSR-E pixels, NWP, in situ time series, and sea ice – CCI approach.

OE setup: Inversion of forward model TOA for individual channels. Uses updated version of Wentz-DMI forward (FW) model. State vector – SST, TCWV, TCLW, WS

Need measurements and FW model error covariance, first guess from NWP, and a priori errors of state variables. Computes most likely state. Implement with iterations: RMS changes between iterations. The RMS rapidly converges after a few iterations (less than 10).

Uncertainty: Say RMSE TB (relative to OE to reproduce BT) can be used as quality indicator and thus for filtering and uncertainty estimates.

Concluded that OE SST better than NWP SST in mid-latitudes, but NWP SST better in the tropics.

OE work now published in Remote sensing.

Rest of presentation – impact of clouds and aerosols on OE SST retrievals

OE SST performance against drifters as function of MODIS cloud fraction – no cloud impact.

Next against CALIPSO number of surrounding pixels with aerosols – also stable – slightly better performance for matchups in regions where there is some aerosol concentration.

Impact from Total Ice Water Content (TIWC) – as TIWC increases, the OE SST performance decreases. Also, some degradation observed with opaque cloud top height and deep convective clouds. Believe all those impacts are related so try to filter out deep convective clouds (affect more than 50% of pixels). See performance increase (0.56 to 0.5 RMS) if remove deep convective clouds.

But OE retrieves more parameters than SST: author thinks that OE retrieved TCLW can be used to help filter out convective clouds, since TCLW retrievals, compared to NWP TCLW, seem to work.

Conclude: Generally good performance. Some effect of deep convective clouds but OE can help retrieve and correct

Future plans: Implement OE for AMSR2.

Questions:

Helen Beggs asked if AMSR2 plans are real time or reanalysis – Pia say for climate

Luo asks – performance relative to retrieval approach? – Answer similar to regression approach, but OE includes uncertainty estimates.

James While asks: Any consideration of horizontal correlations in NWP observations for the background characterization? – Answer no.

A.Harris: Was NWP SST the initial guess – yes. So, when say "less performance than NWP" are you degrading the answer? Yes – price of getting uncertainty information. Andy said this is part of why he encourages MTLS – not so much degradation.

How to take footprint disparity into account? Chelle noted that they used the JAXA resampled BTs: Level 1R BTs from JAXA are remapped to a common footprint; high spatial resolution channels are mapped onto other footprints. Based on 6.9 GHz – all other channels are remapped onto 6.9 GHz using antenna patterns.

Any iterations beyond 10 fail to converge? Very few

Merchant – OE answer is worse than the prior in the tropics. OE shouldn't make things worse – implies that we don't have the error covariance assumptions right.

Harris: This is a problem Prabhat has pointed out over several years.

Beggs: any comments about the lack of microwave data in the Tropical Warm Pool region? Chelle: there are too many islands.

Merchant: CIMR proposed new mission mentioned – potential value of high resolution MW observations near land. CIMR can obtain data within 15-20 km from land masses; also has improved radiometric resolution; hence it would be extremely valuable for SSTs. CIMR is a proposed mission – not guaranteed. Please comment widely that the CIMR mission would be of value if you believe so.

Open discussion led by Session Chair:

Andy: any other PMW thoughts in general?

Andy asks if any possibility to deconvolve sidelobes to improve PW retrievals near land. Chelle say is active area of research with Aquarius – trying to improve retrievals near land – they are getting retrievals, but still higher errors.

Chelle – know the sidelobes, but taking land contributions out is challenging.

Chris – some are retrieving land emissivity and temperature – any effort to go across edge? Chelle thinks no.

Jacob – some work to do across sea ice edge.

Chelle: Computationally, have to map footprint and sidelobe onto land – complicated pattern – not straightforward. Chris say would be revolutionary. Chelle say an interesting path forward and could be topic for a student thesis. Let's put in a proposal.

Helen: Has anyone mapped what the improved coverage from CIMR would be? Telling for managers. Can someone put together a figure showing the positive impact of CIMR on spatial coverage relative to AMSR?

Jacob say will show slide after break.

Andy: Any other viewpoint on aerosol and shortwave?

Helen: there has been a lot of science work on improving L2 products, but what, overall, has been the improvement in SST from the retrievals vs the sensors themselves. What gives the "best bang for the buck" in improving SST? What more can be done?

Andy: with many channels, the problem becomes more linear and there is little benefit from more sophisticated retrievals. Physical retrieval is a way to remove regional biases and include aerosols in the retrievals. Also, physical retrieval gives pixel-by-pixel uncertainty estimates. So even when physical retrievals do not improve performance, at least we know where the uncertainties are.

Andy: highlight benefit of many channels in physical retrievals. It allows you to include as many channels as you can (e.g., additional information on water vapor and winds). Like the 13-micron channel: not very useful for SST, but useful for separating other effects impacting SSTs.

Ignatov: One of the major improvements in SST retrievals recently has been in cloud masking – identifying clear regions. A key aspect for that improvement has come from higher spatial resolution for polar satellites and frequent geostationary temporal sampling. OE is not the only way to go – when have many channels, we have more information. Major areas to improve – revisit atmospheric correction (NLSST) algorithms – get rid of first guess. Don't have to rely on prior.

Andy agreed on cloud masking improvements – one of values of MTLS – makes no assumptions.

Chris – this is why it would be good to see sensitivity calculations for MTLS.

Andy – mathematically hard to do.

Chris – once regression is done, have terms. Can then propagate perturbations.

Prabhat – issue with priors. Sasha agrees with Prabhat.

Chris – all algorithms use priors (NLSST, MCSST included), just in some cases we don't know.

Andy – distinction between initial guess and a prior. A prior is an initial guess with an uncertainty estimate attached to it.

IMPROVING SATELLITE RETRIEVED INFRARED SEA SURFACE TEMPERATURES IN AEROSOL CONTAMINATED REGIONS

Bingkun Luo[1], Peter J. Minnett[1], Chelle Gentemann[2], Goshka Szczodrak[1]

1 Rosenstiel School of Marine and Atmospheric Science, University of Miami
4600 Rickenbacker Causeway, Miami, Florida, USA, Email: LBK@rsmas.miami.edu
2 Earth and Space Research, Seattle, Washington, USA.

Abstract

Infrared satellite retrievals of sea surface temperature (SST) have become essential for many applications in meteorology, climatology, and oceanography. Satellite infrared imaging radiometers passively measure the energy emitted and reflected by the Earth's surface and atmosphere. Tropospheric aerosols increase infrared signal attenuation, degrading the accuracy of infrared satellite SST retrievals. In this study, to assess the radiative effects of aerosols satellite-derived skin SSTs (SST_{skin}) are compared with quality-controlled, collocated SST_{skin} measurements from the Marine-Atmospheric Emitted Radiance Interferometer (M-AERI) deployed on ships during the Aerosols and Ocean Science Expeditions (AEROSE), and subsurface temperatures measured by thermistors on drifting buoys. In this region, SST_{skin} retrievals from the MODerate-resolution Imaging Spectroradiometer (MODIS) aboard the Aqua satellite are generally cooler than the M-AERI shipboard SST_{skin} measurements. In the Saharan outflow area, where aerosol optical depths are greater than 0.5, satellite SST_{skin} are more than 1 K cooler than the *in situ* data. The goal of this study is to understand better the characteristics of aerosol effects on satellite retrieved infrared SST, and to derive empirical formulae for improving accuracies of infrared-derived SSTs in aerosol-contaminated regions. A new method to derive a night-time Dust-induced SST Difference Index (DSDI) algorithm based on simulated brightness temperatures (BTs) at infrared wavelengths of 3.9, 8.7, 10.8 and 12.0 μm, was developed using the Radiative Transfer for TOVS (RTTOV) model. The satellite SST_{skin} biases and standard deviations are reduced by 0.25 K and 0.19 K after the DSDI correction.

Introduction

SST derived from satellites is one of the key parameters in the research and prediction of climate variability, numerical weather prediction, and oceanographic research. Generating SST Climate Data Records (CDRs), requires an absolute temperature error of 0.1 K and stability of better than 0.04 K per decade (Ohring *et al.*, 2005). Therefore, it is necessary to quantify the errors and uncertainties accurately to understand where there is evidence of systematic shortcomings in the current retrieval algorithms.

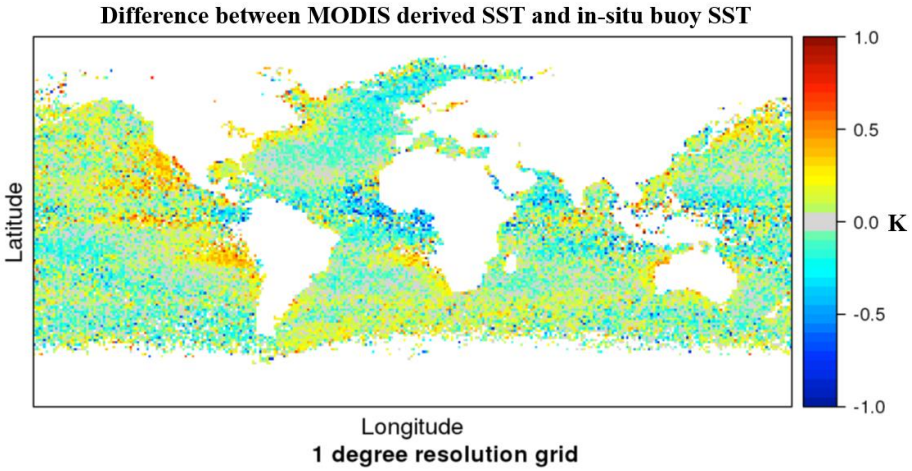

Figure 13. Distribution of Terra MODIS SST matchups with in situ drifting buoy (Minnett et al. 2016). The color indicates the SST difference between MODIS SSTs with in situ measurements from drifting buoy.

Analysis of comparisons of MODIS SSTs with *in situ* measurements from drifting buoys over the missions of Terra and Aqua show that, generally, mean biases are ~ 0.17 K and standard deviation ~ 0.25 K (Minnett *et al.* 2016). The spatial distribution of the difference between MODIS derived SSTs with in situ buoys temperatures (Figure 1), shows a pronounced negative difference in the Saharan outflow area. Szczodrak, *et al.* (2014) discussed the effects of anomalously low moisture layers on the accuracy of MODIS SST_{skin} and quantified these effects using data from measurements taken during research cruises and simulations from numerical atmospheric radiative transfer models (RTMs). They found that for deep dry layers, the errors can be greater than 1 K, and the dry layer altitude affects the sign of the error. In the area of the Saharan Outflow, the dry layers are often accompanied by dust aerosols, but these were not considered by Szczodrak *et al.* (2014). The absorption and re-emission of infrared radiation (IR) by the aerosol layers affect the satellite observed brightness temperatures (BTs), so an aerosol-specific atmospheric correction algorithm is needed to reduce errors (Závody *et al.*, 1995).

Data and Method

The study methods include analysis of in situ data, satellite data and modeled fields. Ship-based measurements were taken during cruise of AEROSE, a series of tropical Atlantic Ocean cruise campaigns. This research will use the in situ datasets from 2006 to 2015. The satellite-derived SST_{skin} are from MODIS on board Aqua from 2006 to 2016 (Kilpatrick et al., 2015). The reanalysis model datasets from the NASA Modern-Era Retrospective analysis for Research and Applications, Version 2 (MERRA-2; Gelaro et al., 2017) will be used as data fields for the RTTOV model simulations during August 18, 2017 12:00 AM, as during this time there is a strong Sahara dust outbreak. Considering the Sahara dust area, the research area is between 90° W to 90° E and 20° S to 35° N.

Our goal is to better understand the characteristics and physical mechanisms of the aerosol layer effects on satellite-retrieved infrared SST_{skin}, and to derive an empirical formula that leads to improved corrections for the aerosol-related effect. The goal can be divided into seven main objectives; the specific steps to reach each main objective are then described:

a. Preprocess the data: collocate MODIS Aqua satellite data with the in situ measurements.

b. Apply quality control and generate match-ups.

c. Evaluate the accuracy of satellite SST_{skin}. Assess the impact of aerosols on satellite retrieved SST_{skin}.

d. Use the RTMs - RTTOV to simulate the SST_{skin} differences with AOD and derive the DSDI based on ancillary data from MERRA-2.

e. Use 80% of the Match-up database (MUDB) to obtain coefficients for the DSDI algorithm.

f. Apply the new algorithm to this region, compare the new, aerosol corrected SST_{skin} with in situ SST.

g. Having derived an empirical correction formula, using the remaining 20% of the data to validate this approach.

Results

The BT_{11}-BT_{12}, $BT_{3.8}$-BT_{12}, and $BT_{3.8}$-$BT_{8.9}$ differences are more useful to derive the DSDI. We examined the night-time MODIS SST_{skin} difference respect to *in situ* measurement versus MODIS BT difference when AOD>0.2 and derived the new-version MODIS Aqua DSDI:

$$DSDI = a + (b + c \times S_0) \times (BT_{3.8} - BT_{12}) + d \times (BT_{3.8} - BT_{3.9}) + (e + f \times S_0) \times (BT_{11} - BT_{12}) + (g + h \times S_0) \times (BT_{11} - BT_{12})^2$$

where $S_0 = sec(\theta) - 1$. θ is the satellite zenith angle.

We ran the model with aerosol and without aerosol present to derive the SST_{skin} difference, the coefficients for the DSDI are derived by multi-dimensional regressions of the BTs difference and SST_{skin} difference using the RTTOV model simulations.

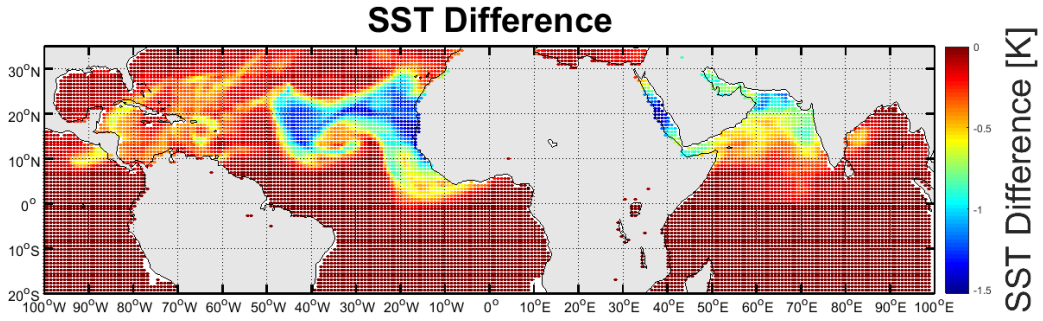

Figure 2. Difference in simulated SST_{skin} when aerosols are present or not. The SST_{skin} difference is related to the aerosol distribution.

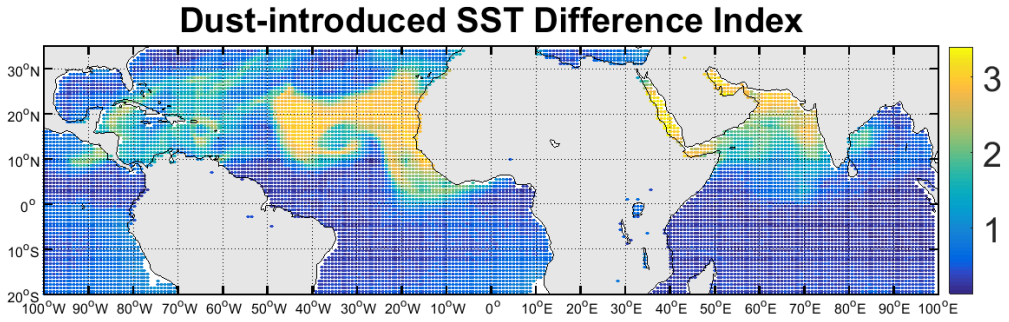

Figure 3. Derived Dust-introduced SST Difference Index. Compared to Figure 2, the derived DSDI distribution is clearly related to the SST_{skin} difference.

Encouraged by the RTTOV simulations, we use the MODIS SST_{skin} data in the MUDBs with quality levels of 0, 1 and 2; representing both cloud free data, and some with possible cloud/aerosol contamination. Deriving coefficient from the simulations of aerosol effects is not appropriate as these would relate to the difference between derived SST_{skin} in conditions where there are aerosols present compared to those without. The correction being sought is one to be applied when the effects of aerosols are present, but not appropriately corrected for, in the satellite-derived SST_{skin}. Thus, using 80% of MUDBs data, regression against *in situ* data is used to determine the coefficients in the MODIS night-time DSDI.

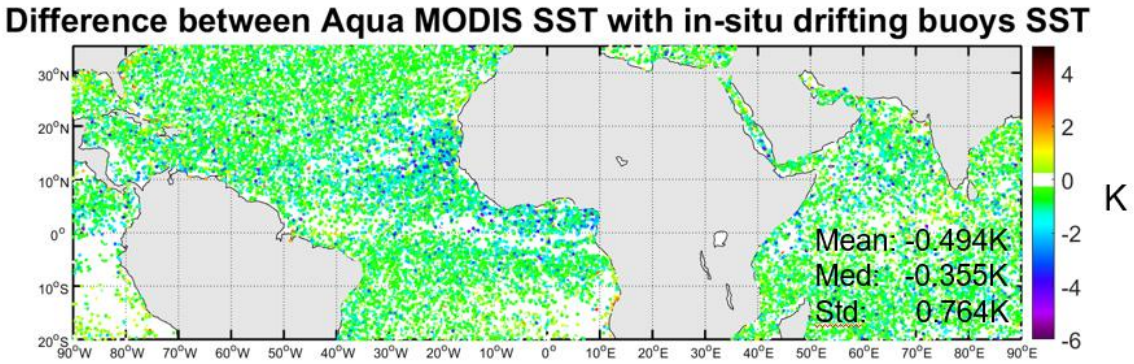

Figure 4. MODIS Aqua SST difference near the Saharan Outflow area, the quality flag values of MODIS Aqua are 0, 1 and 2.

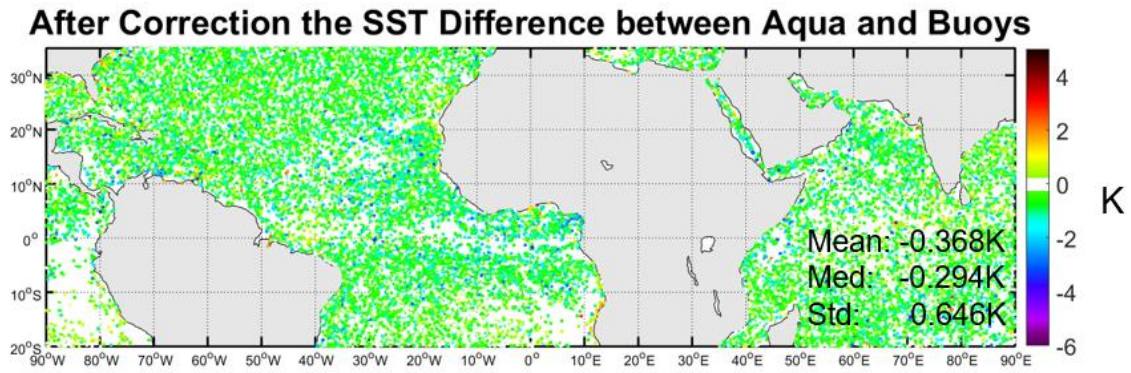

Figure 5. Difference between Aqua MODIS SST_{skin} with in situ buoy SST after correction. From the histograms of the SST_{skin} difference after correction. The mean SST_{skin} difference has decreased by 0.126K. There are a few SST_{skin} differences below -2K after correction.

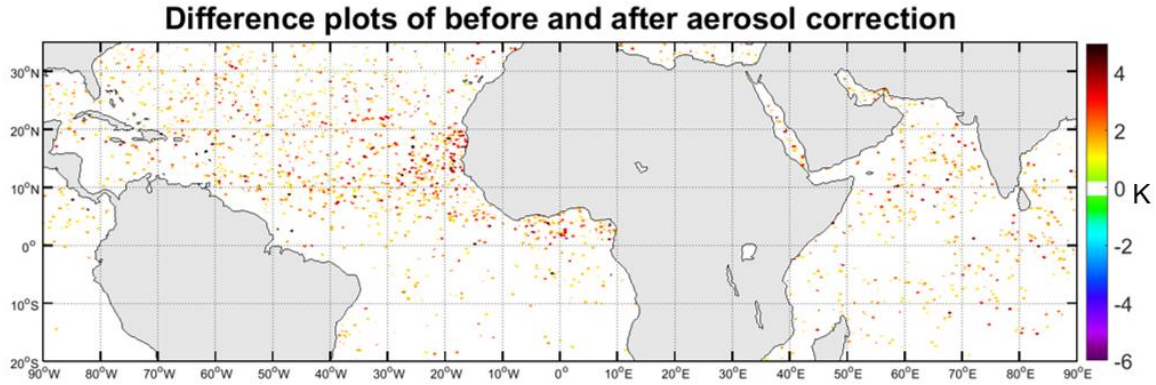

Figure 6. SST_{skin} (before correction) minus SST_{skin} (after correction) is high near Saharan dust outflow region.

Figure 5 shows the differences between SST_{skin} and in situ temperatures after applying the DSDI correction term to the derived SST_{skin} based on MODIS DSDI. Compared to the data in Figure 4, the mean bias has decreased by 0.13 K. Table 1 shows the error statistics at different MODIS quality flags. Compared to quality flags 0 and 1, there is much more benefit for quality flag 2 data, the average increase being 0.296 K. Thus, this correction method works well for the data that are usually categorized as poor quality, which means the DSDI correction can improve the fraction of useful data available instead of being discarded. The effects of the DSDI correction is plotted in Figure 6, showing there are improvements near Saharan outflow region.

Table 1. Differences statistics according to MODIS quality flag

Quality Flag	N	Before correction (K)			After correction (K)		
		Mean	Median	STD	Mean	Median	STD
0	86092	-0.217	-0.190	0.458	-0.192	-0.180	0.442
1	47030	-0.482	-0.435	0.649	-0.376	-0.360	0.616
2	50919	-0.974	-0.830	1.003	-0.657	-0.585	0.834
All	184041	-0.494	-0.355	0.764	-0.368	-0.295	0.646

References

Kilpatrick, K., Podesta, G., Walsh, S., Evans, R., & Minnett, P. (2014). Implementation of Version 6 AQUA and TERRA SST processing. White Paper.

Merchant, C. J., Embury, O., Le Borgne, P., & Bellec, B. (2006). Saharan dust in nighttime thermal imagery: Detection and reduction of related biases in retrieved sea surface temperature. Remote Sensing of Environment, 104, 15–30.

Minnett, P.J., Knuteson, R.O., Best, F.A., Osborne, B.J., Hanafin, J.A., & Brown, O.B. (2001). The Marine-Atmospheric Emitted Radiance Interferometer (M-AERI), a high-accuracy, seagoing infrared spectroradiometer. Journal of Atmospheric and Oceanic Technology 18, 994-1013.

Minnett, P.J., Smith, M., & Ward, B. (2011). Measurements of the oceanic thermal skin effect. Deep Sea Research Part II: Topical Studies in Oceanography 58, 861-868. 10.1016/j.dsr2.2010.10.024

USE OF 3.9 µM CHANNEL FOR DAYTIME SEA SURFACE TEMPERATURE RETRIEVAL

Prabhat Koner

ESSIC, University of Maryland, USA, Email: pkoner@umd.edu

Abstract

Determination of satellite-based sea surface temperature (SST) dates back to the 1970s, and it was derived using measured brightness temperature (BT) of 11 and 12 µm channels only. Although triple-window algorithm (TWA) including 3.7 µm is proven better options for SST retrieval, generation of linear coefficients including shortwave channels during daylight hours is extremely challenging due to the highly nonlinear contribution of solar reflection and scattering. Most of the older generation polar satellite imagers except MODIS were having only one 3.7 µm channel at short-wave infrared (SWIR) region and developed inertia in the community not to use SWIR channels for daytime operational SST retrieval. On the other hand, most of geo-stationary imagers are having a channel of 3.9 µm in SWIR. This talk will discuss the difference characteristics between 3.7 and 3.9 µm channels for daytime SST retrieval from theoretical point of view as well as applying on real data from MODIS. Use of 3.9 µm channel for daytime SST retrieval using physical deterministic (PD) method is accepted, but it will be shown that 3.9 µm channel for daytime SST retrieval using regression is a sound choice too. A successful operational implementation of 3.9 µm channel for SST retrieval from GOES(13-15) measurement using PD method will be also included in this presentation.

OPTIMAL ESTIMATION OF SEA SURFACE TEMPERATURE FROM AMSR-E

Pia Nielsen-Englyst[(1)], Jacob L. Høyer,[(1)], Leif Toudal Pedersen[(2)], Chelle L. Gentemann[(3)], Emy Alerskans[(1)], Tom Block[(4)] and Craig Donlon[(5)]

(1) Danish Meteorological Institute, Lyngbyvej 100, DK-2100 Copenhagen Ø, Denmark, Emails: pne@dmi.dk (P.NE.); jlh@dmi.dk (J.L.H.); ea@dmi.dk (E.A.)
(2) DTU-Space, Technical University of Denmark, DK-2800 Lyngby, Denmark, Email: ltp@eolab.dk
(3) Earth and Space Research, Seattle,WA 98121, USA, Email: cgentemann@gmail.com
(4) Brockmann Consult GmbH, Max-Planck-Str. 2, 21502 Geesthacht, Germany, Email: tom.block@brockmann-consult.de
(5) European Space Agency/European Space Research and Technology Centre (ESA/ESTEC), 2201 AZ Noordwijk, The Netherlands, Email: craig.donlon@esa.int

1. Introduction

Sea surface temperature (SST) is an essential climate variable used for climate monitoring, understanding of air–sea interactions, and numerical weather prediction. Since the early 1980s SST has been observed from thermal infrared (IR) satellite instruments. However, these observations are limited by clouds and biased by aerosols (Reynolds, 1993; Reynolds et al., 2002; Vázquez-Cuervo et al., 2004). SST observations from passive microwave (PMW) sensors are widely recognized as an important alternative to the IR observations (Donlon et al., 2007; Donlon and Co-Authors., 2010) as these are not prevented by non-precipitating clouds and the impact from aerosols is small (Chelton and Wentz, 2005; Wentz et al., 2000).

SST retrievals using the optimal estimation (OE) method have already been developed for IR retrievals (Merchant et al., 2008, 2009; Merchant and Embury, 2014). The OE methodology utilizes a forward model that includes a priori information on the ocean and atmosphere to simulate brightness temperatures. Using the OE method leads to improvements in the accuracy of IR SST retrievals and it was used to generate the first IR SST climate data record from the European Space Agency Climate Change Initiative (ESA-CCI) project (Merchant et al., 2008, 2014). The strength of using an OE algorithm is that it can be designed to estimate both retrieval uncertainty and sensitivity (Merchant et al., 2013).

The OE method has previously been used on multi-frequency PMW data (Pedersen, 1994) and results from AMSR-E retrievals were reported by Melsheimer et al. (2009) and Scarlat et al. (2017), where SST was among the retrieved parameters, but the focus was on the retrieval of sea ice parameters. The OE method has also been applied for WindSat retrievals (Bettenhausen et al., 2006), where SST also was among the retrieved parameters but with focus on wind vector retrievals. The aim of this study is to develop a retrieval algorithm which provides an optimal and physically consistent retrieval with a specific focus on retrieving SST to be used for generation of a climate data record. This study is based on the work done in Nielsen-Englyst et al. (2018) extended with an assessment of atmospheric impacts on the SST retrievals and possible screening methods.

2. Data

This study uses the spatially resampled L2A swath data product AMSR-E V12 (Ashcroft and Wentz, 2013), produced by Remote Sensing Systems (RSS) and distributed by NASA's National Snow and Ice Data Center (NSIDC; https://nsidc.org/data/ae_l2a). The spatial resampling is generated by applying the Backus–Gilbert method to the L1A data. The RSS L2A product includes

brightness temperatures for all AMSR-E channels that have been calibrated to the RSS version 7 standard, which includes inter-calibration with other satellite radiometers, and a correction to the AMSR-E hot load used during the calibration (Wentz, n.d.). Here, we use the re-sampling to 6.9 GHz resolution (75 × 43 km) for the 5 lowest frequencies.

The in situ dataset used for algorithm testing and validation is composed of quality-controlled measurements taken from the International Comprehensive Ocean-Atmosphere Dataset (ICOADS) version 2.5.1 (Woodruff et al., 2011), and the Met Office Hadley Centre (MOHC) Ensembles dataset version 4.2.0 (EN4) (Good et al., 2013), where measurements from drifting buoys constitute the main source of observations. Temperature observations are also used from the Argo profiling floats (Roemmich et al., 2009).

The OE method uses a priori information about the state of the ocean and atmosphere as first guess. We use Numerical Weather Prediction (NWP) information from the ERA-Interim NWP data (Dee et al., 2011) as first guess. The ERA-Interim NWP SST fields are from the Operational Sea Surface Temperature and Ice Analysis (OSTIA) level 4 SST analysis, which is generated from IR and PMW satellite observations blended with in situ data from drifting buoys (Donlon et al., 2012; Stark et al., 2007).

For the assessment of atmospheric effects on the retrievals we use observations from the Cloud-Aerosol Lidar with Orthogonal Polarization (CALIOP) instrument onboard the Cloud–Aerosol Lidar and Infrared Pathfinder Satellite Observations (CALIPSO). CALIOP is a two-wavelength polarization-sensitive lidar which provides high-resolution vertical profiles of aerosols and clouds (Liu et al., 2009; Winker et al., 2007, 2009). We use the CALIPSO Level 2 lidar vertical feature mask data product that describes the vertical and horizontal distribution of clouds and aerosols layers observed by CALIOP. The data are recorded in nominal increments of 15 consecutive laser pulses, which is nominally equivalent to a distance of 5 km along the laser ground-track.

2.1. The multi-sensor matchup databases

The basis for the retrieval algorithmic development and tuning is a Multi-sensor Matchup Dataset (MMD) pioneered by the ESA-CCI SST project. It includes AMSR-E orbital data matched to in situ observations from drifting buoys and Argo floats, requiring a maximal geodesic distance of 20 km and a maximal time difference of 4 h. ERA-Interim NWP data have been referenced to each AMSR-E pixel and each in situ measurement and spatially interpolated to the data raster (Schulzweida et al., 2010). Developing an accurate retrieval algorithm relies on the quality of the satellite observations and auxiliary fields used for the retrieval and validation. Erroneous matchups have been flagged as described in Nielsen-Englyst et al. (2018).

For the assessment of the atmospheric effects another MMD has been developed where AMSR-E observations have been matched with in situ observations, and the CALIOP data. Here, we use a 5-year long CALIOP matchup dataset covering 2007-2011, generated following the same matchup procedure as described above.

3. The OE algorithm

The OE algorithm uses dual polarization observations (v-pol and h-pol) at the frequencies: 6.9, 10.7, 18.7, 23.8, 36.5 GHz. Four geophysical parameters are considered to be the leading terms controlling the observed microwave brightness temperatures in the measurement situation (considering open-ocean only):

$$x = [WS, TCWV, TCLW, SST], \quad (1)$$

where WS is the wind speed, TCWV is the integrated columnar atmospheric water vapor content, TCLW is the integrated (columnar) cloud liquid water content, and SST is the sea surface temperature.

The variations of the retrieved geophysical parameters are restricted by the use of a priori information from NWP about the mean (a priori state) and covariances of the parameters. The covariance matrix of x is:

$$S_a = \begin{bmatrix} e_{WS}^2 & 0 & 0 & 0 \\ 0 & e_{TCWV}^2 & 0 & 0 \\ 0 & 0 & e_{TCLW}^2 & 0 \\ 0 & 0 & 0 & e_{SST}^2 \end{bmatrix}, \quad (2)$$

where e_{WS} = 2 m·s−1, e_{TCWV} = 0.9 mm, e_{TCLW} = 1 mm and e_{SST} = 0.50 K. The uncertainties on the WS, TCVW and TCLW are best estimates based upon published validation results (see e.g., (Chelton and Freilich, 2005; Dee et al., 2011; Jakobson et al., 2012; Jiang et al., 2012; Li et al., 2008)), while the SST uncertainty is derived from a comparison with Argo floats.

The quality can be assessed by comparing the simulated and observed brightness temperatures. This is quantified through the root-mean-square error ($RMSE_{TB}$). Figure 1a shows the $RMSE_{TB}$ value for each iteration performed using a subset of the MMD. A convergence test is applied to decide whether a retrieval process has converged to sufficient precision or if more iterations are needed. A maximum of 10 iterations are allowed and a failure to meet the above convergence criterion within 10 iterations leads to an exclusion of the data (<0.1%). Figure 1b shows the number of iterations performed for all drifter matchups during 2010 and convergence is typically reached after 3–4 iterations.

The OE method assumes an unbiased prior and forward model, which is not necessarily the case. We have applied two corrections two improve the forward model based on the difference between simulated and observed brightness temperatures (Nielsen-Englyst et al., 2018).

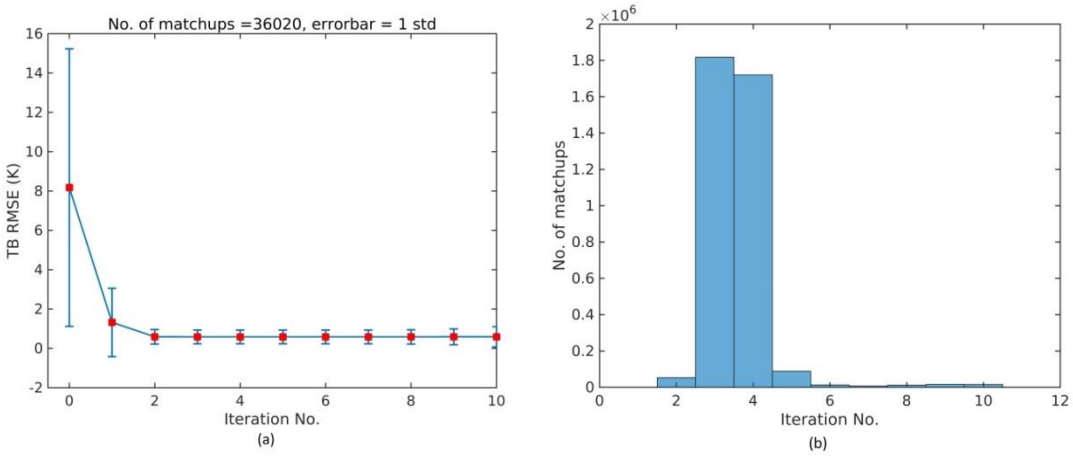

Figure 1. (a) The mean $RMSE_{TB}$ for all channels is plotted for each iteration number. Uncertainty bars show one standard deviation; (b) number of iterations performed for all drifter matchups during 2010.

4. Results

The OE algorithm has been run for 3,764,798 drifter matchups in 2010 and the statistics of the OE SSTs against drifter SSTs are given in Table 1.

Table 1. Comparison of retrieved SSTs and NWP SSTs against drifter SSTs for various subsets.

Filter	**Bias/K**	**std/K**	**Bias/K**	**std/K**	**N (10^6)**	
	OE-Drifter	**OE-Drifter**	**NWP-Drifter**	**NWP-Drifter**		
Convergence test passed	0.02	0.57	−0.04	0.50	3.7429	=100%
$RMSE_{TB}$ < 1 K	0.02	0.51	−0.04	0.50	3.4329	=92%
$RMSE_{TB}$ < 0.50 K	0.02	0.47	−0.04	0.48	2.3953	=64%
$RMSE_{TB}$ < 0.35 K	0.02	0.45	−0.04	0.47	1.5681	=42%

In Figure 2 all retrievals which have passed the convergence test have been binned with respect to $RMSE_{TB}$ with a bin size of 0.1 K. The number of members in each bin is shown in the bottom plot (blue curve) together with the cumulative percentage (red curve). The middle plot displays the binned distribution of OE SST minus drifter SST (with bin size of 1 K) as a function of binned $RMSE_{TB}$, where the color bar is the number of matchups in each bin. The top plot shows the mean (solid) and standard deviation (dashed) of OE SST minus drifter SST as a function of the binned $RMSE_{TB}$ statistic. We notice a large increase in scatter as $RMSE_{TB}$ increases. This makes the $RMSE_{TB}$-value an efficient indicator of the quality of the OE SST retrieval. Limiting $RMSE_{TB}$ to 1 K

removes only 8% of the converged retrievals and leaves the remaining 92% with a bias of 0.02 K and standard deviation of 0.51 K (see Table 1).

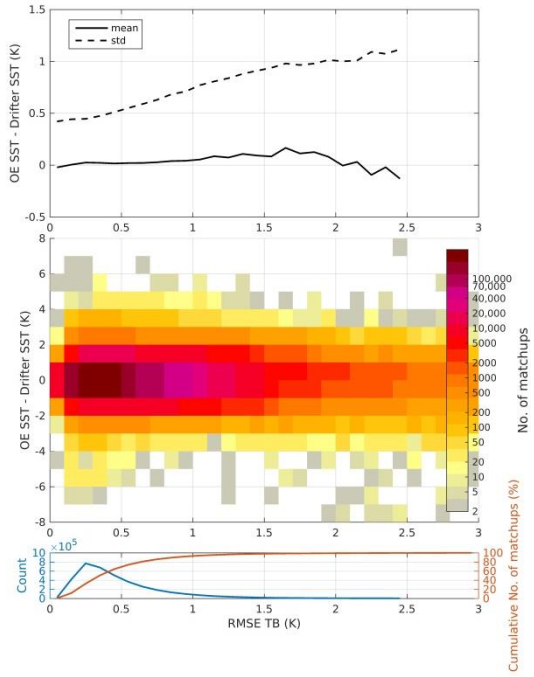

Figure 2. OE SST minus drifter SST as a function of binned $RMSE_{TB}$. The dashed line is standard deviation while the solid line is bias in the upper figure. The surface plot in the middle figure shows the number of matchups in each bin, while the bottom plot shows the number of matchups (blue) and the cumulative percentage of matchups (red) in each $RMSE_{TB}$ bin.

Figure 3a-b shows the gridded (grid size = 5 degrees) mean and standard deviation of OE SST minus drifter SST, respectively, for the 64% best retrievals. Figure 3a reveals a dependency on latitude, with positive bias at mid-latitudes and negative bias in high latitudes and the equatorial region, likely linked to surface emissivity issues (dependent on wind speed and direction) and atmospheric effects. Figure 3b shows areas with high standard deviations in e.g., the Gulf Stream Extension, the Kuroshio Current and the Aghulas Retroflection areas. These regions are known to be very dynamical with high mesoscale activity and large SST gradients over smaller scales (Legeckis, 1978; Pascual et al., 2006). The mesoscale SST gradients will result in enhanced differences when the large (64 × 32 km native instantaneous field of view at 6.9 GHz) satellite footprints are compared with in situ observations. The larger standard deviations in these regions are therefore not related to the quality of the OE SST retrieval.

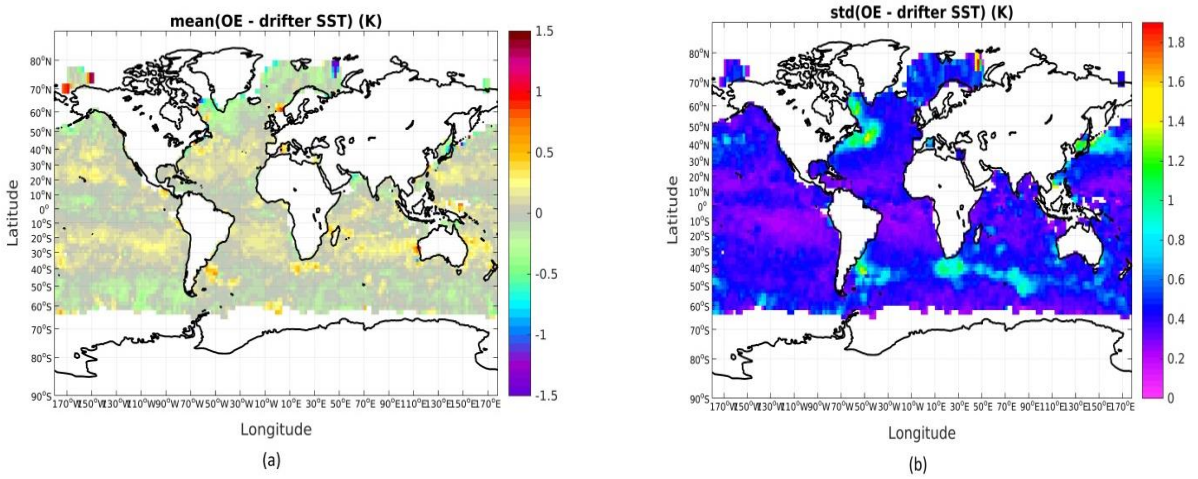

Figure 3. (a) Mean OE SST minus drifter SST; (b) Mean standard deviation of the OE retrieved minus drifter SST difference. Only retrievals with a corresponding RMSETB < 0.5 K are plotted in the figures.

Figure 4 shows the latitudinal difference in standard deviations of OE and NWP SST compared against drifters and Argo floats, respectively. The OE SST performs better than NWP SST in both northern and southern mid-latitudes, while NWP SST performs better in the tropics. The latitudinal pattern in the relative performance is remarkably similar for both the drifting buoys and the Argo floats.

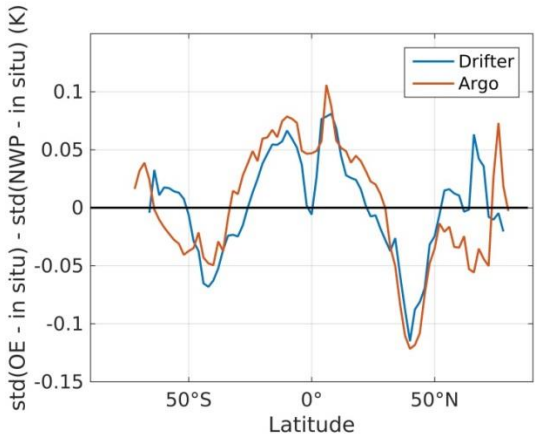

Figure 4. The latitudinal difference in standard deviations of OE and NWP SST compared against in situ SST. The blue curve is the comparison against drifters, while the red curve shows the comparison against Argo floats.

The OE technique offers several options to estimate an uncertainty for each individual retrieval. From Figure 2, it is evident that the quality of the SST retrieval is closely connected to the $RMSE_{TB}$ value. For that reason, we have set up an uncertainty indicator based on a scaled $RMSE_{TB}$ value, using a scaling factor of 0.55. Figure 5 shows the validation results for the uncertainties, where the OE SSTs minus drifter SSTs are displayed versus the theoretical uncertainties obtained from the $RMSE_{TB}$ values. The dashed line represents the ideal uncertainty with the assumptions that drifting buoys have a total uncertainty of 0.2 K and that the sampling uncertainty is 0.3 K. The point to satellite footprint sampling difference is estimated based on the results in Høyer et al. (Høyer et al.,

2012). The mean modeled uncertainty is estimated to 0.48 K including the in situ and sampling uncertainty.

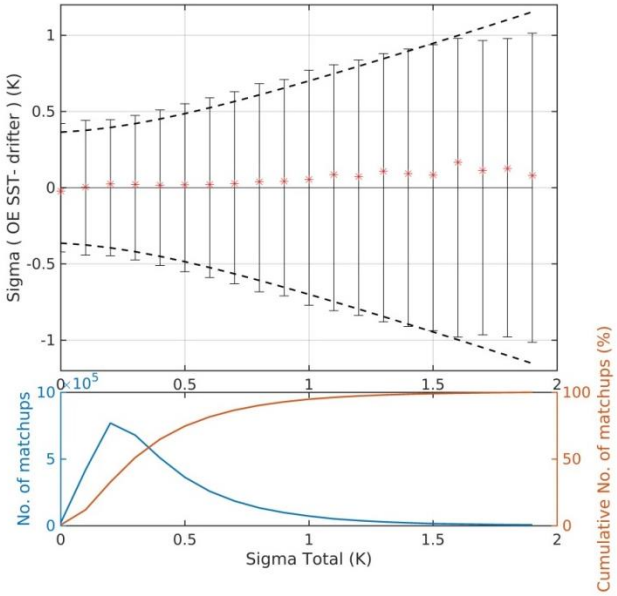

Figure 5. OE SST uncertainty validation with respect to drifter SST. Dashed lines show the ideal uncertainty model accounting for uncertainties in drifter SST and the sampling error. Solid black lines show one standard deviation of the retrieved minus drifter differences for each 0.1 K bin and the red symbols mark the mean bias. The bottom plot shows number of matchups (blue) and the cumulative percentage of matchups for each bin (red).

4.1. Atmospheric effects

This section examines the influence from atmospheric effects, such as cloud cover, ice and water content and aerosols, using the MMD containing observations from CALIOP. It is found that extreme cases with deep convective clouds do have an impact on the SST retrievals. This can be seen from Figure 6a where the performance (OE SST minus in situ SST) is plotted as a function of the number of deep convective cloud contaminated pixels in a pixel extract, containing 15 pixels. Figure 6b shows how well the estimated uncertainty captures these effects from deep convective clouds. It is found that the uncertainty increases with the number of pixels contaminated by deep convective clouds.

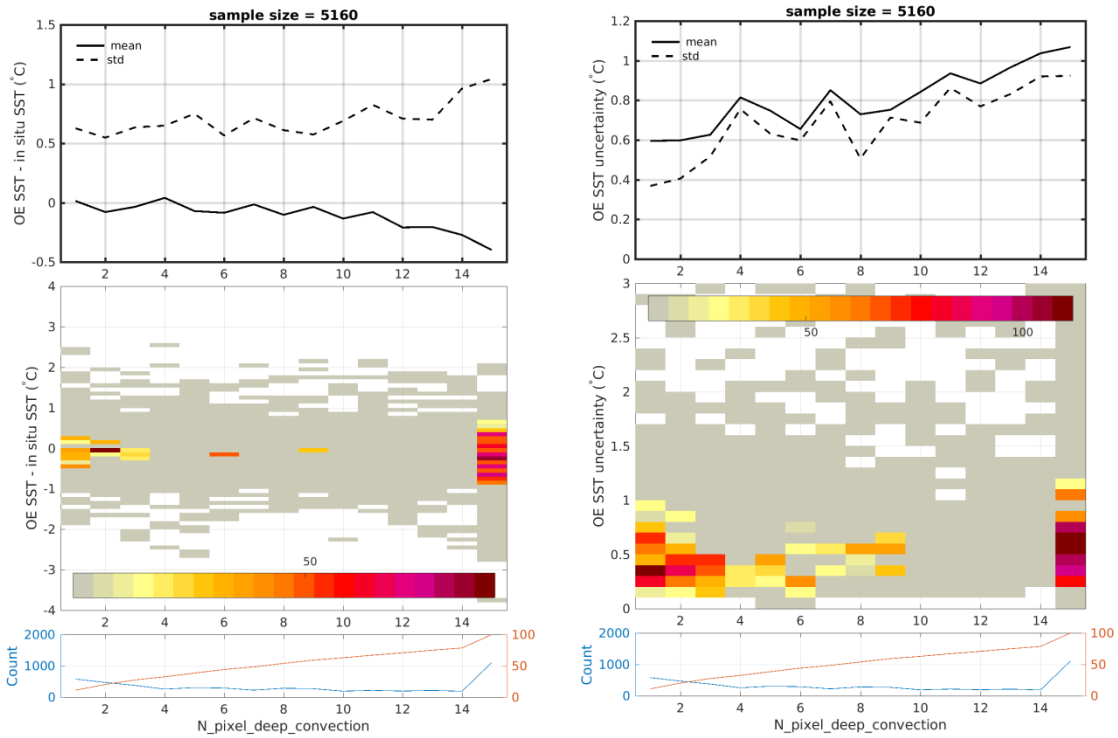

Figure 6 Retrieved SST minus in situ SST (a) and estimated SST uncertainty (b) as a function of number of pixels containing deep convective clouds (ranging from 1 to 15) from 2007-2011. Top panels: solid and dashed lines are mean and standard deviation of bias, respectively. Middle panels: Number of matchups in each bin. Bottom panels: the total number of matchups (blue) and the cumulative percentage of matchups (red) in each bin (for 1 pixel). A minimum of 30 matchups in each bin is applied for statistics calculation in the top figures. Note that 82% of the total matchups are found no DCCs (i.e. N_pixel = 0) and hence excluded from this figure.

Figure 7a shows the OE retrieved TCLW as a function of deep convective clouds, while Figure 7b shows the NWP TCLW as function of the number of pixels contaminated by deep convective clouds. The retrieved TCLW is correlated well with the number of deep convective clouds, while the NWP TCLW is not.

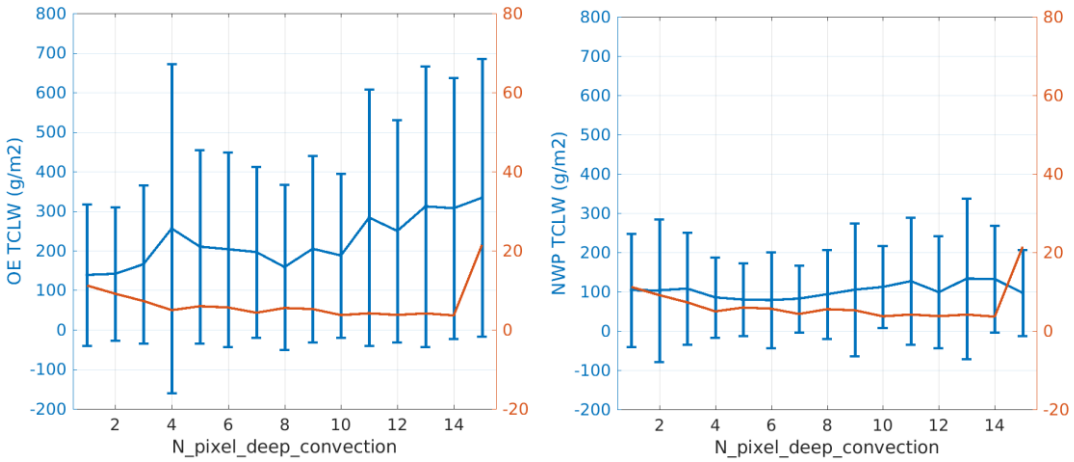

Figure 7 OE retrieved total cloud liquid water (TCLW) and NWP TCLW as a function of the number of pixels containing deep convective cloud from 2007-2011. On the left y-axis: solid lines and error bars represent mean and standard deviation of each bin, respectively. The right y-axis shows normalized histogram of bins. A minimum of 30 matchups in each bin is applied for statistics calculation.

5. Conclusion

The optimal estimation (OE) method has been used to retrieve sea surface temperature (SST) from passive microwave (PMW) satellite observations. The OE SST has an overall bias (OE SST - drifter SST) of 0.02 K and standard deviation of 0.47 K when considering the 64% matchups, where the simulated and observed brightness temperatures are most consistent. The modeled uncertainty estimates, available for each retrieval, have proven to be accurate and reliable, when compared to in situ observations. The main advantage of the OE technique is its capability to provide valuable information on pixel level about the quality of the satellite observations, which can be used directly to identify and discard erroneous retrievals (e.g., contamination from extreme wind, atmospheric attenuation and emission, sun-glint, land/ice, rain and RFI). We have found that deep convective clouds do influence the performance of the retrievals. However, the effects from deep convective clouds are easily identified by the estimated uncertainty, or can be removed by using the retrieved TCLW, which has turned out to be correlated with the deep convective clouds. The findings provide an important contribution to understanding PMW SST observations and towards combining PMW and IR observations.

6. References

Ashcroft, P. and Wentz, F. J.: AMSR-E/Aqua L2A Global Swath Spatially-Resampled Brightness Temperatures (Tb), Version 3, , doi:10.5067/AMSR-E/AE_L2A.003, 2013.

Bettenhausen, M. H., Smith, C. K., Bevilacqua, R. M., Nai-Yu Wang, Gaiser, P. W. and Cox, S.: A nonlinear optimization algorithm for WindSat wind vector retrievals, IEEE Trans. Geosci. Remote Sens., 44(3), 597–610, doi:10.1109/TGRS.2005.862504, 2006.

Chelton, D. B. and Freilich, M. H.: Scatterometer-Based Assessment of 10-m Wind Analyses from the Operational ECMWF and NCEP Numerical Weather Prediction Models, Mon. Weather Rev., 133(2), 409–429, doi:10.1175/MWR-2861.1, 2005.

Chelton, D. B. and Wentz, F. J.: Global Microwave Satellite Observations of Sea Surface Temperature for Numerical Weather Prediction and Climate Research, Bull. Am. Meteorol. Soc., 86(8), 1097–1115, doi:10.1175/BAMS-86-8-1097, 2005.

Dee, D. P., Uppala, S. M., Simmons, A. J., Berrisford, P., Poli, P., Kobayashi, S., Andrae, U., Balmaseda, M. A., Balsamo, G., Bauer, P., Bechtold, P., Beljaars, A. C. M., van de Berg, L., Bidlot, J., Bormann, N., Delsol, C., Dragani, R., Fuentes, M., Geer, A. J., Haimberger, L., Healy, S. B., Hersbach, H., Hólm, E. V., Isaksen, L., Kållberg, P., Köhler, M., Matricardi, M., McNally, A. P., Monge-Sanz, B. M., Morcrette, J.-J., Park, B.-K., Peubey, C., de Rosnay, P., Tavolato, C., Thépaut, J.-N. and Vitart, F.: The ERA-Interim reanalysis: configuration and performance of the data assimilation system, Q. J. R. Meteorol. Soc., 137(656), 553–597, doi:10.1002/qj.828, 2011.

Donlon, C., Rayner, N., Robinson, I., Poulter, D. J. S., Casey, K. S., Vazquez-Cuervo, J., Armstrong, E., Bingham, A., Arino, O., Gentemann, C., May, D., LeBorgne, P., Piollé, J., Barton, I., Beggs, H., Merchant, C. J., Heinz, S., Harris, A., Wick, G., Emery, B., Minnett, P., Evans, R., Llewellyn-Jones, D., Mutlow, C., Reynolds, R. W. and Kawamura, H.: The Global Ocean Data Assimilation Experiment High-resolution Sea Surface Temperature Pilot Project, Bull. Am. Meteorol. Soc., 88(8), 1197–1213, doi:10.1175/BAMS-88-8-1197, 2007.

Donlon, C. J. and Co-Authors.: Successes and Challenges for the Modern Sea Surface Temperature Observing System, in Proceeding of OceanObs'09: Sustained Ocean Observations and Information for Society, vol. 2, Hall, J., Harrison, D.E. & Stammer, D., ESA Publication WPP-306, Venice Italy, 21-25 September 2009., 2010.

Donlon, C. J., Martin, M., Stark, J., Roberts-Jones, J., Fiedler, E. and Wimmer, W.: The Operational Sea Surface Temperature and Sea Ice Analysis (OSTIA) system, Remote Sens. Environ., 116, 140–158, doi:10.1016/j.rse.2010.10.017, 2012.

Good, S. A., Martin, M. J. and Rayner, N. A.: EN4: Quality controlled ocean temperature and salinity profiles and monthly objective analyses with uncertainty estimates: THE EN4 DATA SET, J. Geophys. Res. Oceans, 118(12), 6704–6716, doi:10.1002/2013JC009067, 2013.

Høyer, J. L., Karagali, I., Dybkjær, G. and Tonboe, R.: Multi sensor validation and error characteristics of Arctic satellite sea surface temperature observations, Remote Sens. Environ., 121, 335–346, doi:10.1016/j.rse.2012.01.013, 2012.

Jakobson, E., Vihma, T., Palo, T., Jakobson, L., Keernik, H. and Jaagus, J.: Validation of atmospheric reanalyses over the central Arctic Ocean: TARA REANALYSES VALIDATION, Geophys. Res. Lett., 39(10), n/a-n/a, doi:10.1029/2012GL051591, 2012.

Jiang, J. H., Su, H., Zhai, C., Perun, V. S., Del Genio, A., Nazarenko, L. S., Donner, L. J., Horowitz, L., Seman, C., Cole, J., Gettelman, A., Ringer, M. A., Rotstayn, L., Jeffrey, S., Wu, T., Brient, F., Dufresne, J.-L., Kawai, H., Koshiro, T., Watanabe, M., LÉcuyer, T. S., Volodin, E. M., Iversen, T., Drange, H., Mesquita, M. D. S., Read, W. G., Waters, J. W., Tian, B., Teixeira, J. and Stephens, G. L.: Evaluation of cloud and water vapor simulations in CMIP5 climate models using NASA "A-Train" satellite observations: EVALUATION OF IPCC AR5 MODEL SIMULATIONS, J. Geophys. Res. Atmospheres, 117(D14), doi:10.1029/2011JD017237, 2012.

Legeckis, R.: A survey of worldwide sea surface temperature fronts detected by environmental satellites, J. Geophys. Res., 83(C9), 4501, doi:10.1029/JC083iC09p04501, 1978.

Li, J.-L. F., Waliser, D., Woods, C., Teixeira, J., Bacmeister, J., Chern, J., Shen, B.-W., Tompkins, A., Tao, W.-K. and Köhler, M.: Comparisons of satellites liquid water estimates to ECMWF and GMAO analyses, 20th century IPCC AR4 climate simulations, and GCM simulations, Geophys. Res. Lett., 35(19), doi:10.1029/2008GL035427, 2008.

Liu, Z., Vaughan, M., Winker, D., Kittaka, C., Getzewich, B., Kuehn, R., Omar, A., Powell, K., Trepte, C. and Hostetler, C.: The CALIPSO Lidar Cloud and Aerosol Discrimination: Version 2 Algorithm and Initial Assessment of Performance, J. Atmospheric Ocean. Technol., 26(7), 1198–1213, doi:10.1175/2009JTECHA1229.1, 2009.

Melsheimer, C., Heygster, G., Mathew, N. and Toudal Pedersen, L.: Retrieval of sea ice emissivity and integrated retrieval of surface and atmospheric parameters over the Arctic from AMSR-E data., J. Remote Sens. Soc. Jpn., 29(1), 236–241, 2009.

Merchant, C. J. and Embury, O.: Simulation and Inversion of Satellite Thermal Measurements, in Experimental Methods in the Physical Sciences, vol. 47, pp. 489–526, Elsevier., 2014.

Merchant, C. J., Le Borgne, P., Marsouin, A. and Roquet, H.: Optimal estimation of sea surface temperature from split-window observations, Remote Sens. Environ., 112(5), 2469–2484, doi:10.1016/j.rse.2007.11.011, 2008.

Merchant, C. J., Le Borgne, P., Roquet, H. and Marsouin, A.: Sea surface temperature from a geostationary satellite by optimal estimation, Remote Sens. Environ., 113(2), 445–457, doi:10.1016/j.rse.2008.10.012, 2009.

Merchant, C. J., Le Borgne, P., Roquet, H. and Legendre, G.: Extended optimal estimation techniques for sea surface temperature from the Spinning Enhanced Visible and Infra-Red Imager (SEVIRI), Remote Sens. Environ., 131, 287–297, doi:10.1016/j.rse.2012.12.019, 2013.

Merchant, C. J., Embury, O., Roberts-Jones, J., Fiedler, E., Bulgin, C. E., Corlett, G. K., Good, S., McLaren, A., Rayner, N., Morak-Bozzo, S. and Donlon, C.: Sea surface temperature datasets for climate applications from Phase 1 of the European Space Agency Climate Change Initiative (SST CCI), Geosci. Data J., 1(2), 179–191, doi:10.1002/gdj3.20, 2014.

Nielsen-Englyst, P., L. Høyer, J., Toudal Pedersen, L., L. Gentemann, C., Alerskans, E., Block, T. and Donlon, C.: Optimal Estimation of Sea Surface Temperature from AMSR-E, Remote Sens., 10(2), 229, doi:10.3390/rs10020229, 2018.

Pascual, A., Faugère, Y., Larnicol, G. and Le Traon, P.-Y.: Improved description of the ocean mesoscale variability by combining four satellite altimeters, Geophys. Res. Lett., 33(2), doi:10.1029/2005GL024633, 2006.

Pedersen, L. T.: Merging microwave radiometer data and meteorological data for improved sea ice concentrations, EARSeL Adv. Remote Sens., 3(2–XII), 81–89, 1994.

Reynolds, R. W.: Impact of Mount Pinatubo Aerosols on Satellite-derived Sea Surface Temperatures, J. Clim., 6(4), 768–774, doi:10.1175/1520-0442(1993)006<0768:IOMPAO>2.0.CO;2, 1993.

Reynolds, R. W., Rayner, N. A., Smith, T. M., Stokes, D. C. and Wang, W.: An Improved In Situ and Satellite SST Analysis for Climate, J. Clim., 15(13), 1609–1625, doi:10.1175/1520-0442(2002)015<1609:AIISAS>2.0.CO;2, 2002.

Roemmich, D., Johnson, G., Riser, S., Davis, R., Gilson, J., Owens, W. B., Garzoli, S., Schmid, C. and Ignaszewski, M.: The Argo Program: Observing the Global Oceans with Profiling Floats, Oceanography, 22(2), 34–43, doi:10.5670/oceanog.2009.36, 2009.

Scarlat, R. C., Heygster, G. and Pedersen, L. T.: Experiences With an Optimal Estimation Algorithm for Surface and Atmospheric Parameter Retrieval From Passive Microwave Data in the Arctic, IEEE J. Sel. Top. Appl. Earth Obs. Remote Sens., 10(9), 3934–3947, doi:10.1109/JSTARS.2017.2739858, 2017.

Schulzweida, U., Kornblueh, L. and Quast, R.: CDO user's guide – Climate Data Operators, Technical Report, Max Planck Institute for Meteorology., 2010.

Stark, J. D., Donlon, C. J., Martin, M. J. and McCulloch, M. E.: OSTIA : An operational, high resolution, real time, global sea surface temperature analysis system, pp. 1–4, IEEE., 2007.

Vázquez-Cuervo, J., Armstrong, E. M. and Harris, A.: The Effect of Aerosols and Clouds on the Retrieval of Infrared Sea Surface Temperatures, J. Clim., 17(20), 3921–3933, doi:10.1175/1520-0442(2004)017<3921:TEOAAC>2.0.CO;2, 2004.

Wentz, F. J.: SSM/I Version-7 Calibration Report, Remote Sensing Systems, Santa Rosa, CA., n.d.

Wentz, F. J., Gentemann, C., Smith, D. and Chelton, D. B.: Satellite Measurements of Sea Surface Temperature Through Clouds, Science, 288(5467), 847–850, doi:10.1126/science.288.5467.847, 2000.

Winker, D. M., Hunt, W. H. and McGill, M. J.: Initial performance assessment of CALIOP, Geophys. Res. Lett., 34(19), doi:10.1029/2007GL030135, 2007.

Winker, D. M., Vaughan, M. A., Omar, A., Hu, Y., Powell, K. A., Liu, Z., Hunt, W. H. and Young, S. A.: Overview of the CALIPSO Mission and CALIOP Data Processing Algorithms, J. Atmospheric Ocean. Technol., 26(11), 2310–2323, doi:10.1175/2009JTECHA1281.1, 2009.

Woodruff, S. D., Worley, S. J., Lubker, S. J., Ji, Z., Eric Freeman, J., Berry, D. I., Brohan, P., Kent, E. C., Reynolds, R. W., Smith, S. R. and Wilkinson, C.: ICOADS Release 2.5: extensions and enhancements to the surface marine meteorological archive, Int. J. Climatol., 31(7), 951–967, doi:10.1002/joc.2103, 2011.

SECTION 3: POSTERS

POSTERS LISTS

Posters are published on the GHRSST website and can be found in the 'Event Resources' of the G-XIX meeting page (https://www.ghrsst.org/agenda/g-xix/). They are available - as presented - in the 'Monday 4th June' and 'Tuesday 5th June' sections, under 'Interactive presentations'.

Where posters are available, individual links are also provided below.

MONDAY 4TH JUNE 2018 – INTERACTIVE PRESENTATIONS		
Nr	**Presenter**	**Title**
1		Withdrawn
2	Helen Beggs	A new 2 km SST atlas of the Australian regional seas (SSTAARS)
5	Chuqun Chen	The property of temperature profile of water surface layer detected by instrument, the Buoyant Equipment for Skin Temperature (best)
6	Caroline Cox	Retrieval of radiatively consistent Sea Surface Temperature under aerosol conditions using an optimal estimation scheme across the visible and infrared.
9	Lydia Gates	The Marine Climate Data Centre of Deutscher Wetterdienst in Hamburg
10	Lucile Gaultier	New discovery and analysis tools for multisensor exploitation
13	Tsutomu Hihara	Bias correction of satellite SST for ocean assimilation product using LETKF
14	Jacob Høyer	Consistency between Sea Surface Temperature and Sea Ice products in Arctic and Antarctic
17	Alexander Ignatov	Exploring MERRA-2 global meteorological and aerosol reanalyses for improved brightness temperature simulations and SST retrievals in the NOAA ACSPO system
18	Alexey Kaplan	Near-Lagrangian Platform (Drifting Buoy) + Near-Conservative Variable (SST) = ?
21	Prabhat Koner	Ocean micro-skin temperature profile retrieval from M-AERI measurement
22	Yukio Kurihara	SST Data from SGLI onboard the Shikisai Satellite
24		Withdrawn
25	Bingkun Luo	Coastal diurnal warming – a study of the Great Barrier Reef

MONDAY 4TH JUNE 2018 – INTERACTIVE PRESENTATIONS		
Nr	**Presenter**	**Title**
26	Bingkun Luo	Accuracy assessment of MERRA-2 temperature and humidity profiles over the tropical ocean using AEROSE Observations
29	David Meldrum	Towards improved drifter SST: a collaboration between the satellite community and the Data Buoy Co-operation Panel
30	Peter Minnett	Simultaneous Retrievals of Sea-surface Temperature and Column Water Vapor from MODIS measurements with Optimal Estimation
33	Nodoka Ono	Three-Way Error Analysis between GCOM-W, Himawari-8, and In Situ Surface Temperature Observations
34	Gang Pan	Seasonal variability of Sea Surface Temperature gradients in the south coast of Sri Lanka
36	Kyung-Ae Park	Sea Surface Current Retrieval Algorithm of Geo-KOMPSAT-2A/Advanced Meteorological Imager
38	Matthew Pennybacker	Towards Second VIIRS SST Reanalysis (RAN2)
41	Swathy Sunder	Exploring Machine Learning Techniques to Estimate Cloud Free Daily Sea Surface Temperatures (SST) from MODIS Aqua across South Eastern Arabian Sea
43	Jorge Vazquez	A review of the importance of high resolution SSTs: Application to a Coastal Upwelling Region
45	Gary Wick	Subpixel Variability and Quality Assessment of Satellite Sea Surface Temperature Data Using a Novel High Resolution Multistage Spectral Interpolation Technique
46	Xuepeng Zhao	Transition of Global Satellite Pathfinder SST Climate Data Record Production System to NOAA/NCEI for Operational Production

TUESDAY 5TH JUNE 2018 – INTERACTIVE PRESENTATIONS		
Nr	**Presenter**	**Title**
3	Marouan Bouali	On the use of NLSST and MCSST products for the study of spatio-temporal trends in ocean thermal gradients
4	Brahim Boussidi	The need for the measurement spatial response function for optimal deconvolution of AMSR-E SSTs
7	Prasanjit Dash	Towards an Enterprise Monitor for simultaneous monitoring of multiple ocean parameters: SST, salinity, height, wind and colour
8	Craig Donlon	The Copernicus Microwave Imaging Radiometer (CIMR) Mission
11	Irina Gladkova	ACSPO Regional Monitor for SST: ARMS v2.1
12	Lei Guan	Comparison of SUOMI NPP VIIRS SST with shipboard skin SST measurements in the Northwest Pacific
15	Jacob Høyer	Construction of an SST Climate Data Record from Passive Microwave measurements
16	Alexander Ignatov	In situ SST Quality Monitor version2 (iQuam2)
19	Ioanna Karagali	The increasing importance of SST for wind energy applications
20	Jaegwan Kim	Improvement for Operational SST Observed by the COMS at KMA
23	Wen-Hao Li	Differences in Three Unique High Resolution VIIRS Sea Surface Temperature Datasets
27	Bingkun Luo	Comparison of Sentinel-3a/SLSTR and MSG/SEVIRI derived diurnal warming estimates with CMEMS drifting buoy data
28	Eileen Maturi	NOAA's New High-Resolution Sea Surface Temperature Blended Analyses
31	Peter Minnett	Sea-Surface Temperature Fields from MODIS and VIIRS – an Update
32	Peter Minnett	Improved cloud mask for NASA sea-surface temperature products from MODIS and VIIRS
35	Kyung-Ae Park	Sea Surface Temperature Algorithm of Geo-KOMPSAT-2A/Advanced Meteorological Imager

TUESDAY 5TH JUNE 2018 – INTERACTIVE PRESENTATIONS		
Nr	**Presenter**	**Title**
37	Matthew Pennybacker	Update in NOAA SST Quality Monitor 2 (SQUAM2)
39	Boris Petrenko	Training regression SST algorithms for geostationary sensors against analysis L4 SST fields
40	Jean-François Piollé	A tool for the quantitative assessment of long time series of satellite SST
42	Igor Tomazic	Sentinel-3 SLSTR Cal/Val Activities for Sea Surface Temperature Measurements
44	Jorge Vazquez	CEOS Ocean Variables Enabling Research and Applications for GEO: COVERAGE

POSTERS EXTENDED ABSTRACTS

BIAS CORRECTION OF SATELLITE SST FOR OCEAN ASSIMILATION PRODUCT USING LETKF

Tsutomu Hihara[(1)], Yasumasa Miyazawa[(2)], Toru Miyama[(3)], Misako Kachi[(4)], Hiroshi Murakami[(5)], Yukio Kurihara[(6)]

(1) APL, JAMSTEC, Yokohama, Japan, Email: hiharat@jamstec.go.jp
(2) APL, JAMSTEC, Yokohama, Japan, Email: miyazawa@jamstec.go.jp
(3) APL, JAMSTEC, Yokohama, Japan, Email: tmiyama@jamstec.go.jp
(4) EORC, JAXA, Tsukuba, Japan, Email: kachi.misako@jaxa.jp
(5) EORC, JAXA, Tsukuba, Japan, Email: murakami.hiroshi.eo@jaxa.jp
(6) Triple-i, Tokyo, Japan, Email: kurihara@triple-i.co.jp

1. Introduction

Several earth observation satellites detect sea surface temperature (SST) with spatiotemporally high-resolution. However, the satellite SST data include missing areas caused by atmospheric and/or satellite orbit conditions. Additionally, satellites cannot detect information of vertical oceanic conditions. On the other hand, numerical ocean models are able to provide information of whole three-dimensional oceanic structures without any missing part, but they are suffering from errors due to model biases and unrealistic initial conditions. Data assimilation techniques effectively combining the observation data and the numerical model results allow us to reproduce more realistic oceanic conditions as compared to both the original observation and model data. By utilizing a data assimilation technique, we examine feasibility of producing ocean data set with temporally and spatially uniform quality as Level-4 SST data targeting south of Japan. Here we show that bias correction of satellite SST is required prior to data assimilation.

2. Observation data

2.1. Assimilated data

We assimilate SST products obtained by four satellites with three type sensors (Table 1). Most of products: Global Climate Observation Mission - Water (GCOM-W), Aqua, and Terra, detect SST every 12 hours, but Himawari-8 allows higher frequency, 1 hour. Advanced Himawari Imager (AHI) and Moderate Resolution Imaging Spectroradiometer (MODIS) measure SST covering wide areas from open ocean to nearshore regions with higher spatial resolution but the data quality easily deteriorates owing to the cloud noises. On the other hand, the measurement by Advanced Microwave Scanning Radiometer 2 (AMSR2) is relatively robust to the cloud noises but misses SST nearshore areas.

In addition, we assimilate sea surface height anomaly (SSHA) data obtained by four altimetry satellites and in-situ data provided by Global Temperature and Salinity Profile Programme (GTSPP). The altimetry satellites/ sensors are Jason-2, -3/Poseidon, CryoSat-2/Synthetic Aperture Interferometric Radar Altimeter - 2 (SPIRAL-2), Satellite with Argos and AltiKa (SARAL)/Altimeter in Ka-band (AltiKa). We downloaded SSHA data from the Copernicus - Marine environment monitoring service (CMEMS) website. Temperature and salinity vertical profiles obtained by ships, moored buoys, and floats are included in the GTSPP product.

Satellite	Himawari-8	GCOM-W	Aqua, Terra
Type of orbit	Geo-stationary	Sun-synchronous polar orbit	
Sensor name	AHI	AMSR2	MODIS
Sensor type	Infrared radiometer	Microwave radiometer	Infrared radiometer
Data provider	JAXA		NASA

Table 1: List of assimilated satellite SST data

2.2. Validation data

We use the in-situ SST data provided by iQUAM and observed by the Kuroshio-Bokujyo buoys which are moored off Shikoku Island (Figure 1). iQUAM data are used to confirm biases included in satellite SST data in section 4.1. Kuroshio-Bokujyo buoys data are used to validate the analysis data calculated by the data assimilation system described in section 4.2. These in-situ data are not assimilated, and thus independent from the analysis data. Note that nearshore locations of the buoys (Figure 1) are uncovered by the GCOM-W/AMSR2 measurement.

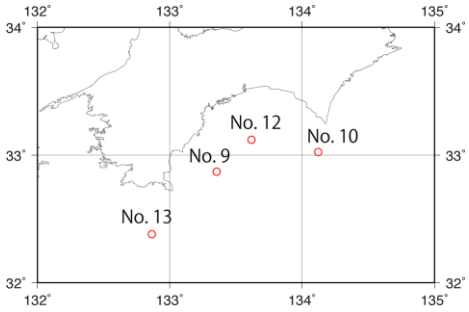

Figure 1: Locations of Kuroshio-Bokujyo buoys

3. Assimilation system

We show the status of assimilation system in Table 2. We constructed an ocean nowcast/forecast system assimilating observation data in a daily-basis using Stony Brook Parallel Ocean Model (sbPOM; Jordi and Wang, 2012) with Local Ensemble Transformation Kalman Filter (LETKF; Hunt et al., 2007). This system has been originally developed for investigating usability of Moderate Resolution Imaging Spectroradiometer (MODIS) sea surface temperature (SST) data south of Japan (Miyazawa et al., 2013).

sbPOM is a parallelized version of the widely adopted Princeton Ocean Model (Jordi and Wang, 2012), which is available to the general public. Choices of spatial and vertical resolution are 1/36˚ and 47 sigma levels, respectively. Surface forcing data are calculated by bulk formulae using the National Centers for Environmental Prediction (NCEP)/National Center for Atmospheric Research (NCAR) reanalysis atmospheric data (wind speed at 10m, temperature at 2m, water vapor at 2m, cloud amount). A clear-sky shortwave radiation is calculated by the method of Rosati and

Miyakoda (1988). Lateral boundary conditions are provided from a modified version of Japan Costal Ocean Predictability Experiment 2 model (JCOPE2M; Miyazawa et al., 2017).

LETKF is a variant of Ensemble Kalman filter (EnKF; Evensen 1994) and is an efficient upgrade of the local ensemble Kalman filter (LEKF; Ott et al. 2004). A LETKF code used in this study, was developed by Miyoshi et al. (2010).

Assimilation method	Local ensemble transformation Kalman filter (LETKF, Hunt et al., 2007)
Ensemble member	20
Assimilated data	Satellite SST, Satellite SSHA, in-situ data (temperature and salinity)
Ocean Model	Stony Brook Parallel Ocean Model (sbPOM, Jordi and Wang, 2012)
Forcing data	NCEP/NCAR Reanalysis
Boundary condition	Japan Coastal Ocean Predictability Experiment 2M (JCOPE2M, Miyazawa et al., 2017)
Analysis area	South of Japan (128-142˚E, 28-36˚N)
Horizontal resolution	1/36˚ (3km)

Table 2: Status of assimilation system.

4. Results

4.1. Bias Correction

First we directly compare satellite SST products around Japan. Figure 3a (b) shows that Himawari-8 SST is lower (higher) than AMSR2 SST in winter (summer). MODIS SST tends to have opposite tendency (Fig.3c, d), suggesting each non-negligible specific bias included in each product. Difference between Himawari-8 and MODIS in summer exceeds 1 ˚C in Pacific Ocean (cf. Fig.3b, c).

We validate the satellite SST data using iQUAM in-situ SST data. Figure 4 shows that seasonal changes of biases: negative (positive) in winter and positive (negative) in summer, are represented in the Himawari-8 (MODIS) SST data. On the other hand, no significant bias is detected in the AMSR2 SST data.

Various factors of errors could be included in the satellite SST data, so it is difficult to exactly describe possible causes for differences detected in these results. In particular, since both Himawari-8 and MODIS SST data are detected by infrared radiometers, the large difference exceeding 1˚C in summer is difficult to be explained by specific mechanisms associated with actual

physical phenomena. We just suggest that these differences could come from the technical differences in the SST detecting algorithms.

From the comparison of snapshots of clouds distribution and Himawari-8 SST (not shown here), we perceive that Himawri-8 SST data show significantly low values on edges of clouds where MODIS SST data are usually missing. This indicates that cloud contamination causes the negative bias of Himawari-8. A time series of Himawari-8 SST shows variations in weekly time scale (Fig.5a) that might be affected by changes in weather/cloud conditions in winter. Other satellite SST products do not show such phenomena.

These differences among satellite SSTs are more evident in 7-days moving average (Figs. 5c and 6c). To remove the biases in the Himawari-8 and MODIS SST, we developed a bias correction method using 7-days moving average of AMSR2 SST as a reference for correction, because significant difference between AMSR2 SST and iQUAM SST is not found (Fig. 4). Time series of corrected satellite SST in Figs. 5b and 6b show that the biases are reasonably excluded. This method is very effective to remove the biases varying in weekly and/or longer time scales.

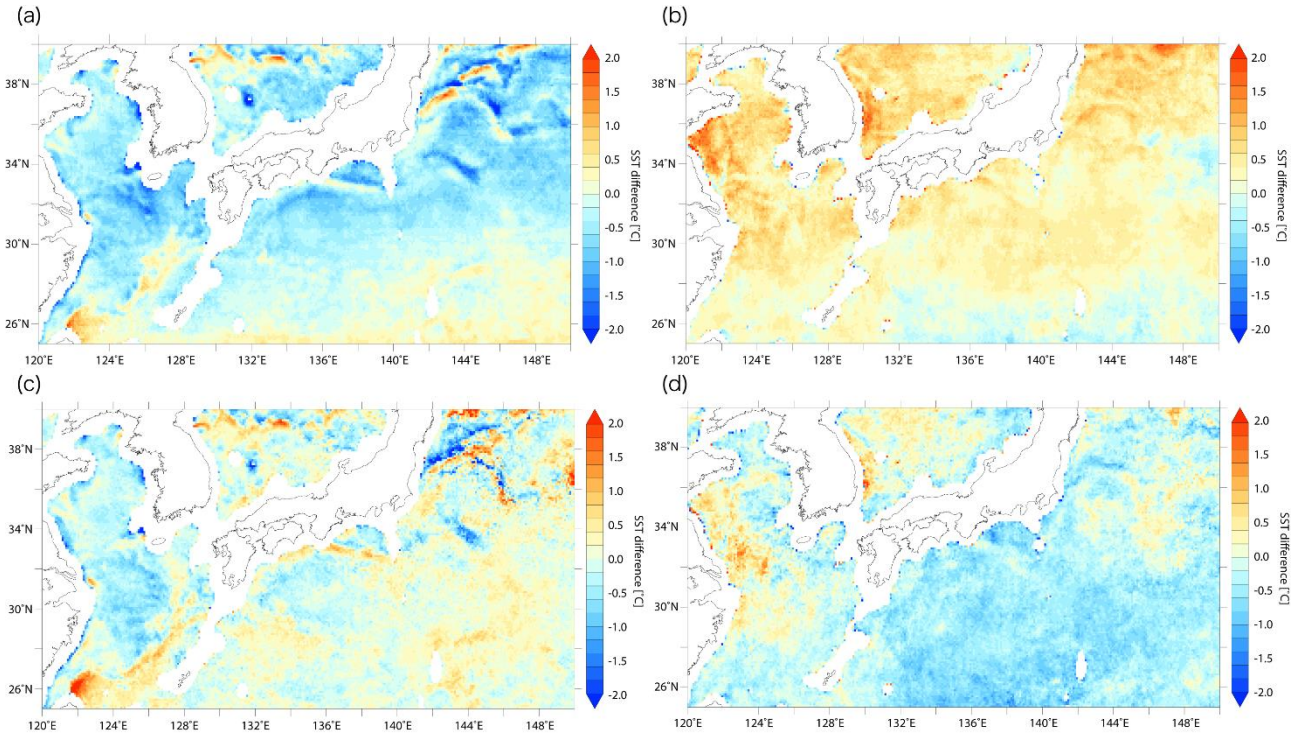

Figure 3: Spatial distributions of monthly average difference of (a)H8-A2 in February 2017, (b) H8-A2 in August 2017, (c) MA-A2 in February 2017, and (d) MA-A2 in August 2017.

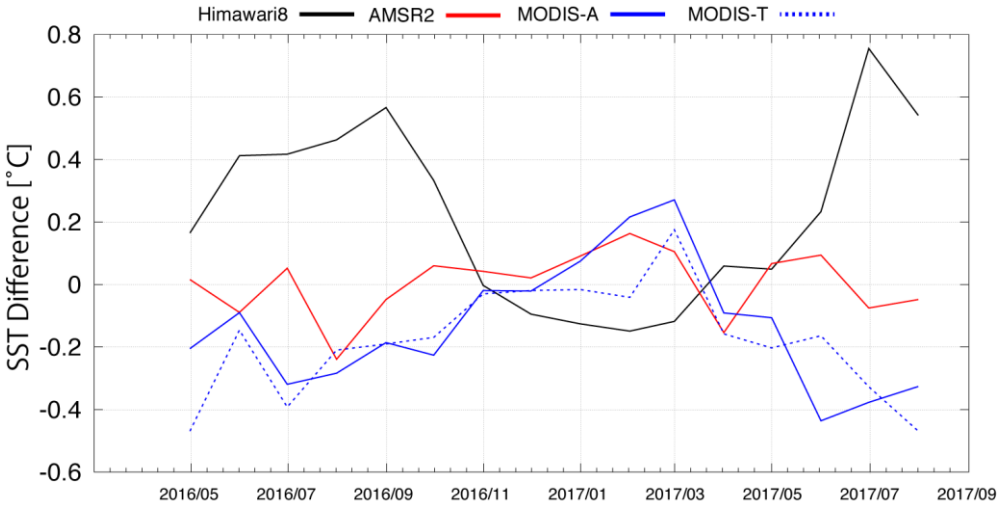

Figure 4: Monthly average difference between Satellite SST and iQUAM in-situ SST in 120-150˚E, 25-40˚N. Match up condition is ±30min. and 0.1˚ grid.

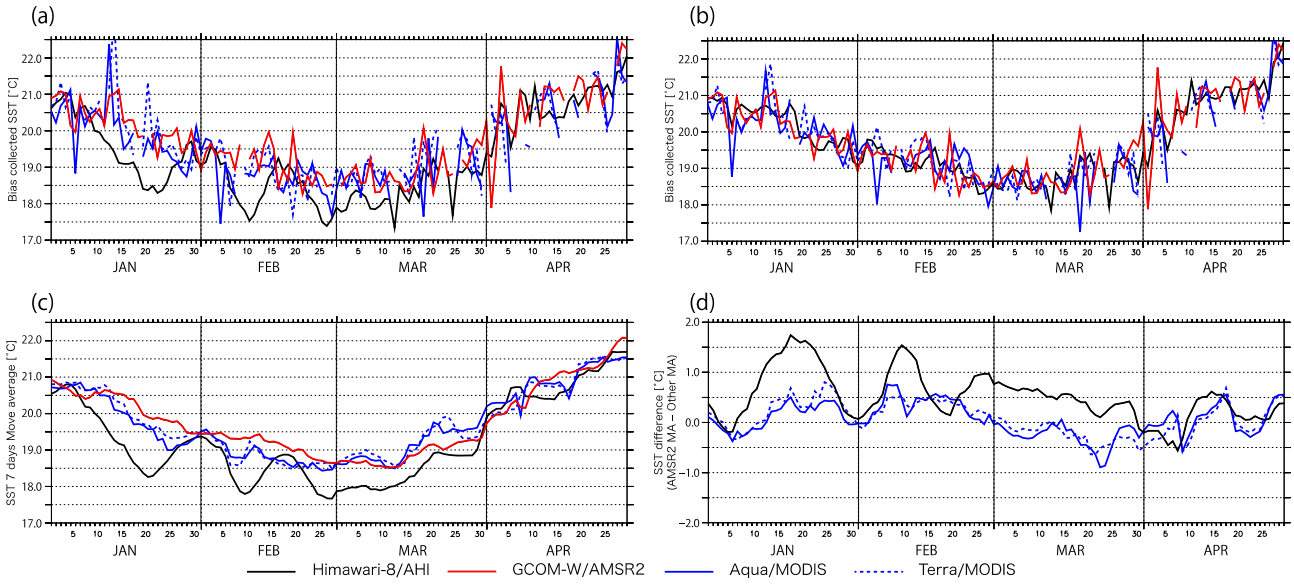

Figure. 5: Time series of (a) original data, (b) bias corrected data, (c) 7-days moving averaged data, and (d) correction parameter, averaged in 133-136˚E, 31-32˚N from January to April 2017.

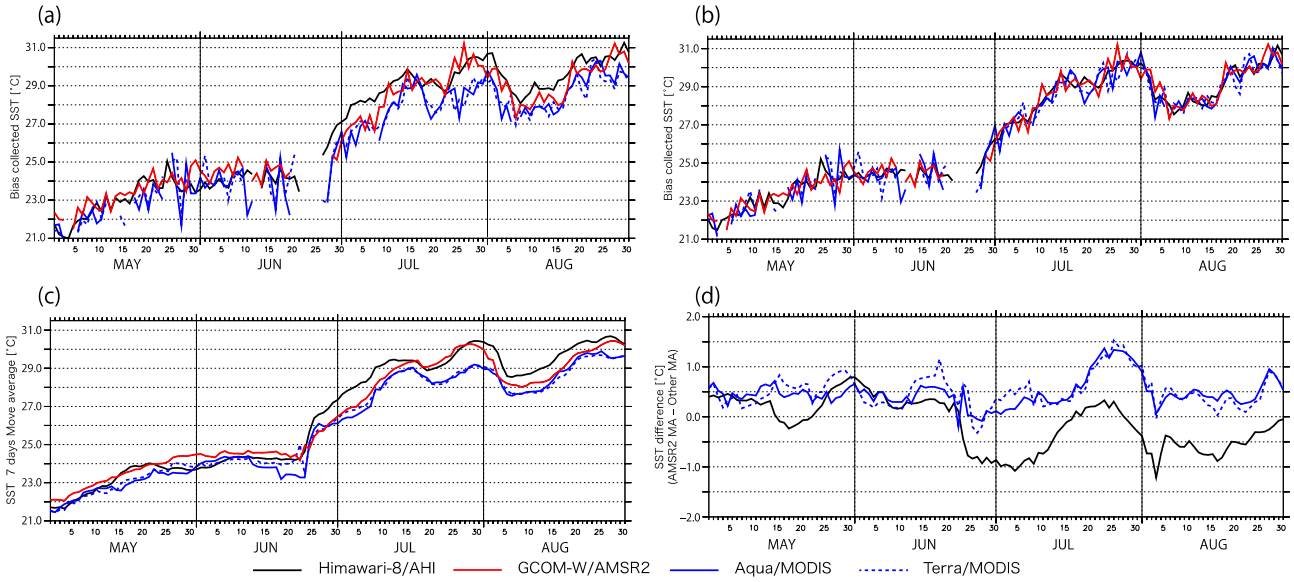

Figure. 6: Same as Figure 5 except from May to August 2017.

4.2. Data Assimilation

We conducted six cases of data assimilation experiments to confirm effects of our bias collection method and sensitivity of each satellite SST product to the analysis data (Table 3). Analysis period is from January to August, 2017.

Figure 7 plots time series of spatial average difference between NO-SAT and others for clarifying effects of satellite SST data assimilation. Time series of analysis data assimilating each one satellite SST product show the same characteristics as the satellite SST data shown in Figures 5 and 6. The result of ALL-SAT is affected by the original satellite biases; especially it is more visible in winter. Time series of ALL-SAT after July indicates that SST difference between Himawari-8 and MODIS is canceled each other by the data assimilation. On the other hand, the time series of ALL-BC exhibits its independence from the all satellite SST biases and they are similar to that of A2 which is used as the reference data for bias correction.

We validate the analysis data using in-situ SST data observed by the Kuroshio-Bokujyo buoys that are moored in an AMSR2 missing area (Table 4 and Figure 8). In this validation, we separate the data into two periods because the characteristics of satellite SST are opposite in each period. ALL-BC shows the best fitting to the in-situ data. On the other hand, fitting of ALL-SAT is worse than those of the analysis data with assimilation of one satellite SST. Bias correction of assimilated satellite SST data is thus important to make a more reliable level-4 SST product.

	Assimilated satellite SST data
NO-SAT	No satellite SST
ALL-SAT	All satellite SST
BC-SAT	Bias corrected satellite SST
H8	Himwari-8/AHI
A2	GCOM-W/AMSR2
MO	Aqua, Terra/MODIS

Table 3: Experiment settings

Table 4: Validation of analysis data using Kuroshio-Bokujyo Buoys.

		NO-SAT	ALL-SAT	ALL-BC	H8	A2	MO
Rank (Point)		6 (29)	5 (24)	1 (11.5)	3 (21)	4 (23.5)	2 (17)
Jan-Apr	BIAS	-0.360 (4)	-0.378 (5)	-0.197 (1)	-0.500 (6)	-0.265 (3)	-0.208 (2)
	RMSE	1.076 (5)	0.985 (4)	0.884 (2)	0.896 (3)	1.087 (6)	0.774 (1)
	Corr.	0.831 (4)	0.823 (6)	0.857 (2)	0.851 (3)	0.829 (5)	0.899 (1)
May-Aug	BIAS	0.590 (6)	0.222 (2)	0.399 (3)	0.533 (4)	0.573 (5)	0.025 (1)
	RMSE	0.875 (5)	0.837 (3)	0.824 (1)	0.840 (4)	0.826 (2)	0.915 (6)
	Corr.	0.957 (5)	0.961 (4)	0.962 (2.5)	0.963 (1)	0.962 (2.5)	0.954 (6)

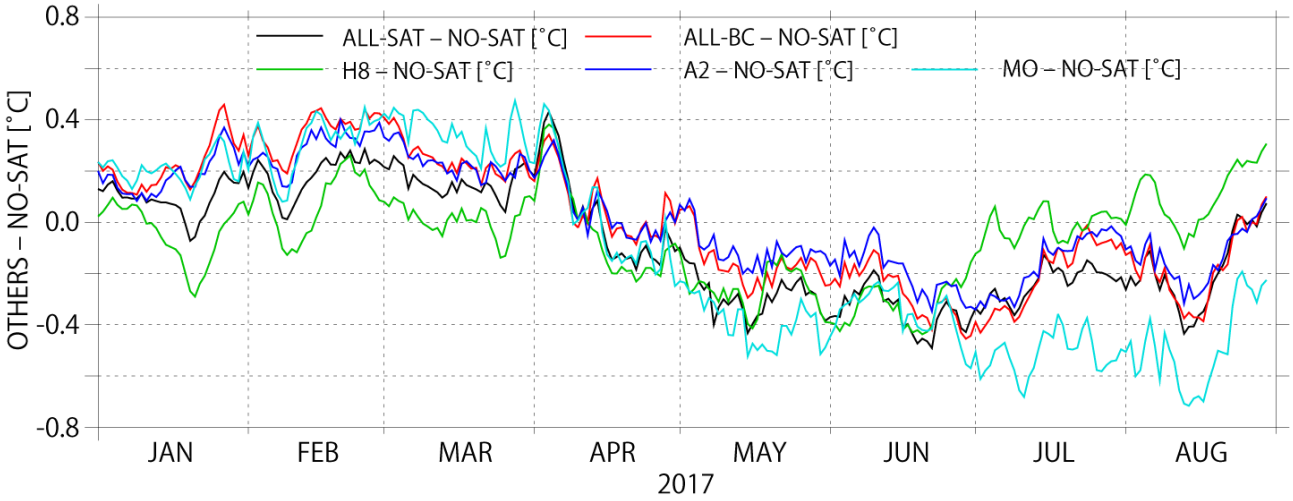

Figure. 7: Time series of SST difference between NO-SAT and others averaged in analysis area.

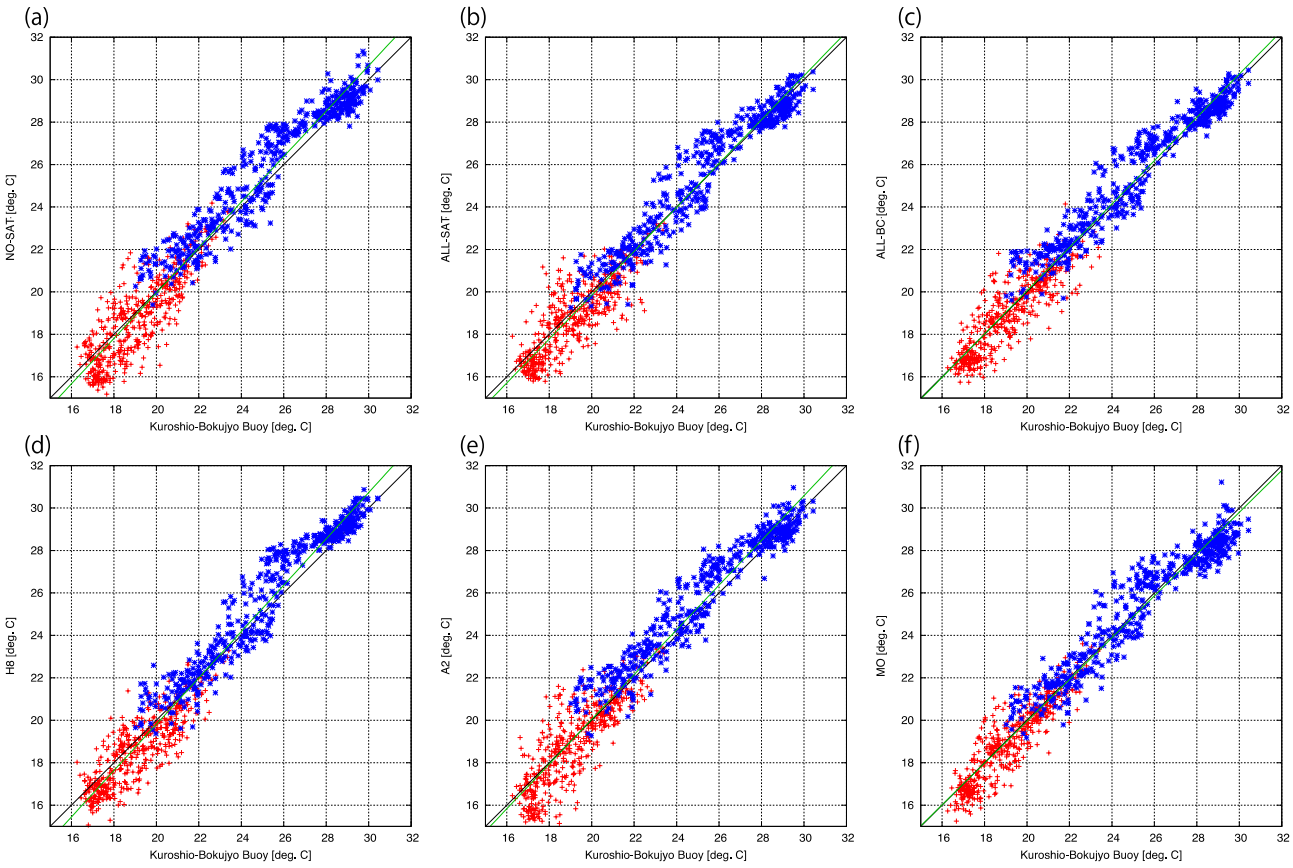

Figure. 8: Scatter plots of SST data observed by Kuroshio-Bokujyo buoys and detecte analysis data.

5. Conclusion

We constructed an ocean data assimilation system with the aim of making the Level 4 SST product around Japan using the LETKF data assimilation technique. Validation of the satellite SST data

using in-situ data provided by iQUAM showed that seasonal changes of bias: negative (positive) in winter and positive (negative) in summer, were found in the Himawari-8 (MODIS) SST data. On the other hand, significant bias was not detected in the AMSR2 SST data. A bias correction method using 7-days moving average of AMSR2 SST as a reference for correction. Validating six cases of data assimilation experiments with independent in-situ data demonstrated clear improvements in quality of the data assimilation product caused by the bias correction of the original SST products.

6. References

Evensen, G., Sequential data assimilation with a nonlinear quasi-geostrophic model using Monte Carlo methods to forecast error statistics, *J. Geophys. Res.* **99** (C5), 10 143-10 162, 1994.

Hunt, B. R., E. J. Kostelich and I. Szunyogh, Efficient data assimilation for spatiotemporal chaos: A local ensemble transform Kalman filter, *Physica D* **230**, 112–126, 2007.

Jordi, A. and D.-P. Wang, sbPOM: A parallel implementation of Princenton Ocean Model, *Environ. Modell. Softw.* **38**, 59-61, 2012.

Miyazawa, Y., H. Murakami, T. Miyama, S.M. Varlamov, X. Guo, T. Waseda and S. Sil, Data assimilation of the high-resolution sea surface temperature obtained from the Aqua-Terra satellites (MODIS-SST) using an ensemble Kalman filter, *Remote Sens.* **5,** 3123-3139, 2013.

Miyazawa, Y., S. M. Varlamov, T. Miyama, X. Guo, T. Hihara, K. Kiyomatsu, M. Kachi, Y. Kurihara and H. Murakami, Assimilation of high-resolution sea surface temperature data into an operational nowcast/forecast system around Japan using a multi-scale three dimensional variational scheme, *Ocean Dynam.* **67**, 713-728, 2017.

Miyoshi, T., Y. Sato and T. Kadowaki, Ensemble Kalman Filter and 4D-Var Intercomparison with the Japanese Operational Global Analysis and Prediction System, *Mon. Weather Rev.* **138**, 2846-2866, 2010.

Ott, E. and Coauthors, A local ensemble Kalman filter for atmospheric data assimilation, *Tellus* **56A**, 415–428, 2004.

Rosati, A. and K. Miyakoda, A general circulation model for upper ocean simulation, *J. Phys. Oceanogr.* **18**, 1601-1626, 1988.

Acknowledgement

This project was supported by JAXA for utilization of the satellite sea surface temperature data including Himawari-8 and GCOM-W.

SST DATA FROM SGLI ONBOARD THE SHIKISAI SATELLITE

Yukio Kurihara (ykuri.kiyo@gmail.jcom)[(1)], Kazunori Ogata[(2)], Hiroshi Murakami[(2)], Misako Kachi[(2)]

(1) Triple-i, Shibuya-ku, Tokyo, Japan
(2) Japan Aerospace Exploration Agency (JAXA), Tsukuba, Ibaraki, Japan

Abstract

JAXA launched the Global Change Observation Mission-Climate (GCOM-C) satellite: SHIKISAI, on 23 December 2017. The SHIKISAI satellite carries an optical sensor: the Second Generation Global Imager (SGLI) that is the successor to the Global Imager (GLI) onboard the JAXA's Advanced Earth Observing Satellite-II (ADEOS-II). SGLI consists of two components: the Visible and Near-infrared Radiometer (VNR) and the Infrared Scanner (IRS). VNR has 11 non-polarization channels and two polarization channels that measure the reflected and emitted radiations at the wavelengths from visible to near infrared. IRS has four channels for the short wavelength infrared radiation and the split window channels for the thermal infrared radiation. SGLI has switchable spatial resolutions from 250 m x 250 m to 1 km x 1 km. Sea surface temperatures are determined by using the split-window data of IRS. The SST algorithm and the cloud screening algorithm are based on the algorithms for the JAXA's Himawari-8 SST product. A preliminary validation result shows biases and standard deviations as -0.18 K and 0.69 K for daytime and -0.37 and 0.45 K for nighttime, respectively against buoy data. SGLI SST is now under development toward the publication by the end of this year.

1. Introduction

The Global Change Observation Mission-Climate "SHIKISAI" (GCOM-C) is JAXA's new sun-synchronous orbital satellite. SHIKISAI was launched from the Tanegashima Space Center on 23 December 2017. SHIKISAI aims monitoring of geophysical parameters related to the global climate system to contribute to the global climate watch and forecast. SSTs are determined from the split-window data of the Second Generation Global Imager (SGLI): an optical sensor onboard the SHIKISAI satellite. It is noteworthy that SGLI has the spatial resolution of 250m that will be powerful on the monitoring of coastal regions, inland seas, and so on. SGLI SST will be released by the end of 2018.

2. Algorithm and data

SGLI SSTs are determined by using the split window data measured at the 10.8- (T1) and the 12-micron (T2) channels of SGLI (Table 1). The SST algorithm is based on the quasi-physical method developed for Himawari-8 SST[1]. We modified and applied the method to the SGLI split window data. Coefficients for the SST determination were calculated by using the simulated SGLI data that we generated by using RTTOV, an RTM of NWPSAF. NWP data, the input to RTTOV, were provided by JMA.

Table 1 SGLI channel specifications

Ch.	λ [nm]	Δλ [nm]	L_{std}, L_{max} [W/m²/sr/μm]		SNR at L_{std}	IFOV [m]
VN1	380	10	60	210	675	250 / 1000
VN2	412	10	75	250	800	250 / 1000
VN3	443	10	64	400	517	250 / 1000
VN4	490	10	53	120	865	250 / 1000
VN5	530	20	41	350	482	250 / 1000
VN6	565	20	33	90	1040	250 / 1000
VN7	673.5	10	23	62	1002	250 / 1000
VN8	673.5	20	25	210	549	250 / 1000
VN9	763	8	40	350	1646	250 / 1000
VN10	868.5	20	8	30	491	250 / 1000
VN11	868.5	20	30	300	498	250 / 1000
P1	670	20	20	250	655	1000
P2	865	20	30	300	723	1000
SW1	1050	20	57	248	951	1000
SW2	1380	20	8	103	346	1000
SW3	1640	200	3	50	100	250 / 1000
SW4	2210	50	1.9	20	379	1000
Ch.	**λ [μm]**	**Δλ [μm]**	**T_{std}, T_{max} [K]**		**NEΔT at T_{std}**	**IFOV [m]**
T1	10.8	0.7	300	340	0.39	250 / 500 / 1000
T2	12.0	0.7	300	340	0.69	250 / 500 / 1000

Cloud/clear algorithm is based on the Bayesian inference method. Cloud probability is calculated for each pixel as the posterior probability of the given data, such as the satellite data, a priori data, etc. Probability density functions (PDFs) are defined by using the statistics calculated for each condition: clear sky, cloudy sky, and the mix of clear and cloudy sky. Here, the clear/cloudy classification is based on the comparison of the SGLI SST and buoy data. Visible data measured at the 673.5 nm channel (VN8) and split window data are currently used for the cloud probability determination. Analyzed SSTs are not used because of negative impacts of the errors in analyzed SSTs. The Gaussian distribution is assumed for the PDFs. Uncertainties in the satellite data, in determined SSTs, and in other data are implicitly taken into account in the PDFs; this is an advantage of statistics. A disadvantage of statistics is that reliable statistics requires a huge amount of data.

3. Result and discussions

We validated the SGLI SSTs using buoy data downloaded from iQuam of NOAA[2]. The PDFs for cloud probability were preliminarily generated by using the data from March to May in 2018. SGLI SSTs from 1 to 20 June 2018 were compared with the nearest buoy data. The match-up window is 3-hour and 3 km. The result shows good agreement between SGLI SST and buoys data (Fig. 1). Biases and standard deviations (STDs) are stable at each satellite zenith angle, meanwhile, these statistics are likely to depend on latitudes (Fig. 2). Latitudinal biases are possibly generated by the SST algorithm; however, we need further investigation to conclude this. Further improvements of the SST algorithm will be left for future.

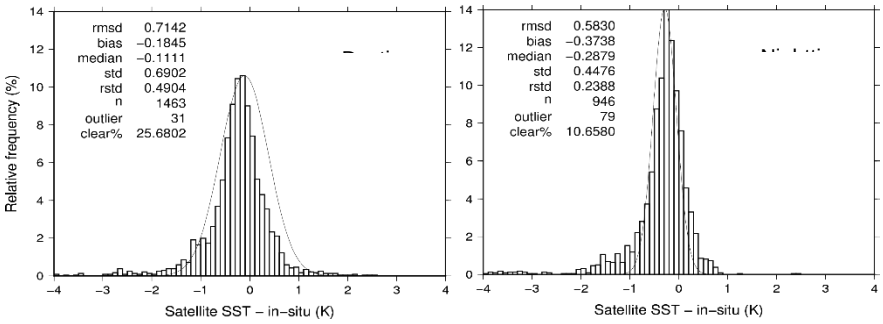

Fig. 1 Histogram of the differences between SGLI SST and buoy data (SGLI SST minus buoy)

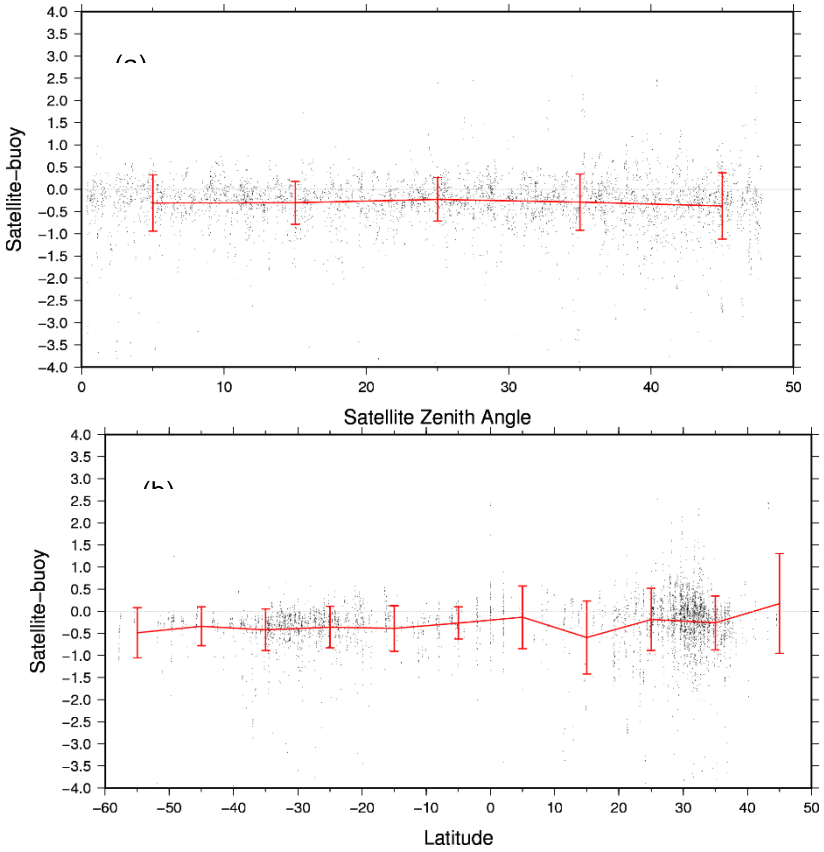

Fig. 2 Bias and standard deviation (STD) as a function of the satellite zenith angles (a) and as a function of the latitudes (b)

The long cold tail, that we reported on the poster at GHRSST XIX, was improved. Bias and STD were also improved with the improvement of the long cold tail. Meanwhile, clear sky percentage hardly changed. Fig. 3 shows SGLI SSTs of the latest version that reveals the Kuroshio current meandering south of Japan. Cloud contaminations are well masked without missing the data along the strong SST front associated with Kuroshio.

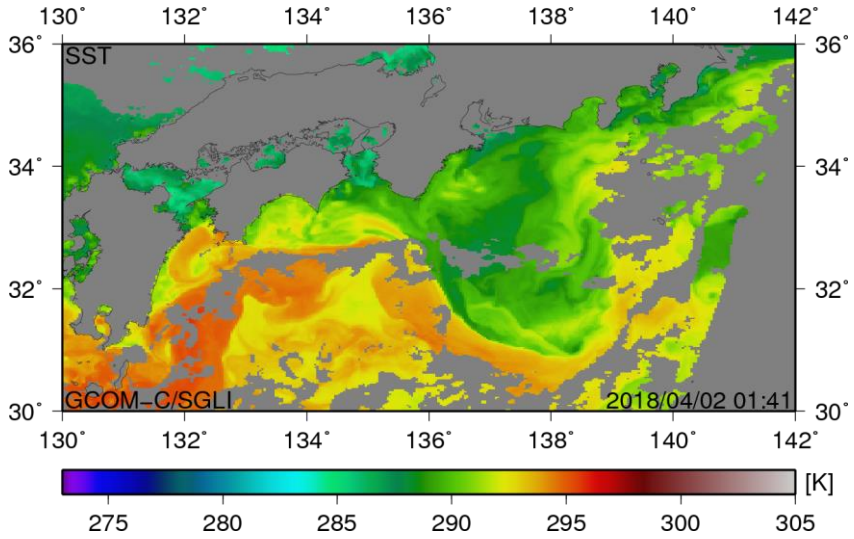

Fig. 3 SGLI SSTs (2 April 2018)

4. Summary

SGLI SST product is under development as of the end of June 2018. A preliminary result shows good agreement between SGLI SST and the buoy data. SGLI SST will be published from G-Portal of JAXA[3] by the end of 2018. SGLI SST is expected to improve the monitoring of the coastal and inland seas with the 250m spatial resolution.

5. Acknowledgment

RTTOV, that we used to simulate SGLI data, is developed and provided by NWPSAF of EUMETSAT. NWP data, the input to RTTOV, were provided by JMA. Buoy data were downloaded from the in-situ SST quality monitor (iQuam) of NOAA.

6. References

[1] Y.Kurihara, H. Murakami, and M. Kachi. Sea surface temperature from the new Japanese geostationary meteorological himawari-8 satellite. GRL, 2016. dos: 10.1002/2015GL067159.

[2] NOAA in-situ SST quality monitor (iQuam), URL: https://www.star.nesdis.noaa.gov/sod/sst/iquam/

[3] JAXA Glove Portal System (G-Portal), URL: https://www.gportal.jaxa.jp/gp/top.html

SECTION 4: APPENDICES

APPENDIX 1 – LIST OF PARTICIPANTS

**PARTICIPANTS TO THE GHRSST XIX SCIENCE TEAM MEETING,
EUMETSAT, Darmstadt, Germany
4-8 JUNE 2018**

Name	Affiliation	email
Armstrong, Ed	NASA Jet Propulsion Laboratory, United States	edward.m.armstrong@jpl.nasa.gov
Autret, Emmanuelle	Ifremer, France	emmanuelle.autret@ifremer.fr
Bank, Christian	EUMETSAT, Germany	
Barron, Charlie	U.S. Naval Research Laboratory, United States	charlie.barron@nrlssc.navy.mil
Barton, Ian	Retired from CSIRO, Australia	ian.barton@ozemail.com.au
Bauernschubert, Elisabeth	Deutscher Wetterdienst, Germany	Elisabeth.Bauernschubert@dwd.de
Beggs, Helen	Bureau of Meteorology, Australia	helen.beggs@bom.gov.au
Bouali, Marouan	Institute of Oceanography of the University of Sao Paulo, Brazil	marouanbouali@gmail.com
Boussidi, Brahim	University of Rhode Island, United States	bboussidi@uri.edu
Bragaglia-Pike, Silvia	University of Leicester, United Kingdom	sbp9@leicester.ac.uk
Castro, Sandra	University of Colorado, United States	sandrac@colorado.edu
Cayula, Jean-François	Vencore, inc, United States	j.cayula@ieee.org
Chen, Chuqun	South China Sea Institute of Oceanology, China	cqchen@scsio.ac.cn
Ciani, Daniele	National Research Council of Italy, Italy	daniele.ciani@artov.isac.cnr.it
Corlett, Gary	University of Leicester, United Kingdom	gkc1@leicester.ac.uk
Cornillon, Peter	University of Rhode Island, United States	pcornillon@me.com
Dash, Prasanjit	NOAA NESDIS STAR, United States	prasanjit.dash@noaa.gov
Donlon, Craig	ESA, Netherlands	craig.donlon@esa.int
Dumenil-Gates, Lydia	Deutscher Wetterdienst, Germany	lydia.gates@dwd.de
Eastwood, Steinar	Norwegian Meteorological Institute, Norway	s.eastwood@met.no
Gar-Glahn, Eugene V. S.	Liberia Meteorological Service, Liberia	egarglahn@yahoo.com
Gaultier, Lucile	OceanDataLab, France	lucile.gaultier@oceandatalab.com
Gentemann, Chelle	Earth & Space Research, United States	cgentemann@esr.org
Gladkova, Irina	NOAA/CREST at City College of New York, United States	irina.gladkova@gmail.com

Name	Affiliation	email
González-Haro, Cristina	Ifremer, Laboratoire d'Océanographie Physique et Spatiale, France	cristina.gonzalez.haro@ifremer.fr
Good, Simon	Met Office, UK	simon.good@metoffice.gov.uk
Guan, Lei	Ocean University of China, China	leiguan@ouc.edu.cn
Harris, Andy	NOAA-CICS, University of Maryland, United States	andy.harris@noaa.gov
Hihara, Tsutomu	Japan Agency for Marine-Earth Science and Technology, Japan	hiharat@jamstec.go.jp
Høyer, Jacob	Danish Meteorological Institute, Denmark	jlh@dmi.dk
Huang, Thomas	NASA Jet Propulsion Laboratory, United States	thomas.huang@jpl.nasa.gov
Ignatov, Alexander	NOAA STAR, United States	Alex.Ignatov@noaa.gov
Kaplan, Alexey	Lamont-Doherty Earth Observatory of Columbia University, United States	alexeyk@ldeo.columbia.edu
Karagali, Ioanna	DTU - Technical University of Denmark, Denmark	ioka@dtu.dk
Kim, Hee-Young	Seoul National University, South Korea	heeyoungkim@snu.ac.kr
Kim, Jaegwan	National Meteorological Satellite Center of Korea Meteorological Administration (KMA), South Korea	kimjgwan@korea.kr
Koner, Prabhat	ESSIC, University of Maryland, United States	pkoner@umd.edu
Kulkarni, Balasaheb	PVG'S College of Science and Technology, India	balasahebk@yahoo.com
Kurihara, Yukio	Triple-i, Japan	ykuri.kiyo@gmail.com
Lange, Martin	Deutscher Wetterdienst, Germany	martin.lange@dwd.de
Li, Wen-Hao	Raytheon, United States	wen-hao.li@jpl.nasa.gov
Li, Xu	EMC/NCEP/NOAA, United States	Xu.Li@noaa.gov
Liu, Mingkun	1. Ocean University of China 2. University of Reading, China	liumingkun_ouc@126.com
Luo, Bingkun	RSMAS, University of Miami, United States	lbk@rsmas.miami.edu
Marullo, Salvatore	ENEA, Italy	salvatore.marullo@enea.it
Maturi, Eileen	Department of Commerce, United States	eileen.maturi@noaa.gov
McKenzie, Bruce	Naval Oceanographic Office, United States	bruce.mckenzie@navy.mil
Meldrum, David	DML, United Kingdom	David.Meldrum@sams.ac.uk
Merchant, Christopher	University of Reading, United Kingdom	c.j.merchant@reading.ac.uk

Name	Affiliation	email
Minnett, Peter	RSMAS. University of Miami, United States	pminnett@rsmas.miami.edu
Nano-Ascione, Nolwenn	Météo-France, France	nolwenn.nano-ascione@meteo.fr
Nielsen-Englyst, Pia	Danish Meteorological Institute, Denmark	pne@dmi.dk
Nightingale, Tim	STFC, UK	tim.nightingale@stfc.ac.uk
O'Carrolll, Anne	EUMETSAT, Germany	Anne.Ocarroll@eumetsat.int
Ono, Nodoka	Japan Aerospace Exploration Agency (JAXA), Japan	ono.nodoka@jaxa.jp
Pan, Gang	South China Sea Institute of Oceanology, Chinese Academy of Sciences, China	gpan@scsio.ac.cn
Park, Kyung-Ae	Seoul National University, South Korea	kapark@snu.ac.kr
Pennybacker, Matthew	NOAA/STAR and GST, Inc., United States	matthew.pennybacker@noaa.gov
Petrenko, Boris	NOAA/STAR, GST, Inc., United States	boris.petrenko@noaa.gov
Piolle, Jean-Francois	Ifremer, France	jfpiolle@ifremer.fr
Sakurai, Toshiyuki	Japan Meteorological Agency, Japan	tsakurai@met.kishou.go.jp
Santoleri, Rosalia	CNR - Institute of Atmospheric Sciences and Climate, Italy	rosalia.santoleri@artov.isac.cnr.it
Saux Picart, Stéphane	Météo-France, France	stephane.sauxpicart@meteo.fr
Searle, Toby	Met Office, United Kingdom	toby.searle@metoffice.gov.uk
Sunder, Swathy	Indian Institute of Technology, India	swathysunder@iitb.ac.in
Surcel Colan, Dorina	Canadian Meteorological Centre for Environmental Prediction, Environment and Climate Change Canada, Canada	dorina.surcel-colan@canada.ca
Tomazic, Igor	EUMETSAT, Germany	igor.tomazic@eumetsat.int
Tomita, Hiroyuki	Institute for Space-Earth Environmental Research (ISEE), Nagoya University, Japan	tomita@isee.nagoya-u.ac.jp
Traeger-Chatterjee, Christine	EUMETSAT, Germany	christine.traeger@eumetsat.int
Vazquez, Jorge	Jet Propulsion Laboratory/California Institute of Technology, United States	jorge.vazquez@jpl.nasa.gov
Wang, Sujuan	National Satellite Meteorological Center,CMA, China	wangsj@cma.gov.cn
While, James	Met Office, United Kingdom	james.while@metoffice.gov.uk
Wick, Gary	NOAA/OAR/ESRL, United States	gary.a.wick@noaa.gov

Name	Affiliation	email
Wimmer, Werenfrid	University of Southampton, United Kingdom	w.wimmer@soton.ac.uk
Woo, Hye-Jin	Seoul National University, South Korea	hyejinwoo@snu.ac.kr
Zhang, Haifeng	The University of Melbourne, Australia, Australia	haifeng.zhang@unimelb.edu.au
Zhao, Xuepeng	NOAA/NESDIS/NCEI/CCOG, United States	Xuepeng.Zhao@noaa.gov
Zuo, Hao	ECMWF, United Kingdom	hao.zuo@ecmwf.int

APPENDIX 2 –PARTICIPANTS PHOTO

APPENDIX 3 – SCIENCE TEAM 2017-18

Anne O'Carroll (Chair)	**EUMETSAT, Darmstadt, Germany**
Ed Armstrong	NASA JPL PO.DAAC, USA
Viva Banzon	NOAA/NCDC, USA
Helen Beggs	Bureau of Meteorology, Melbourne, Australia
Kenneth S Casey	NOAA/NESDIS NODC, USA
Sandra Castro	University of Colorado, Boulder, USA
Jean–François Cayula	Vencore, Inc, Stennis Space Center, Mississippi, USA
Mike Chin	NASA JPL, USA
Carol Anne Clayson	WHOI, USA
Dorina Surcel Colan	CMC - Environment Canada
Peter Cornillon	University of Rhode Island, USA
Prasanjit Dash	NOAA, USA
Craig J Donlon	European Space Agency, The Netherlands
Steinar Eastwood	Met.no, Norway
Owen Embury	University of Reading, UK
Emma Fiedler	MetOffice, UK
Chelle Gentemann	Earth and Space Research, USA
Simon Good	MetOffice, UK
Lei Guan	Ocean University of China, China
Andrew Harris	NOAA/NESDIS ORA, USA
Simon Hook	NASA JPL, USA
Jacob Høyer	Danish Meteorological Institute, Denmark
Alexander Ignatov	NOAA/NESDIS/STAR, USA
Misako Kachi	Japan Aerospace Exploration Agency (JAXA), Japan
Alexey Kaplan	Columbia University, USA
Ioanna Karagali	Technical University of Denmark, Denmark
Prabhat Koner	ESSIC, University of Maryland, USA
Yukio Kurihara	Japan Aerospace Exploration Agency (JAXA), Japan
W Timothy Liu	NASA JPL, USA
Yang Liu	RSMAS, University of Miami, USA
Salvatore Marullo	ENEA, Italy
Eileen Maturi	NOAA/NESDIS/STAR/SOCD/MECB, USA
Christopher Merchant	University of Reading, UK
Peter Minnett	RSMAS, University of Miami, USA
Jonathan Mittaz	University of Reading, UK
Tim Nightingale	Rutherford Appleton Laboratory, UK
Kyung-Ae Park	Seoul National University, Korea
Jean–François Piollé	IFREMER, France
Rosalia Santoleri	ARTOV.ISAC.CNR, Italy
Stéphane Saux Picart	Météo-France, France
Dorina Surcel Colan	CMC - Environment Canada
Igor Tomazic	EUMESTAT, Darmstadt, Germany
Jorge Vazquez	NASA JPL PO.DAAC, USA
Sujuan Wang	National Satellite Meteorological Center, Met Administration, China
Christo Whittle	CISR, South Africa

Gary Wick	NOAA ETL, USA
Keith Willis	Naval Oceanographic Office, USA
Werenfrid Wimmer	University of Southampton, UK

LAST PAGE